Méthodologie basée sur l'intelligence artificielle pour certifier la conformité de pièces traitées par renforcement superficielle

Sevan Garois

HESAM UNIVERSITÉ

Arts et Métiers Sciences et Technologies

ÉCOLE DOCTORALE Science des Métiers de l'Ingénieur

Procédés et Ingénierie en Mécanique et Matériaux

THÈSE

présentée par : **Sevan GAROIS**
soutenue le : **08 Septembre 2023**

pour obtenir le grade de : **Docteur d'HESAM Université**

préparée à : **École Nationale Supérieur d'Arts et Métiers**

Discipline : **Science**

Spécialité : **Intelligence Artificielle**

Methodology based on artificial intelligence to certify the validity of gears treated by induction hardening

THÈSE dirigée par :
[Prof. CHINESTA Francisco]

et co-encadrée par :
[Dr. DAOUD Monzer]

Jury

M. Amine AMMAR	Professeur, ENSAM Angers	Président
Mme. Marianne BERINGHIER	Maîtresse de conférences, ISAE-ENSMA	Rapporteur
M. Antonio FALCO MONTESINOS	Professeur, Universidad CEU Cardenal Herrera	Rapporteur
M. Souheil-Antoine TAHAN	Professeur, ETS Montréal	Examinateur
M. Mohammed JEBAHI	Professeur associé, ENSAM	Examinateur
M. Monzer DAOUD	Professeur assistant, Dhofar University	Examinateur
M. Francisco CHINESTA	Professeur, ENSAM	Examinateur
M. Khalil TRAID	Docteur, Safran Tech	Invité
M. Pascal LAMESLE	Docteur, IRT-M2P	Invité

Remerciements

J'aimerais tout d'abord remercier le Professeur Francisco Chinesta et Monzer Daoud pour leur aide, leur soutien et leur confiance tout au long de ce long travail. Paco dont les discussions de quelques minutes me permettait d'avancer mes recherches sur plusieurs mois et Monzer dont la rigueur a permis à cette thèse d'être aussi détaillée et exhaustive.

Le travail de l'IRT M2P, et plus globalement des acteurs du projet TRANSFUGE, a été également déterminant pour le bon déroulement de la thèse. Sans eux, cette thèse n'aurait jamais vu le jour.

De même, j'aimerais remercier particulièrement mes coéquipiers du PIMM. Victor avec qui nous avons partagé quotidiennement notre calvaire en se rassurant autour d'une bière. Sergio, Angelo, Maurine et Clara dont les discussions au labo m'ont permis d'avancer plus sereinement. La collaboration enrichissante que j'ai pu faire avec Khouloud qui a donné lieu à un article et beaucoup d'idées. Nicolas et Simon en tant qu'anciens qui m'ont conseillés et accueillis du mieux possible dans cet univers. Et tant d'autres dont l'entraide et la bienveillance m'ont permis de traverser ce périple sans heurt.

Je remercie également La Douzaine, fleuron de l'industrie de la joie et de la bonne humeur entre amis qui m'a permis de m'évader plusieurs fois, le temps d'un week-end, pour me ressourcer mentalement et physiquement.

Pour son soutien inconditionnel, jour après jour, depuis le début de la thèse et jusqu'à la fin, je voudrais exprimer à ma compagne Micaela ma tendre gratitude. Toi qui a partagé mon quotidien, entre la joie et la difficulté, ce succès est aussi le tien.

Pour finir, je remercie ma famille : ma mère et mon père qui sont toujours là après tant d'années à m'épauler quelque soit l'épreuve. Ma soeur et mon frère qui sont toujours prêts à m'aider et me conseiller même si je n'ose pas le demander. Sans vous, il est peu probable que cette thèse ait été finie.

Résumé

La modélisation des systèmes physiques est une étape déterminante dans l'industrie pour optimiser les différents procédés. Les techniques les plus utilisées pour cela sont historiquement la modélisation par éléments finis (MEF) et la modélisation analytique. Néanmoins, la complexité de systèmes multi-physiques sur des géométries complexes, comme le procédé de renforcement superficiel faisant intervenir la chauffe par induction et ensuite la trempe, induit un temps de calcul extrêmement coûteux pour la MEF et une grande approximation au niveau des résultats pour la modélisation analytique. Depuis quelques années, avec l'avènement de l'intelligence artificielle (IA), l'apprentissage automatique (ML) apparaît comme une solution satisfaisante au niveau du temps de calcul et de la précision de la prédiction. Cette thèse a donc pour but de modéliser le procédé de renforcement superficiel sur un pignon à denture droite d'acier C45, plus particulièrement la prédiction de la dureté et dans une moindre mesure la prédiction des contraintes résiudelles.

Premièrement, la collection de données synthétiques provenant de la simulation par MEF et de données expérimentales a été effectuée. La prédiction des profils de dureté en profondeur a été réalisée que ce soit avec un entraînement sur les données de simulation ou les données expérimentales. La première modélisation basée sur la simulation par EF a deux approches: un modèle uniquement basé sur les données et un modèle hybride utilisant de l'information supplémentaire et pertinente via un modèle physique. La deuxième modélisation basée sur les données expérimentales a engendré une multitude de cas variés qui ont été traités. Après la dureté, les profils de contrainte résiduelle ont également été modélisés via les données de simulation par EF. Toutes les modélisations ont été réalisées via des modèles "boite-noire" tel que le eXtrem Gradient Boosting (XGBoost) dont la logique interne nous est inconnue.

De ce fait, une étude d'explicabilité des résultats par ML a été menée pour s'assurer de la véracité et de la cohérence des prédictions par rapport aux principes physiques bien connus. Pour cela, différents

outils ont été utilisés comme la bibliothèque basée sur la théorie du jeu, SHAP, ou encore les modèles de substitution qui miment de manière interprétable les résultats du modèle boite noire. Cela a permis de justifier les résultats obtenus par des implications majeures de différents paramètres du procédé ou par des règles compréhensibles.

Pour finir, une modélisation du problème inverse a été réalisée pour optimiser le procédé en permettant d'obtenir les paramètres procédés en fonction des paramètres de sortie désirés. Cette approche inverse a mis en lumière la difficulté de ce type de modélisation permettant de formuler un problème plus simple qui a menée vers une modélisation avec des résultats intéressants.

Mots-clés : Renforcement superficiel; Chauffage par induction; Trempe; Acier C45; Dureté; Contrainte résiduelle; Modélisation par éléments finis; Apprentissage automatique; Explicabilité de l'intelligence artificielle; Problème inverse

Abstract

Modeling physical systems is a determining step in the industry to optimize various processes. The most used techniques for this purpose are historically the Finite Element Method (FEM) and analytical modeling. However, the complexity of multi-physics systems coupled with complex geometries, such as the induction hardening process involving induction heating and quenching, induces an extremely costly computation time for the FEM and a large approximation for analytical modeling. In recent years, with the advent of artificial intelligence (AI), machine learning (ML) techniques appear to be satisfactory solutions in terms of computation time and modeling accuracy. The aim of this thesis is to model the surface reinforcement process on a C45 steel spur gear, more particularly to predict the hardness and the residual stress.

Firstly, synthetic data from finit element (FE) simulation and experimental data were collected. Prediction of the in-depth hardness profiles was made using both FE and experimental data. The first modeling based on FE was carried out using two approaches: a fully data-driven model, and a hybrid model using additional and relevant information via a physical model. The second modeling, based on experimental data, generated a multitude of different cases and resulted in promising results. Then, after hardness, residual stress profiles were also modeled using FE data. All modelings were carried out using 'black box' models such as eXtrem Gradient Boosting (XGBoost), the internal logic of which is unknown to us.

Therefore, a study of the explicability of the results by ML was conducted to ensure the veracity and consistency of the predictions with respect to the well-known physical principles. For this purpose, different tools were used such as the game theory-based library, SHAP, or the substitution models which mimic in an interpretable way the results of the black box model. This allowed to justify the obtained results by major implications of different process variables or by understandable rules.

Finally, an inverse modeling was done to optimize the process by allowing to obtain the process parameters according to the desired output ones. This inverse approach highlighted the difficulties of this type of modeling allowing to formulate a simpler problem that led to interesting results.

Keywords : Induction hardening; Induction heating; Quenching; C45 steel; Hardness; Residual stress; Finite Element Method; Machine learning; Explainable artificial intelligence; Inverse problem

Résumé en français

0.1 Introduction générale

0.1.1 Contexte industriel et scientifique

La tendance globale des processus industriels, tels que la trempe par induction, est à la rationalisation et à l'économie d'efforts, de temps et de ressources. Ceci est particulièrement important pour améliorer les propriétés mécaniques des composants tels que les engrenages, les barres et les disques, qui sont essentiels dans des industries telles que l'automobile, l'aviation et la production industrielle. Les modes de défaillance les plus courants des engrenages sont la fatigue superficielle (piqûres), l'usure, l'écoulement plastique et la rupture, causés par des problèmes de résistance, de force ou de lubrification. La trempe par induction est une technique largement utilisée pour améliorer la résistance à la fatigue des composants en les chauffant par induction électromagnétique puis en les refroidissant rapidement, ce qui entraîne une phase de martensite à grain fin et une contrainte résiduelle de compression. Les industries utilisent ce procédé pour chauffer avec précision des zones spécifiques, ce qui donne des résultats et un contrôle de haute qualité, tout en respectant l'environnement.

Le procédé de chauffage par induction consiste à induire un courant électrique à l'intérieur de l'engrenage à l'aide d'un champ électromagnétique alternatif, ce qui entraîne un chauffage localisé. Ce chauffage est influencé par des phénomènes tels que l'effet de peau, l'effet de bord, l'effet de bout et la perte d'hystérésis. Les facteurs clés du processus de chauffage sont la fréquence, le niveau de puissance et la durée du chauffage. Les méthodes de chauffage par induction à fréquence unique et à double fréquence sont toutes deux utilisées, la dernière permettant un durcissement complet et uniforme de la couche superficielle dans les formes complexes. La trempe superficielle suit le processus de chauffage par induction et implique un refroidissement rapide de l'engrenage chauffé à l'aide d'eau ou d'un mélange polymérisé.

0.1.2 Problématiques

La modélisation de systèmes physiques tels que la trempe par induction est cruciale pour les industries, car elle permet de comprendre et de contrôler le comportement et les performances du système. La méthode des éléments finis (FEM) et les modèles analytiques sont couramment utilisés pour modéliser la trempe par induction. La méthode des éléments finis permet de comprendre en détail les phénomènes physiques, mais elle est coûteuse en temps et en calcul. Les modèles analytiques sont efficaces au niveau calculatoire mais limités à des géométries simples. Les modèles de régression basés sur l'apprentissage automatique sont apparus comme une alternative, offrant un équilibre entre puissance et précision. Cependant, ils nécessitent des données de haute qualité et en quantité suffisante pour l'apprentissage.

0.1.3 Objectifs de recherche

Le travail de la thèse consiste à trouver une méthode de modélisation évolutive et précise pour les géométries complexes, sans coût de calcul élevé. Les modèles d'apprentissage automatique pourraient constituer une solution appropriée, mais il faut tenir compte des limites des données et du sur-apprentissage. Il est essentiel de trouver un juste équilibre entre puissance et précision pour optimiser le processus de trempe par induction et obtenir les propriétés mécaniques souhaitées dans le produit final.

0.1.4 Organisation de la thèse

La thèse se compose de cinq articles rédigés dans le cadre du projet TRANSFUGE, sur la modélisation et l'optimisation du processus de trempe par induction à partir de données. Voici un résumé de chaque article:

0.1.4.1 Article 1: Data-driven modelling for multi-physics parametrized problems - Application to induction hardening process

Cet article se concentre sur la modélisation du processus de durcissement par induction en utilisant des données synthétiques pour un engrenage en acier C45. Il présente différentes approches, notamment l'utilisation de la méthode des éléments finis via le logiciel FORGE pour générer des données synthétiques précises. La température et le taux d'austénite pendant le processus de chauffage sont

prédits à l'aide de la décomposition orthogonale appropriée (POD), et la dureté est prédite à l'aide de modèles d'apprentissage automatique guidés par les données et de modèles hybrides. L'article met en évidence la collecte et l'analyse de données synthétiques, la modélisation des paramètres pertinents et la combinaison de la modélisation basée sur la physique et de l'apprentissage automatique pour des prédictions précises.

0.1.4.2 Article 2: Data-driven modeling for residual stress prediction after induction heating process of C45 steel

Ce papier présente un modèle guidé par les données qui est basé sur la bibliothèque XGBoost pour prédire les contraintes résiduelles après le processus de durcissement par induction d'un engrenage à denture droite en acier C45. Il utilise des données synthétiques générées par la FEM pour l'étape de trempe. L'article met l'accent sur la prédiction des contraintes résiduelles en profondeur, qui sont cruciales pour la validation d'un engrenage traité.

0.1.4.3 Article 3: Artificial intelligence modeling of induction contour hardening of 300M steel bar and C45 steel spur gear

Cet article présente de nouvelles données expérimentales issues de processus de trempe par induction sur des cylindres en acier 300M et des engrenages à denture droite en acier C45. Il propose un modèle basé sur XGBoost pour prédire la dureté dans les deux cas. L'article met en évidence la collecte et l'analyse des données expérimentales, la différence entre une induction à simple et double fréquence, la modélisation de la dureté pour des géométries simples et complexes, et le lissage de la régression du noyau pour gérer les incertitudes et le bruit dans les données.

0.1.4.4 Article 4: Explaining Hardness Modeling after Induction Hardening with XAI Tools

Cet article explique les résultats de la modélisation de la dureté après la trempe par induction à l'aide d'outils d'intelligence artificielle explicables (XAI). Il explore différentes méthodes XAI telles que l'importance des caractéristiques, les valeurs SHAP et la modélisation de substitution. L'article souligne l'importance de l'XAI pour comprendre la prise de décision du modèle et assurer la cohérence physique.

0.1.4.5 Article 5: Data-driven Inverse Problem for optimizing the Induction Hardening process of C45 Spur-Gear

Cet article explore l'approche des problèmes inverses pour optimiser le processus de durcissement par induction de l'engrenage en acier C45. Il propose une méthode pour estimer l'énergie requise pour les profils de dureté souhaités. L'article simplifie le problème en discrétisant le profil de dureté et en créant des caractéristiques basées sur la physique. Il aborde les défis posés par les problèmes mal posés et présente des résultats prometteurs pour une analyse plus approfondie.

Ces articles contribuent à la compréhension de la modélisation basée sur les données, à l'optimisation et à l'explication du processus de trempe par induction. Ils soulignent l'importance des données synthétiques et expérimentales, ainsi que la combinaison de l'apprentissage automatique et des approches basées sur la physique.

0.2 Revue de littérature

0.2.1 Études expérimentales

La trempe par induction est un procédé utilisé pour durcir la surface des matériaux ferromagnétiques comme l'acier. Il s'agit de générer un champ électromagnétique à l'aide d'un inducteur, qui induit de la chaleur dans le matériau par le biais de courants de Foucault. La couche superficielle de l'acier est chauffée à une température élevée, ce qui entraîne une transformation de sa microstructure. La microstructure transformée donne une couche superficielle plus dure et plus résistante à l'usure du temps et des efforts.

La trempe par induction entraîne également des phénomènes tels que des contraintes résiduelles et des déformations. Les contraintes résiduelles sont des contraintes internes qui subsistent dans le matériau après le processus de durcissement et qui peuvent avoir un impact sur la stabilité dimensionnelle et la durée de vie du composant. La distorsion fait référence au changement permanent de forme causé par la disparité des coefficients de dilatation thermique entre la couche de surface et le matériau de base.

Des études expérimentales ont été menées pour étudier les effets des différents paramètres du processus sur les profils de dureté et les microstructures résultant de la trempe par induction. Les profils de dureté sont généralement mesurés à l'aide de techniques telles que les essais de dureté Vickers, Knoop, Rockwell et Brinell. Les contraintes résiduelles sont mesurées à l'aide de méthodes telles que la diffraction des rayons X et la méthode du trou incrémental.

0.2.2 Algorithmes d'apprentissage automatique

Les algorithmes d'apprentissage automatique, en particulier les algorithmes d'apprentissage supervisé, sont appliqués pour prédire et optimiser divers aspects de la trempe par induction. Des algorithmes tels que XGBoost, les Forêts Aléatoires, les réseaux neuronaux artificiels (ANN), les réseaux neuronaux récurrents (RNN), les machines à vecteurs de support (SVM) et la régression multilinéaire sont couramment utilisés pour les tâches de prédiction.

0.2.3 Explicabilité

L'explicabilité de l'intelligence artificielle (XAI) est un sous-domaine de l'IA qui se concentre sur le développement de modèles et de systèmes qui peuvent être compris et interprétés par les humains. L'XAI vise à rendre les systèmes d'IA transparents et explicables afin d'instaurer la confiance et d'identifier les biais. Dans le contexte du renforcement de l'induction, l'XAI peut aider à expliquer les modèles de boîte noire ou à développer des modèles interprétables pour fournir des informations sur les paramètres du procédé et leurs implications sur le modèle.

0.2.4 Problème inverse

Les problèmes inverses (et mal posés) sont à mettre en opposition avec les problèmes directs. Dans le problème direct, une fonction modèle est utilisée pour déterminer l'effet (phénomène) sur la base de causes connues. Le problème inverse, quant à lui, consiste à déterminer les causes ou à reconstruire une quantité inconnue à partir d'observations ou de mesures.

Les problèmes inverses sont complexes mais déterminants. Ils nécessitent de trouver une fonction qui relie les données observées aux causes inconnues. Ces problèmes impliquent souvent des solutions non uniques et nécessitent des hypothèses supplémentaires ou des techniques de régularisation pour obtenir une solution stable et unique. Diverses approches mathématiques telles que l'optimisation,

la régularisation, l'inférence bayésienne et les algorithmes d'apprentissage automatique peuvent être utilisées pour résoudre les problèmes inverses.

Il existe quelques applications de l'approche des problèmes inverses en métallurgie, en particulier dans le contexte des processus de durcissement par induction. De même, des approches similaires ont été utilisées dans le domaine des systèmes de conduction thermique et de la thermodynamique.

0.3 Méthodes

0.3.1 Données de simulation

La méthode des éléments finis est utilisée pour résoudre les équations aux dérivées partielles qui régissent les phénomènes physiques survenant au cours du processus. Les données synthétiques du processus de trempe par induction sont générées par des simulations par éléments finis à l'aide du logiciel commercial FORGE. L'étude porte sur un engrenage à denture droite en acier C45 présentant des dimensions et des propriétés mécaniques et métallurgiques spécifiques.

Le processus comporte deux étapes principales : le chauffage et la trempe. Lors de l'étape de chauffage, les champs électromagnétiques et thermiques sont combinés et la puissance de chauffage est calculée à l'aide des équations de Maxwell. Cette puissance est ensuite appliquée au solveur thermique pour déterminer la distribution de la température au sein de l'engrenage en résolvant l'équation de la chaleur. Dans l'étape de trempe, un solveur thermo-métallo-mécanique est utilisé pour simuler le processus de refroidissement, en tenant compte du couplage entre les effets thermiques, métallurgiques et mécaniques. L'état résultant du chauffage et de la trempe est utilisé pour calculer la dureté, les contraintes et les déformations.

Pour générer des données précises, plusieurs simulations par éléments finis ont été réalisées avec différents paramètres de processus et coefficients de transfert de chaleur. Les simulations sont conçues en utilisant un plan d'expérience (DOE) afin de minimiser le nombre d'exécutions tout en obtenant les combinaisons les plus pertinentes de paramètres.

0.3.2 Données expérimentales

La première série d'expérience est menée sur des barres cylindriques en acier 300M avec une induction mono-fréquence. La température en surface est obtenue à l'aide d'un pyromètre. La deuxième

série d'expérience est réalisée sur des engrenages à denture droite en acier C45, avec deux engrenages de dimensions et modules différents. Ensuite des mesures de dureté Vickers ont été faites dans le cadre de la collection des données et une modélisation future. Les équipements et les conditions spécifiques d'expérience sont exhaustivement présentés et décrits dans le manuscrit.

0.3.3 Algorithmes d'apprentissage automatique

0.3.3.1 Forêts aléatoires

Les forêts aléatoires est un type d'algorithme utilisé pour les tâches de classification et de régression. Il se compose de plusieurs arbres de décision qui travaillent ensemble pour faire des prédictions. Chaque arbre de décision est construit en divisant récursivement les données sur la base de la caractéristique qui fournit l'erreur quadratique moyenne (MSE) la plus faible pour les valeurs prédites. La prédiction finale d'une forêt aléatoire est la moyenne des prédictions de chaque arbre. Les forêts aléatoires sont efficaces pour saisir les relations complexes entre les caractéristiques et les cibles, disposent de mesures intégrées de l'importance des caractéristiques et sont moins sujettes à l'ajustement excessif que les arbres de décision individuels. Cependant, elles peuvent être coûteuses en termes de calcul et manquer d'interprétabilité.

0.3.3.2 XGBoost

XGBoost, abréviation de Extreme Gradient Boosting, est un autre algorithme basé sur des arbres de décision boostés par le gradient. Il construit séquentiellement une forêt d'arbres de décision. L'algorithme commence par une prédiction initiale, qui est la moyenne des valeurs cibles. À chaque itération, les résidus, qui sont les différences entre les valeurs observées et les prédictions actuelles, sont calculés. Les résidus sont ensuite utilisés pour diviser les données en nœuds feuilles, dans le but de minimiser le score de similarité. Le processus se poursuit de manière itérative, chaque nouvel arbre apprenant à partir des résidus des arbres précédents. XGBoost est connu pour sa capacité à traiter des ensembles de données complexes, son efficacité et sa flexibilité en matière de déploiement.

0.4 Contribution scientifique

La thèse est articulé autour d'article divers qui traitent le sujet de l'optimisation du procédé par induction avec des méthodes d'IA. La totalité de ces articles forme le coeur de la contribution de cette thèse.

0.4.1 Article 1

Ce article traite de la modélisation pilotée par les données pour le processus de chauffage par induction. Le chauffage par induction consiste à appliquer un courant alternatif à une pièce conductrice, ce qui provoque un échauffement par effet Joule. L'étude se concentre sur l'optimisation et l'amélioration du chauffage par induction en tenant compte de divers paramètres tels que le comportement du matériau, les paramètres du processus et les caractéristiques géométriques. Deux paramètres importants du processus, la fréquence et la puissance, sont étudiés tout en maintenant les autres paramètres constants. L'article présente la méthodologie utilisée, qui comprend la collecte de solutions de haute fidélité par le biais de simulations par éléments finis, l'application de techniques de réduction de la dimensionnalité telles que la décomposition orthogonale appropriée (POD) et l'utilisation d'un algorithme d'apprentissage automatique pour la régression.

La température et la transformation de la phase austénitique pendant le processus de chauffage sont considérées comme des quantités physiques importantes. Les auteurs construisent des modèles pour l'évolution temporelle de la température et utilisent la POD pour réduire la dimensionnalité des données. Ils appliquent ensuite une technique de régression non linéaire appelée "sparse Proper Generalized Decomposition" (sPGD) pour ajuster les données réduites. Les résultats montrent une bonne concordance entre les valeurs réelles et prédites des coefficients modaux.

L'article fournit des explications détaillées sur la méthodologie et examine le choix des paramètres, les techniques de prétraitement des données et l'évaluation du modèle. Des figures et des tableaux sont utilisés pour illustrer les concepts et présenter les résultats. Les auteurs soulignent le potentiel de la technique de régression non linéaire appliquée avec un nombre réduit de données.

Dans l'ensemble, l'article se concentre sur l'utilisation de la modélisation guidée par les données et des techniques d'apprentissage automatique pour comprendre et optimiser le processus de chauffage par induction. La méthodologie et les résultats présentés contribuent au domaine du chauffage par

induction et démontrent l'efficacité de l'approche proposée.

L'article traite de l'utilisation de techniques de modélisation hybrides et basées sur les données pour prédire la dureté au cours du processus de trempe. La pièce étudiée est un engrenage, et des simulations utilisant le logiciel FORGE® ont été effectuées pour générer des ensembles de données pendant l'étape de trempe. Les variables d'entrée prises en compte comprennent le pas de simulation, la durée totale de la trempe, la température initiale et les valeurs de température recueillies à différents moments du processus de trempe. Des variables supplémentaires, telles que les gradients de température temporels et spatiaux, ont également été incluses dans l'espace des caractéristiques.

Pour analyser les données, celles-ci ont été divisées en sous-ensembles de formation et de test. En raison de la distribution déséquilibrée des valeurs de dureté, les données ont été regroupées en trois classes à l'aide de l'algorithme K-means afin de créer un ensemble de données de test équilibré. La sélection des caractéristiques a été effectuée à l'aide du test F afin de réduire le nombre de variables d'entrée.

Pour modéliser la dureté, l'algorithme de gradient boosting implémenté dans la bibliothèque XGBoost a été choisi. Les paramètres du modèle ont été optimisés à l'aide d'une recherche aléatoire. La petite taille des ensembles de données a constitué un défi, et diverses techniques ont été employées pour éviter le surajustement et maximiser les performances du modèle. L'erreur quadratique moyenne (RMSE) et l'erreur quadratique moyenne en pourcentage (RMSPE) ont été utilisées pour évaluer la précision de la prédiction.

Les résultats ont montré que les modèles avaient du mal à se généraliser à de nouvelles données, mais qu'ils fournissaient des informations pertinentes. L'ensemble de données d'apprentissage a été bien prédit, tandis que l'ensemble de données de test a montré une marge d'amélioration avec plus de données. L'approche de modélisation hybride, qui combine des modèles axés sur les données et des lois physiques, a également été considérée comme une solution potentielle pour résoudre le problème de la rareté des données. La corrélation entre le taux d'austénite et la dureté a été mise en évidence comme un élément d'information précieux pour la prédiction.

Dans l'ensemble, l'étude a démontré les défis et les solutions potentielles pour la prédiction de la dureté pendant la trempe en utilisant des techniques de modélisation hybrides et basées sur les données.

0.4.2 Article 2

Ce travail traite de l'utilisation du chauffage par induction suivi d'une trempe en tant que processus de traitement thermique de surface pour améliorer la résistance à la fatigue des composants critiques dans les industries automobile et aérospatiale, tels que les engrenages. Le procédé introduit des champs de contraintes résiduelles en compression en surface qui améliorent la résistance à la fatigue du composant. La sélection des paramètres du processus joue un rôle crucial dans la détermination des profils de contraintes résiduelles qui en résultent.

Pour prédire le profil des contraintes résiduelles à l'intérieur d'une pièce en forme d'engrenage, les chercheurs ont développé une approche combinant une technique d'intelligence artificielle et une modélisation par éléments finis du processus de traitement par induction. Ils ont utilisé un modèle d'éléments finis à symétrie périodique 3D pour simuler le processus avec diverses combinaisons de paramètres en utilisant un plan d'expériences par échantillonnage hypercube latin. Les données de simulation ont ensuite été utilisées pour former un modèle piloté par les données basé sur la bibliothèque XGBoost.

Le modèle développé a montré une bonne précision dans la prédiction des profils de contrainte résiduelle et peut être utilisé pour l'optimisation du processus de traitement par induction. L'utilisation de techniques d'intelligence artificielle et de modèles pilotés par les données offre une alternative à la collecte de données expérimentales coûteuses et peut fournir des prédictions précises avec des données disponibles limitées.

0.4.3 Article 3

Après avoir rappelé les conditions des essais expérimentaux sur les cylindres en acier 300M et les engrenages en acier C45 comme présenté précédemment dans la section Méthodes de la thèse.

L'article traite de l'utilisation de l'algorithme XGBoost pour la modélisation de la dureté. XGBoost est un algorithme basé sur les arbres qui est connu pour son efficacité dans les problèmes de prédiction de l'apprentissage automatique. De plus, il est facile à tester et à manipuler, ne nécessitant que quelques hyperparamètres liés aux arbres.

L'algorithme construit une forêt d'arbres de décision boostés par le gradient. À chaque itération de la construction de l'arbre, les résidus entre les valeurs observées et les valeurs prédites sont calculés.

Les résidus sont utilisés pour calculer un score de similarité et l'arbre est divisé en fonction d'un seuil. Les divisions ayant le gain le plus élevé sont choisies, et le processus se poursuit jusqu'à ce que tous les arbres soient construits. La valeur de sortie de l'arbre est exprimée comme la somme des résidus divisée par le nombre de résidus.

Pour la trempe par induction de barres cylindriques et d'engrenages. Les variables de ces cas comprenaient la fréquence, la puissance, les profils de température (calculé à l'aide de la FEM), la profondeur et la durée du chauffage. Les ensembles de données ont été divisés en ensembles d'entraînement (70%) et de test (30%). Les résultats de la prédiction des profils de dureté pour les barres cylindriques à l'aide des modèles XGBoost et Random Forest ont été comparés. XGBoost a donné de meilleures prédictions avec des erreurs relatives plus faibles.

Pour le problème des engrenages, d'autres facteurs ont dû être pris en compte. Des paramètres intermédiaires, tels que les profils de température, sont extraits pour la phase d'entraînement. Dans ce travail, les profils de température ont été considérés comme importants pour décrire la dureté. Ainsi, l'algorithme XGBoost a été utilisé pour prédire, en amont, la température en fonction des paramètres du processus. Les prédictions ont montré une bonne précision par rapport aux températures réelles et permettent leur utilisation en tant que variable d'entrée. Aussi, des techniques de lissage des données, telles que la régression du noyau, ont été appliquées pour réduire le bruit dans les profils de dureté. Les zones de variation expérimentale ont également été prises en compte pour tenir compte de l'incertitude et de la variabilité des mesures.

Plusieurs cas de figures ont été considérés pour la prédiction des profils de dureté pour les engrenages en acier C45 traités. Les prédictions ont été réalisées à l'aide d'un modèle XGBoost. Les profils prédits ont montré des tendances et des niveaux de dureté similaires à ceux des profils mesurés.

Dans l'ensemble, XGBoost s'est avéré être un algorithme efficace pour la modélisation de la dureté dans le contexte de la trempe par induction, que ce soit pour une géométrie simple ou complexe.

0.4.4 Article 4

Ce travail se concentre sur l'utilisation d'outils d'intelligence artificielle explicable (XAI) pour interpréter et expliquer les prédictions d'un modèle XGBoost pour la prédiction de la dureté dans le cadre d'une trempe par induction simultanée à double fréquence. L'étude a été menée sur des

engrenages à denture droite en acier C45 (cas réalisé dans l'article 3). Premièrement, l'outil intégré de la bibliothèque XGBoost pour interpréter l'importance des caractéristiques a été utilisé. Puis, la bibliothèque SHAP pour des explications locales et globales plus avancées. En outre, un modèle de substitution interprétable a été mis en œuvre pour illustrer les règles de prédiction et fournir une explication plus claire. L'étude souligne l'importance d'expliquer les résultats obtenus par les modèles de boîte noire, ce qui permet de justifier la qualité des résultats de manière claire aux acteurs du milieu scientifique.

Les graphiques d'importance des caractéristiques donnés par SHAP indiquent que la profondeur et la température sont les variables les plus importantes pour la prédiction de la dureté. Cependant, il a été noté que ce résultat n'a pas de signification physique. Le modèle a considéré la profondeur comme la variable la plus importante parce que la température n'était disponible qu'en surface, et le modèle a compris que la dureté est liée à la profondeur pour chaque série.

L'analyse SHAP visait à souligner l'impact de toutes les variables sur les résultats du modèle. Les valeurs absolues moyennes de SHAP ont montré que la profondeur a l'impact le plus important sur la prédiction de la dureté. Cependant, d'autres variables contribuent également à la discrimination de la dureté entre les différentes séries à une profondeur donnée.

Une analyse plus poussée a révélé que lorsque la profondeur ne peut plus discriminer la dureté, d'autres variables commencent à avoir un impact. Par exemple, à une profondeur fixe de 30μm (en quasi-surface), la température s'est avérée être le principal paramètre influençant la prédiction de la dureté. Pour valider l'hypothèse selon laquelle l'historique de la température décrit la dureté, une analyse SHAP pour la modélisation de la température a été réalisée. Elle a montré que le temps, suivi des paramètres de puissance, a un impact significatif sur la prédiction de la température de surface.

L'analyse locale s'est concentrée sur un point spécifique où la prédiction n'était pas claire ou incohérente par rapport aux mesures expérimentales. Des diagrammes de force SHAP ont été utilisés pour analyser l'impact des variables sur cette prédiction. Une comparaison a été faite avec un cas bien prédit pour identifier les différences dans les valeurs SHAP. Cette analyse a permis d'expliquer les causes des erreurs de prédiction et de souligner l'importance de variables telles que le temps, la température et la profondeur.

Dans l'ensemble, l'étude a démontré l'importance de la profondeur et de la température dans la

prédiction de la dureté et la façon dont l'analyse SHAP peut fournir des informations sur le comportement du modèle et les contributions des variables. Le modèle s'est avéré cohérent avec les principes physiques.

0.4.5 Article 5

Ce papier aborde le concept du problème inverse, en particulier dans le contexte de la prédiction des paramètres de processus à partir des profils de dureté observés, en utilisant l'apprentissage automatique. L'objectif est de déterminer les paramètres d'entrée qui ont produit un ensemble donné d'observations. Les variables impliquées dans le problème comprennent la moyenne fréquence et la haute fréquence, leurs puissances de générateur respectives, la température, la profondeur, la durée de chauffage et la dureté. L'accent est mis sur l'encodage des profils de dureté dans un ensemble de points caractéristiques afin de simplifier le problème. Les points caractéristiques sont choisis à des profondeurs spécifiques et fixés pour conserver un profil homogène. Un réseau neuronal artificiel (ANN) est utilisé pour résoudre le problème inverse, mais il ne parvient pas à fournir une solution unique, ce qui démontre la non unicité d'une telle solution.

Pour résoudre le problème de non-unicité, une approche basée sur la physique est proposée. La combinaison des paramètres de sortie est basée sur des principes physiques, tels que la prise en compte séparée de la pointe et de la racine de la dent et le calcul de l'énergie en fonction du temps et de la puissance pour chaque fréquence. Le problème inverse est reformulé comme un problème de régression, visant à prédire l'énergie de haute fréquence et l'énergie de moyenne à partir des mesures de dureté à la pointe et à la racine de la dent, de manière séparée.

Différents modèles d'apprentissage automatique, notamment XGBoost, Forêts Aléatoires, Régression multilinéaire et Regresseur à Vecteur de Support, sont testés pour la tâche de modélisation inverse. Les résultats montrent des performances satisfaisantes, avec des erreurs inférieures à 10%. La sélection des mesures de dureté caractéristiques s'avère utile pour obtenir des prédictions précises. Le modèle de régression multi-linéaire est mis en évidence à titre d'exemple, démontrant des prédictions réussies dans les plages d'énergie fixées.

En outre, la cohérence du problème est validée par l'utilisation des paramètres de sortie prédits pour estimer les profils de dureté. La sélection des points de dureté en fonction de la profondeur fixe permet de prédire plusieurs sorties à partir d'une seule variable d'entrée.

Dans l'ensemble, l'étude démontre la faisabilité de l'utilisation de l'apprentissage automatique et des approches informées par la physique pour résoudre le problème inverse de la prédiction des paramètres de processus à partir des profils de dureté observés. Les résultats indiquent que des algorithmes plus simples peuvent traiter efficacement le problème simplifié et que les prédictions obtenues peuvent également être utilisées pour le problème inverse.

0.5 Conclusion

Cette thèse porte sur l'étude du processus de trempe par induction (IH) à l'aide de techniques d'IA. L'étude porte sur différents types de processus de trempe par induction, tels que la trempe par induction simultanée à double fréquence sur un engrenage en acier C45 et la trempe par induction à simple fréquence sur des cylindres en acier 300M. L'objectif est de proposer des approches pour modéliser, expliquer et optimiser les processus IH dans un contexte industriel.

Dans un premier temps, des données synthétiques générées par un logiciel de simulation sont utilisées pour prédire la dureté. Les résultats sont prometteurs, en particulier avec l'utilisation d'une technique de sélection et de combinaison de caractéristiques appelée XGBoost, ainsi qu'un modèle hybride incorporant le ratio d'austénite en plus des données de base. L'étude explore également la prédiction de la contrainte résiduelle avec des résultats satisfaisants. Alors que les données synthétiques constituent un point de départ, les données expérimentales sont considérées comme plus pertinentes en raison des défis du monde réel tels que les biais, le bruit et les données manquantes.

Les données expérimentales sont collectées à partir de diverses expériences IH. La modélisation commence par une géométrie simple avec des cylindres en acier 300M, où les informations sur la température obtenues par la méthode des éléments finis (FEM) permettent d'obtenir des prédictions de dureté précises. Des expériences ont également été menées sur des engrenages à denture droite en acier C45 avec différents paramètres géométriques, ce qui a permis d'étudier de nombreux cas, y compris la prédiction de la dureté basée sur le profil. Le modèle démontre son efficacité, sa précision et sa concordance avec les mesures expérimentales.

L'étude examine ensuite la cohérence et la véracité des résultats à l'aide d'outils d'intelligence artificielle explicable (XAI), en se concentrant spécifiquement sur la modélisation de la dureté basée sur le profil. Divers outils, tels que l'importance des caractéristiques de XGBoost et la bibliothèque

SHAP avec les valeurs de shap, sont utilisés pour comprendre l'implication des caractéristiques dans les prédictions et analyser les erreurs de prédiction. En outre, un modèle de substitution est développé pour illustrer la prise de décision sous forme de règles. Tous les outils et modèles confirment la cohérence physique du modèle.

En conclusion, la thèse propose une méthode de modélisation inverse basée sur le cas de la dureté basée sur le profil, qui inclut la discrétisation des données et la création de caractéristiques basées sur la physique. Des résultats prometteurs conduisent à une vérification du problème en amont.

Les résultats de ce travail présentent plusieurs opportunités pour des études ultérieures, y compris l'impact de la température en profondeur sur les prédictions de dureté, la modélisation d'autres paramètres d'intérêt (par exemple, les contraintes résiduelles et la distorsion), la généralisation de la méthode à différentes géométries en utilisant des techniques telles que les réseaux neuronaux géométriques (GNN), l'exploration de différents traitements de trempe et matériaux, l'augmentation de la représentation et de l'augmentation des données, l'incorporation de modèles basés sur la physique pour des prédictions précises, et le développement d'un outil convivial pour les ingénieurs et les techniciens afin de visualiser et de justifier les résultats de la modélisation en utilisant le XAI.

List of Acronyms

ANN	artificial neural network
DOE	design of experiment
DT	decision tree
FEM	finite element modeling
GBM	gradient boosted machines
GBT	gradient boosted trees
GRU	gated recurrent unit
HTC	heat transfer coefficient
IH	induction hardening
LIME	local interpretable model-agnostic explanation
LORE	local rule-based explanations
LSTM	long short-term memory
MAAPE	mean arctangent absolute percentage error
PGD	proper generalized decomposition
POD	proper orthogonal decomposition
QoI	quantities of interest
ReLu	rectified linear unit
RF	random forest
RMSE	root mean squared error
RMSPE	root mean squared percentage error
RNN	recurrent neural network
SHAP	shapley additive explanations
SVM	support vector machine
SVR	support vector regressor
XAI	explicable artificial intelligence
XGBoost	extrem gradient boosting

Contents

List of Tables

List of Figures

General Introduction and Organization

This chapter presents a complete industrial context on induction hardening process and the historical solutions for modeling. The limiting issues of this latter are highlighted to show the relevancy of introducing machine learning. A quick presentation of all the articles providing the scientific content completes the introduction.

0.6 Industrial and scientific context

Nowadays, the global trend is towards streamlining, enhancing, and conserving effort, time, and resources in all industrial processes, especially those widely utilized such as induction hardening. Researchers and industrialists aim to enhance the mechanical properties of important components such as gears, bars, and discs. These components are a fundamental part of engineering machines, particularly in industries such as automobiles, airplanes, and industrial production of workpieces. The failure modes of steel workpieces such as steel gears inside machines can impact their performance. Indeed, gears are considered as critical components as they are used to transmit motion while increasing speed or force. The most common failure modes of gears are [4, 5, 6] :

(a) The surface fatigue (pitting) which is the repeated surface or sub-surface stresses beyond the endurance limit of the material

(b) The wear which describes loss of material from the contacting surface

(c) The plastic flow is the gear tooth surface deformation when subjected to high contact stress under rolling or sliding action

(d) The breakage which is basically the final failure mode

They occur due to various reasons such as strength, force, or lubrication issues [7] as depicted in Figure 1.

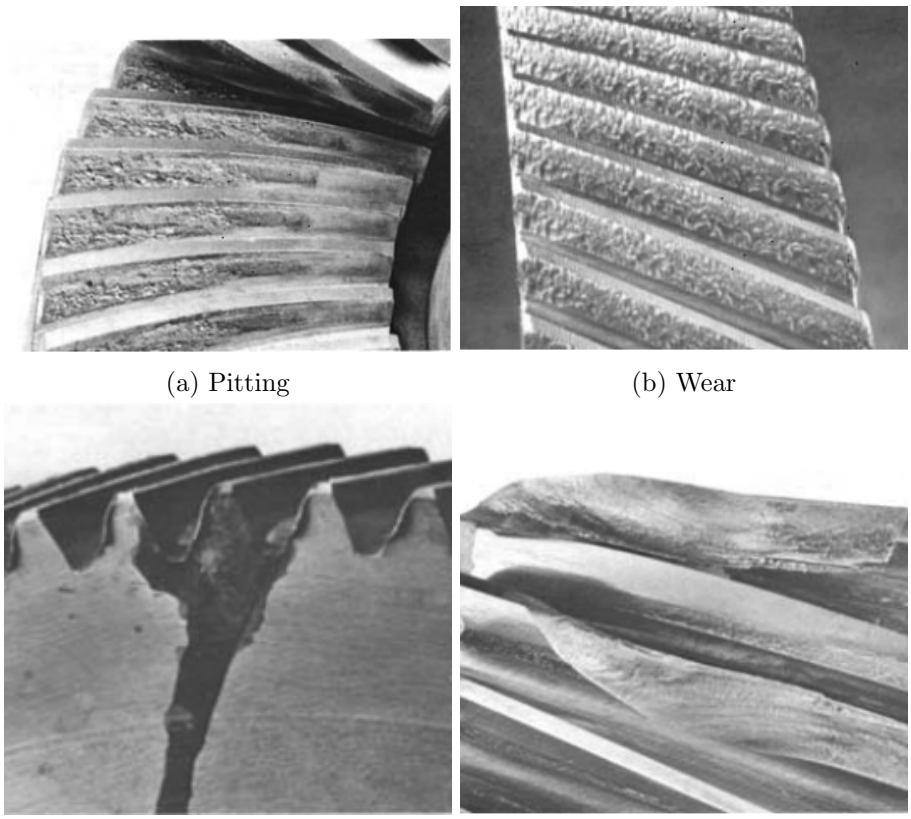

(a) Pitting (b) Wear

(c) Plastic flow (d) Breakage

Figure 1: Different failures modes of a gear [1]

Various techniques such as induction hardening [8] have been utilized to increase behavior against failure modes and therefore delay them. Induction hardening is a combination of two-phases process that enhances the fatigue life of engineering components [9, 10]. The gear is nearly instantaneously heated to a high temperature [11] (heating phase), then quickly cooled (quenching phase) with water, oil or polymerous mixture, leading to the creation of a fine-grain martensite phase [12, 13] and a compressive residual stress field [2]. These mechanical changes are induced under the action of non uniform plastic deformation, itself caused by thermal gradient and localized volume variation resulted from phase transformation [14] within the superficial layer without affecting the metallurgy of the bulk material. Therefore, the first enhances hardness, wear resistance, and contact fatigue strength. In addition, the presence of the latter allows the gear to be resistant to crack propagation and impact [15].

Industries are increasingly using this process for fast and precise heating of specific zones with

high-quality result and control of the treated areas without affecting the bulk material metallurgy [16]. Also, this process is highly repeatable, easily set in production operations and responsible for environmental issues compared to thermochemical process. The system is illustrated in Figure 2.

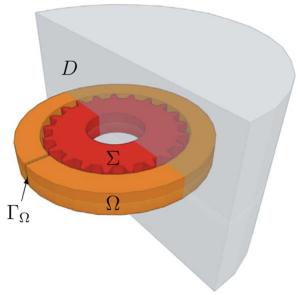

Figure 2: Induction hardening system [2]

where Σ is a steel gear, Ω an inductor-quencher i.e. during the process it can change its function to first heat and then quench, the electrical port given as interface by Γ_Ω. The whole space including the system as well as the ambient air is described by D such that $D = \{Air \cup \Omega \cup \Sigma\}$

0.6.1 Induction heating

Induction heating is the process in which the steel gear is heated by inducing an electrical current within it, through the application of an alternating electromagnetic field. It is based on the principle of electromagnetic induction, which states that when the gear is placed within an alternating magnetic field generated by the inductor, the magnetic field induces eddy currents within the material as described by Lenz's law. These eddy currents generate heat due to the resistance of the material to the flow of electrical current, according to Joule's law. All these phenomena are illustrated in Figure 3.

The generated heat is concentrated within the material, resulting in a rapid and localized increase in temperature. The amount of heat depends on the frequency and intensity of the electromagnetic field, as well as the electrical conductivity and magnetic permeability of the material being heated. However, the distribution of the heat within the gear is not heterogeneous. Based on the complex geometry and the material of the gear, several phenomena causes this as follows:

– Skin effect: it is a phenomenon where the alternating current (AC) used in induction heating

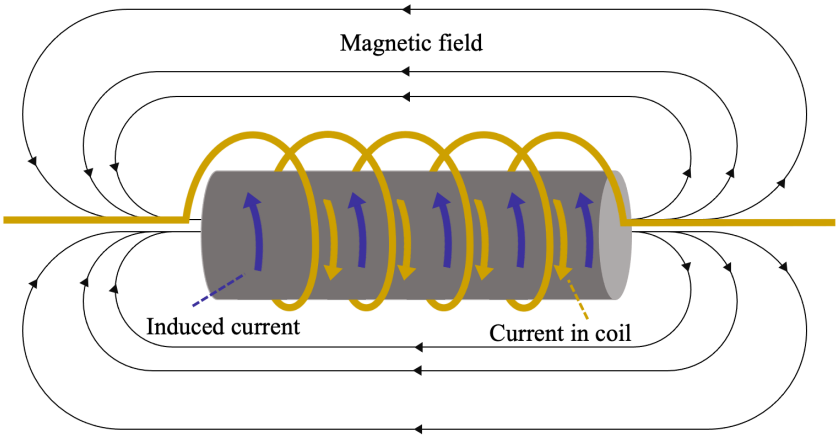

Figure 3: Illustration of the phenomena involved during induction heating

concentrates near the surface of the material being heated. This means that the surface of the gear heats up more quickly than the interior.

- Edge effect: it refers to the the phenomenon in which the edges of the material being heated experience a higher temperature than the center. This is because the edges are exposed to a higher magnetic flux density, which results in more intense heating. It is particularly present in complex geometry such as gears.

- End effect: contrary the latter effects, the end effect refers to the ends of the material being less heated.

- Hysteresis loss: it is a phenomenon occurring specifically with magnetic and ferromagnetic materials. It is the wasted energy in the form of heat caused by the work done by the magnetising force against the internal friction of the molecules of the magnetic material.

Overall, the combination of those phenomena contribute to the heating of the gear during the induction heating phase. By carefully controlling these effects, it is possible to achieve a desired heating distribution within the gear.

The key factors in the heating process are the frequency, power level of the source currents used, and heating duration. There are two common heating methods based on how the frequency is applied: single-frequency induction and a combination of medium and high frequencies applied together or in sequence. Both methods have been studied through experiments and numerical models resulting in

different levels of precision and treatment quality [17]. Although, double-frequency induction heating is able to provide a complete and uniform hardening of the surface layer in complex shapes, which may not be achieved with single-frequency heating [18], both techniques are still utilized a lot. In fact, for the case of a spur-gear, during double-frequency induction, the tooth root is heated by the medium frequency, while the tooth tip is treated by the high frequency as illustrated in Figure 4.

Figure 4: Hardening zone of the gear after induction with high frequency (left), medium frequency (middle) and double frequency (right) [3]

0.6.2 Superficial quenching

As mentioned previously, the quenching step, illustrated schematically illustrated in Figure 5, is dedicated to stabilize the austenite phase by transforming it into the desired martensite, which gives the gear its hardened layer on surface. The liquid of the quenching is generally water but can be optimize with polymerous mixture.

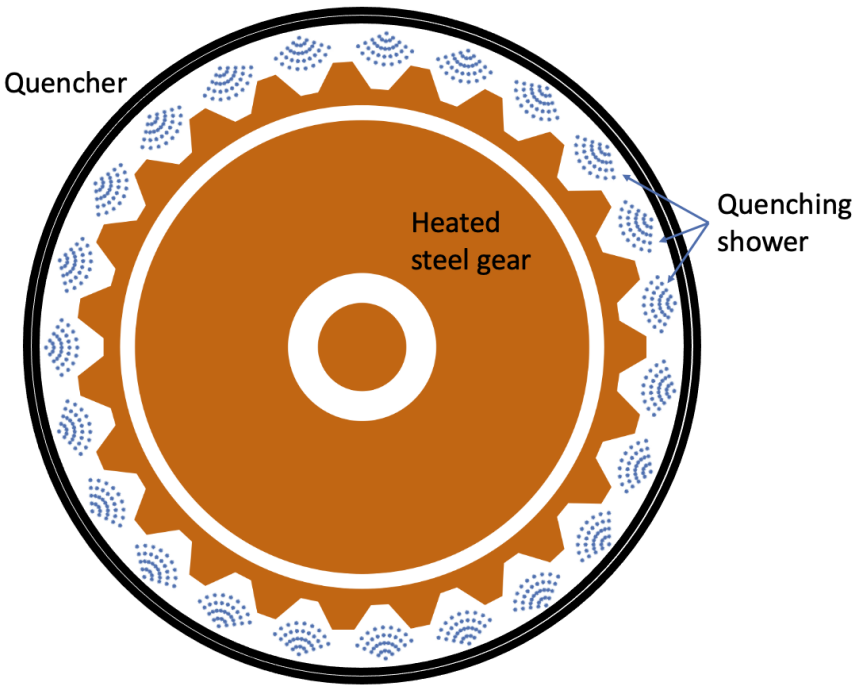

Figure 5: Illustration of the quenching step

Just like induction heating step, several phenomena are involved during quenching such as:

- Thermal expansion which causes high thermal stress within the gear as the metal contracts when rapidly cooled.
- Heat transfer: used as a quenching control parameter, the heat transfer is the thermal flux from the gear to the inductor.

Finally, the physical phenomena involved in induction heating and superficial quenching for induction hardening are complex and depend on various factors such as the material, the geometry of the material, the heating process parameters and the quenching medium. Understanding these phenomena is essential to optimize the quenching process and achieve the desired mechanical properties in the final product.

0.7 Problematic

Modeling physical systems is important for industries for several reasons :

- It provides insight and understanding into the behavior and performance of the system. This can help design and engineering decisions, aid in problem solving, optimize operations, and improve efficiency and productivity.
- It helps to identify potential risks, predict system behavior under different conditions, and facilitate virtual testing before industrialization.
- It is useful for industries to make data-driven decisions that lead to cost savings, improved performance, and increased safety by modeling physical systems.

The modeling allows a control of parameters such as temperature, heating time, cooling rate, and material composition and their effect on the system which is essential for obtaining the desired properties of the hardened material. Modeling also allows to predict parameters of interest as output of the system after treatment. Predicting these parameters within a physical system such as induction hardening is critical because it allows for precise control and optimization of the hardening process. Indeed, the prediction of the hardness, residual stresses, and distortion helps to ensure consistent quality, avoid defects, and achieve the final desired properties within the workpiece.. In the published literature, many research works based on several methods were carried out on the hardening process to analyze and model it.

The first one, is the finite element method (FEM). It is a numerical method for solving partial differential equations that describe the physical behavior of the system. It is widely used for modeling physical system like induction hardening because it can solve physical equations behind the system and thus display temporally and spatially the physical fields in complex geometries with precision. It allows to a better understanding of physical phenomena.

Moreover, FEM can handle non-linear material behavior. Hence, FEM is particularly useful for optimizing the hardening process and avoiding defects. However, FEM requires a lot of computational resources and is time-consuming, especially for complex systems [19, 20, 21, 22]. It can also be sensitive to mesh size and the definition of material properties used in the model. Several works have been conducted with the help of FEM in the context of induction hardening, not only for different workpieces such as aeronautical gears [23], 42CrMo4 cylinders [24], or AISI 1045 steel [25], but also for different steps or parametric analysis such as the heating step [26] or the rolling contact fatigue [27].

The second one is the analytical models. They use mathematical equations to describe the phys-

ical behavior of the system. These models are typically based on simplifying assumptions, such as cylindrical symmetry, uniform material properties, and uniform heating. Analytical models are computationally efficient and provide quick solutions for simple geometries. They are also easy to understand and can provide insight into the physical behavior of the system. However, they are limited to simple geometries and may not be accurate for more complex systems [28, 29, 30], like spur-gears usually used in industry. They also cannot account for variations in material properties and heating conditions, which can lead to significant errors. Just like FEM, analytical models are widely used in the literature for induction hardening problems for modeling the system [31, 32] or more specifically for sensitive study [33], fatigue analysis [34] or different workpieces such as aluminum billet [35]

Hence, the problem lies in the computational power which can be very expensive for small use for industries and the geometries of the parts processed in the industry are mainly complex, especially with spur or helical teeth. A proper combination between efficiency and accuracy could be carried out using machine learning, this solution is often proposed in literature over the other solutions [36, 37, 38]. In the case of hardening, regression models develop a function of the input parameters (e.g., frequency, current) to predict the output parameters (e.g. temperature, hardness). Unlike FEM, they are often quick to train and to set while providing satisfying predictions. Moreover they can account for variations in material properties and heating conditions, contrary to analytical models. However they are limited by the quality and quantity of the data used to develop the model. It is an important point to handle complex and non-linear problems with complex geometries with a small quantity of data. Also, the predictions may not be physically interpretable and the model can overfit, resulting in poor generalization to out-of-sample data.

Machine learning could be a suitable technique for modeling physical systems such as induction hardening. But modeling alone is often not enough as machine learning can lack of transparency or exhibit bias. In fact, the use of complex machine learning algorithms has evolved significantly over the years [39]. Algorithms such as decision trees, linear regression, and logistic regression were used to solve relatively simple problems before. However, as the availability of data and computing power increased, more complex algorithms such as neural networks, deep learning, gradient boosting, and ensemble models are widely utilized now. One reason for this evolution is that complex algorithms can often achieve higher accuracy and better performance than simpler ones, especially for tasks on non-linear and complex problems such as the ones involved in physical system. However, using complex

algorithms over simple ones, what is gained in precision and overall performance is lost in terms of interpretability or explicability of results [40]. Hence, it is then determining, especially in the industrial context, to explain and justify the results of the modeling thanks to eXplainable Artificial Intelligence (XAI) as it ensures trust, accountability, and quality of the proposed predictions.

Also, some works focus now on a new way to model physical systems: a combination of two approaches. One makes the model of the system and the other helps it by correcting it or by bringing knowledge such as equation solutions or new variables. This type of modeling, known as hybrid modeling, allows a good approximation while being fast and physically consistent [41, 42].

Consequently, the goal of this thesis is to find a method based on machine learning to predict induction hardening output parameters. In addition, it should combine satisfying accuracy and low computing time, even for complex systems or geometries with small number of available data but also provides a relevant justification of the model to ensure physical consistency.

0.8 Research objectives

This thesis belongs to a research project launched in 2019 by the Institute of Technological Research (IRT) Materials Metallurgy Processes (M2P) which is entitled: TRANSmission FUture GEneration (TRANSFUGE). The general objective of this research work, which brings together industrial partners and relies on the expertise of the PIMM laboratory at Arts et Métiers ParisTech, is to optimize the induction hardening process by developing a methodology based on artificial intelligence and specifically machine learning techniques to predict the critical identified process parameters while carrying out low computational cost, error result and inference time. In particular, the specific objectives of the proposed research are to:

1. Extract and treat the data coming from simulation or experiments while identifying the required output parameters. Raw data is often incomplete or noisy. The treatment also depends on the further machine learning work.

2. Analyze the data, find correlations, and remove irrelevant variables that add noise or bias. Some variables are often informative and related only for the simulation (e.g. the id of the simulation) or the experiment (e.g. the name of the engineer who carried out the experiments or the label

of the run). Moreover, variables must be analyzed through the scope of the known physical principles: variables irrelevant physically for the hardening process must be removed.

3. Model the output parameters such as the hardness or the residual stresses. Each type of data and each process requires a specific method to be adapted in function of the issues. In fact, the number or the nature of the variables are often not the same. Several modeling are, hence, needed. Hardness is modeled with both synthetic and experimental data based on different geometries in the context of induction hardening.

4. Justify and explain the results obtained from the machine learning are now critical for industries. As a new subfield of machine learning, no academic study have been carried out in the context of induction hardening to explain hardness modeling.

5. Model the process parameters from the induced hardness profile of induction hardening experiments. Inverse modeling is a challenging field but it allows a great optimization of the process. Hence, no study has been conducted on this topic yet.

0.9 Organization of the thesis

The thesis is segmented into five parts, each comprising a research article that was produced as a part of this project to fulfill the goals outlined in Chapter 2. The subsequent sections provide a description of each article, along with its relevancy to the presented objectives.

0.9.1 Article 1: Data-driven modelling for multi-physics parametrized problems - Application to induction hardening process

This article introduces different approaches for modeling the induction hardening process with synthetic data for C45 steel spur-gear. The heating and quenching steps are modeled with the help of FEM and the software FORGE, generating accurate and consistent synthetic data. Then, the temperature and austenite ratio are predicted during the heating process with the use of Proper Orthogonal Decomposition (POD). Finally, the hardness is predicted at the end of quenching step using two approaches. The first one is a fully data-driven one, using temperature history, cooling in time and space. The second one uses the previously predicted austenite ratio to make an hybrid model

which is the combination of data-driven modeling and physics-based knowledge and find even more accurate predictions.

The main contributions of this paper are:

- The collection and analysis of synthetic data about induction hardening process.
- The modeling of several relevant parameters along the process (temperature, austenite ratio, and hardness)
- The management of difficulties linked to synthetic data such as physical inconsistency or weak data representation due to the Design of Experiment (DoE)
- The combination of physical modeling and machine learning to form an hybrid model capable of very accurate predictions and low computational cost.

This article opens to future works for studying the process experimentally or for other parameters with synthetic data such as the residual stresses. This article was published in the "Metals", volume 11, issue 5, pages 738 in April, 2021. This journal focuses on research related to the science and engineering of metals, including their properties, processing, and applications. This article was written by the author of this thesis for the machine learning and hybrid part for hardness prediction. The synthetic data generation and the temperature and austenite modeling was made by Khouloud Derouiche.

0.9.2 Article 2: Data-driven modeling for residual stress prediction after induction heating process of C45 steel

This article presents a data-driven model based on the XGBoost library for residual stress predictions. The system and the synthetic data are from an induction hardening process for C45 steel spur-gear generated by the FEM. In fact, they are the same data from the Article 1. Only the quenching step is considered. The main contributions of this paper is the prediction of the in-depth residual stresses which is a determining parameter for the validation of a treated gear. This article was made for ICRS11 conference. This international conference is specifically focused on novel works and study for residual stresses. This article was written by the author of this thesis.

0.9.3 Article 3: Artificial intelligence modeling of induction contour hardening of 300M steel bar and C45 steel spur gear

This article introduces new experimental data from two different workpieces and different induction hardening approaches. First, 300M steel cylinders are treated with single-frequency induction. Second, simultaneous double-frequency induction hardening experiments are carried out on C45 steel spur-gear. The article proposes a model based on XGBoost for both types of induction process to predict hardness with appealing results.

The main contributions of this paper are:

- The collection and analysis of experimental data for two induction hardening processes.
- The modeling of hardness for simple geometries (cylinders) with the help of in-depth temperature collected with FEM.
- The raising of difficulties from experimental data such as the uncertainty and their noisy nature and the solution with the smoothing of Kernel Regression.
- The modeling of hardness for complex geometries (spur-gear) with different cases based on the input parameters.

This article opens to explaining the presented results under the scope of XAI and inverse problems for further optimization of the induction hardening process. This article is accepted for publication in the "International Journal of Material Forming". The journal focuses on research related to the science and technology of material forming processes, including metal forming, polymer processing, and other related fields. This article was written by the author of this thesis.

0.9.4 Article 4: Explaining Hardness Modeling after Induction Hardening with XAI Tools

This paper proposes a novel and relevant approach with a study on the explicability of the machine learning results for induction hardening modeling. XAI is new in the field of AI and is determining for justifying the results at an industrial level. Different methods are highlighted such as the feature importance from in-built machine learning libraries, external libraries specialized in explaining global and local results, and surrogate modeling. The explained results are from a specific case explored in the previous article.

The main contributions of this paper are:

- The introduction and presentation of utilized XAI methods and tools.
- The analysis of feature importance under the scope of in-built methods.
- The exploration of global explicability by SHAP. Also, the comparison between well and bad predicted instances to discuss the possible causes of model misprediction.
- The general prediction behavior highlighted by a decision tree surrogate model.
- The insurance that the model is physically consistent.

This article shows why it is important to use XAI as it is possible to understand what is the model decision-making and to insure that the model is consistent with physical principles. It opens that XAI could be the next good-practice in engineering when manipulating data. This article is submitted for publication in the "International Journal of Material Forming". This article was written by the author of this thesis.

0.9.5 Article 5: Data-driven Inverse Problem for optimizing the Induction Hardening process of C45 Spur-Gear

The last paper explores the approach of inverse and ill-posed problems. They are challenging but allow to predict causal parameters and hence, to fine-tune and optimize a physical system for a desired output. The article, after experiencing ill-posed problem issues, proposes a simple method to estimate the energy required to insure hardness profiles.

The main contributions of this paper are:

- The simplification of the problem by descritizing the hardness profile into 5 variables
- The physic-based feature creation turning time and power generator into energy to limit the prediction to a single output feature
- The division of the problem into localized problem (teeth and root) for high and medium frequencies energies

This article presents how unstable the problem is and how to simplify. Yet, the lack of data imply an instability of the results depending on the randomly selected train and test set. It opens that the problem could be treated with more certainty about the robustness of the model. However, the results are promising for further analysis and works. This article is submitted for publication in "Metals". This article was written by the author of this thesis.

Chapter 1

Literature review

This chapter is about the state-of-the-art of the induction hardening process, the relevancy of machine learning techniques for this work, and explicability of artificial intelligence theory.

1.1 State-of-the-art of induction hardening

The main purpose of induction hardening is to harden the surface of ferromagnetic materials, such as steel. An inductor is used to generate an electromagnetic field to induce Foucault's currents in the material, which generates heat. The surface layer of the steel is heated to a temperature that is high enough to cause a transformation in the microstructure. The microstructure of the steel workpiece consists of a mixture of ferrite and pearlite at room temperature. When the temperature of the surface layer is raised during induction hardening, the ferrite transforms into austenite. When austenization reached the required rate, the gear is quickly quenched by a powerful water, oil or polymerous mixture shower. Thus, quenched that way, the austenite to transform into martensite. Martensite is a hard, brittle form of iron that has a higher carbon content than austenite. It results in a surface layer that is harder and more wear-resistant than the original material. The increased hardness of the surface layer is due to the formation of fine, hard carbides within the martensite microstructure. The hardness is the main studied parameter to certify the quality of a treated workpiece. A typical hardness profile is depicted in Figure 1.1.

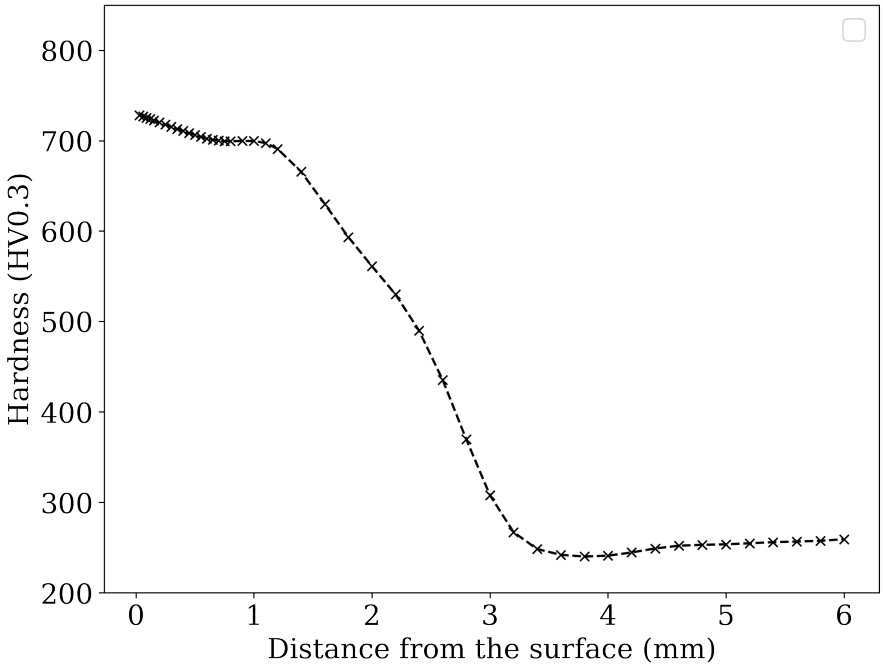

Figure 1.1: Typical hardness profile

Induction hardening also induce other phenomena such as residual stress and distortion. Residual

stresses are internal stresses that remain in a material after it has been subjected to an external load or thermal treatment. During the induction hardening process, the rapid heating and cooling of the surface layer of the steel workpiece cause stresses to develop in the material. These residual stresses can have a significant impact on the dimensional stability and fatigue life of the steel component. On one hand, a compressive residual stress field enhances fatigue life of treated workpieces [43]. In fact, the presence of compressive residual stresses leads to crack closure, which effectively delays the initiation time of fatigue cracks and reduces the force for crack propagation [44]. On the other hand, a tensile residual stress field can

A typical residual stress profile after induction hardening is illustrated in Figure 1.2.

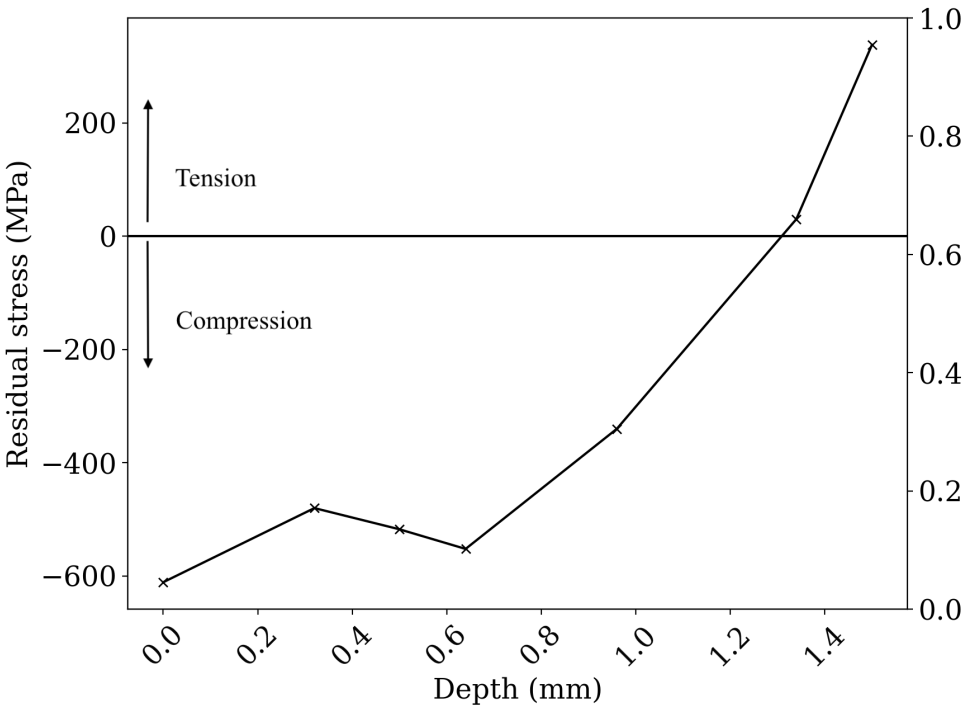

Figure 1.2: Example of residual stress profile normal to the surface

Distortion is the permanent change in shape that occurs as a result of the residual stresses formed during the induction hardening process. As the surface layer of the steel workpiece is heated, it expands. When the workpiece is rapidly cooled during the quenching process, the surface layer contracts, but the core material remains at a higher temperature and does not contract. This mismatch in the

thermal expansion coefficients of the surface layer and the core material causes the workpiece to deform. The extent of the distortion is influenced by factors such as the size and shape of the workpiece, the heating and cooling rates, and the residual stress distribution in the material. Over the years, different approaches of induction hardening are developed in order to optimize the process to be more effective.

Single frequency induction hardening [45, 46, 47, 48] involves using a single frequency of the alternating magnetic field to heat the surface of the component. The frequency is chosen based on the size and geometry of the component to ensure that the heat is distributed evenly across the surface. The frequency and current penetration depth is inversely proportional, it means that the treated hardness depth is higher with lower frequencies.

In contrast, double frequency induction hardening uses two different frequencies of the alternating magnetic field to heat the surface of the component. The frequencies used are chosen to heat the surface of complex geometries, allowing for a more controlled and precise contour hardening than single-frequency process [49]. In fact, for a gear, the tooth root and tip depends on the medium and high frequency, respectively [50]. There are two approaches for this case: sequential or simultaneous double frequency induction hardening. [51, 52]. On one hand, sequential double-frequency induction hardening involves using two frequencies in succession during the process. The medium frequency is first used to heat the gear root, followed by the higher frequency to heat the gear tip. This approach can include a time delay between the two frequencies to control the temperature distribution in the component more precisely. On the other hand, simultaneous double-frequency induction hardening applies both medium and high frequencies at the same time to create a more uniform temperature distribution, especially on curved surfaces such as gear tooth profiles. This method allows for adjusting the energy percentage of the two frequencies, providing greater flexibility in controlling temperature distribution for complicated part shapes. Both approaches are used in the literature [53, 54, 55].

1.2 Experimental studies on induction hardening

1.2.1 Hardness

The effects of different process parameters on post-treatment hardness profile and microstructure have been the subject of numerous experimental studies [56, 57, 58, 59]. Four major techniques are

used to experimentally measure hardness profiles [60]. Vickers hardness testing (HV) is based on measuring the diagonal length of the indentation caused by a diamond indenter under a fixed load and multiple studies work with it [61]. Another pyramid-shaped diamond indenter testers are the Knoop and Rockwell hardness testing. They measure the length of the indentation caused under a very light load and a fixed load, respectively [62, 63]. The Brinell hardness testing [64] measures the hardness by verifying the diameter of the indentation caused by a steel ball of a fixed size and load [65, 66]. The principle behind these tests is that the hardness of a material is directly proportional to the resistance to permanently indenting the surface.

1.2.2 Residual stress

The effect of hardening process and the involved parameters on the residuals stresses within the processed workpiece is studied in several works in literature [67, 68]. In the context of induction hardening, residual stresses are typically measured using different techniques such as X-ray diffraction (XRD) or the hole drilling method, as these methods can accurately measure residual stresses. XRD [69, 70, 71] method uses X-rays to measure the crystal lattice spacing of the material, which can be affected by residual stress, allowing for the determination of the residual stress levels [72, 73, 74, 75, 76, 77]. The hole drilling method is also used in some works [78] in the context of induction hardening. In this method, a small hole is drilled into the workpiece. This removal of stressed material results in localized stress and strain relaxations around the hole location. This strain relaxations could be measured using a strain gauge rosette and can be related to the residual stress levels in the workpiece [79, 80].

1.3 Machine learning algorithms

Artificial Intelligence (AI) is a field of computer science that focuses on the creation of intelligent machines that can perform tasks that usually require human intelligence. It involves the development of algorithms and systems that enable computers to understand, learn, and make decisions. Machine Learning (ML) is a subfield of AI about with the development of algorithms and statistical models [81, 82] that allow computers to learn and improve from observations and experience without being explicitly programmed. It involves the use of various algorithms and techniques to analyze and interpret data, identify patterns or relationships, and make data-driven predictions or decisions.

Machine learning algorithms can be divided into three types: supervised learning, unsupervised learning, and reinforcement learning. In supervised learning [83], the algorithm learns to predict an output variable (also known as the dependent variable) from input variables (also known as the independent variables), based on a labeled dataset. The labeled dataset contains examples of inputs and corresponding outputs, and the algorithm learns to generalize this mapping to new, unseen examples. Supervised learning algorithms can be used to solve a wide range of problems, such as classification (qualitative target variable) and regression (quantitative variable to predict). Then, in unsupervised learning [84], the algorithm learns to find patterns and structure in an unlabeled dataset, without any explicit guidance. Unsupervised learning algorithms can be used to solve problems such as clustering (unlabeled classification) and dimensionality reduction (finding a lower-dimensional representation of a high-dimensional dataset). Finally for reinforcement learning [85], the algorithm learns to make decisions based on feedback from its environment. The algorithm interacts with the environment by taking actions and receiving rewards or penalties based on those actions. Reinforcement learning algorithms are widely used in robotics.

There are many different machine learning algorithms within each of these categories. In this thesis, only supervised learning problems are considered using tabular data or time series. Hence, several algorithms can be listed considering their presence in the literature including XGBoost [86, 43, 87], Random Forest (RF) [88, 89, 90, 91], Artificial Neural Networks (ANN) [92, 93, 94], Recurrent Neural Networks (RNN) [95, 96], Support Vector Machine (SVM) [97, 98] and Multi-linear regression.

1.4 Explicability

Explainable Artificial Intelligence (XAI) is a subfield of AI about developing models and systems that can be understood, trusted, and interpreted by humans. XAI aims to ensure that the decisions made by AI systems are transparent and explainable, so that their actions can be understood and their results can be trusted. XAI is built on several aspects such as transparency, interpretability, fairness, and responsibility [99]. XAI is relevant and important for industries [100] as it can help to build trust in AI systems, particularly in sensitive applications where decisions made by AI systems can have significant consequences. Furthermore, XAI can help to identify and mitigate biases in AI systems, which can lead to more accurate and fair outcomes.

It is therefore necessary to find techniques to prevent the black box effect from persisting on the given model. This is precisely the type of model considered in this thesis. It is possible to either explain the black-box model or take a classifier that is "transparent" [101]. The interest for the thesis is more in the first category because it is more about having a model like a neural network and being able to explain it and not taking another model that is clearer or more explicit. That being said, the problem of explaining a black box can actually be divided into three distinct problems:

1.4.1 Explaining the model

The method consists in giving a global explanation of the black box model b through an interpretable and transparent model c. The idea is that c can mimic the behavior and results of model b by an approximation while being understandable by a human user. This predictor c is assumed to be derived from the black-box model. The problem defined [101] is such that: Let b and X be the black-box model and the input data, respectively. The problem is to find an explanation $E \in \mathcal{E}$ belonging to a domain E interpretable by human experts through an interpretable predictor $c_g = f(b, X)$ derived from model b and X using $f(\cdot, \cdot)$. The explanation $E \in \mathcal{E}$ is obtained by c_g if $E = \epsilon_g(c_g, X)$ with $\epsilon_g(\cdot, \cdot)$ a logical explanation function that reasons between c_g and X. The whole difficulty of this method lies in how to find the function $f(\cdot, \cdot)$ that finds the explanation. An interpretable model such as a decision tree or a feature contribution summary which is trained on the predicted values of b can be a suitable solution. Hence, explaining the model can be done by using a surrogate models [102].

1.4.2 Explaining the output

The problem of explaining the output is, in sum, the same as explaining the model but at the local level. Thus, an explanation $e \in \mathcal{E}$ can be obtained via a local and interpretable predictor $c_l; c_l = f(b, x)$ if $e = \epsilon_l(c_l, x)$ with $\epsilon_l(\cdot, \cdot)$ the logical explanation reasoning via c_l and x.

1.4.3 Model inspection

The definition of model inspection is such that: let a black-box model b with X the input data. We look for a representation r such that $r = f(b, X)$ with a function $f(\cdot, \cdot)$. This function f could for example be a sensitive analysis. Sensitive methods are due to localization, gradients and perturbations i.e. sensitivity to input noise [101]. The model inspection can also be a graphical representation of

the most important variables with respect to the predictions that could be interpreted by different experts in the field. This can be referred to as interpretability methods by mathematical structure [103]. Thus, it is seen here that the apprehension and explicability of the model does not necessarily involve the entire explanation of the model or what is going on inside the black box but rather seeing and understanding the results obtained.

1.4.4 Solutions to the problems

The literature review has shown many solutions such as SHAP [104], LIME [105], LORE [106], to name a few, to better explain black boxes algorithms including Neural Networks, Random Forests, SVM, and XGBoost. It is also useful to specify that all these methods can be used with spreadsheets data, images and text.

1.5 Inverse and ill-posed problems

In the literature, the inverse and ill-posed problems are opposed to the direct (or forward) problem. The latter is defined in physics by the model an occurred phenomena, considering the causes as input. Hence, the forward problem is described by :

$$f(x) = y \tag{1.1}$$

where x is the known causes and f the model function that lead to the phenomena y.

For inverse problems the goal is to determine the causes of the given effect, or to reconstruct an unknown quantity from observations or measurements. They are critical and challenging problems. According to Eq. 1.1, the inverse problem can be described as the search of function g such as $g = f^{-1}$ and :

$$\begin{aligned} g \cdot f(x) &= g(y) \\ x &= g(y) \end{aligned} \tag{1.2}$$

where y is the known observations or measurements, x are the unknown causes, and g the model function to find.

Inverse problem often requires making assumptions and using mathematical models to estimate the unknown parameters that are responsible for the observed data. Moreover, they also often involve non-unique solutions and high computational power demands. In fact, an ill-posed problem either has no solutions in the desired class, or has many (two or more) solutions, or the solution is unstable (i.e., sensitive to small perturbations). These problems are usually more difficult to solve than well-posed problems and require additional assumptions or regularization to obtain a unique and stable solution. In fact, they can be solved using a variety of mathematical techniques such as optimization [107, 108], regularization [109, 110, 111], Bayesian inference [112, 113, 114], and machine learning algorithms [115, 116].

Several works in the field of metallurgy and more precisely for induction hardening process have been conducted with the inverse problem approach. To name a few, they are related to the estimation of the power levels using the temperature as input in steel cylinders [117] and the heat transfer coefficient using the surface temperature in a steel billet [118] or more generally in heat conduction system [119] and thermodynamics [120].

Chapter 2

Methods

The chapter presents the techniques used for providing the synthetic and experimental data of induction hardening process, the machine learning algorithms used for modeling, and the XAI library to explain the obtained results.

2.1 Simulation of C45 steel spur-gears induction hardening

The finite element method (FEM) represents an efficient way to solve the models describing the physical phenomena that appeared in the induction hardening process, where the system is discretized in space and time and partial differential equations are solved. When experimental data are not available for study, the FEM is a suitable technique to generate accurate data. In order to generate such synthetic data of induction hardening process, several finite element (FE) simulations are carried out using the commercial FE software FORGE®. A C45 steel spur-gear having a module of 2.5 and 22 teeth is studied. For computational purpose, only one half of the gear is considered as two symmetry planes are imposed. The material properties of C45 steel is taken from the literature.

During the heating step, electromagnetic and thermal fields in addition to the metallurgical phase transformation associated with the temperature evolution are combined. In this step, FORGE® uses two coupled solvers. The electromagnetic solver where the workpiece, the inductor, and the surrounding air are introduced and a tetrahedral global mesh is created such that a fine mesh of 0.2 mm is defined around the gear tooth - inductor interface and a coarse one far from the common interface. Indeed, the electromagnetic solver solves Maxwell's equations and consequently gives rise to a heating power. The calculated heating power is then applied to the thermal solver to obtain the temperature field by solving the heat equation. The workpiece with a tetrahedral mesh of 0.2 mm on the studied zones is defined for this solver.

In the quenching step, a thermo-metallo-mechanical solver is used, where a strong coupling between these latter physical fields is insured. The last state of the heating step is considered by FORGE® to compute the hardness in addition to the stresses and strains. For these simulations, the heating part and the quenching step share the same mesh. Figure 2.1 shows the IH simulation and the coupling between the different physical fields.

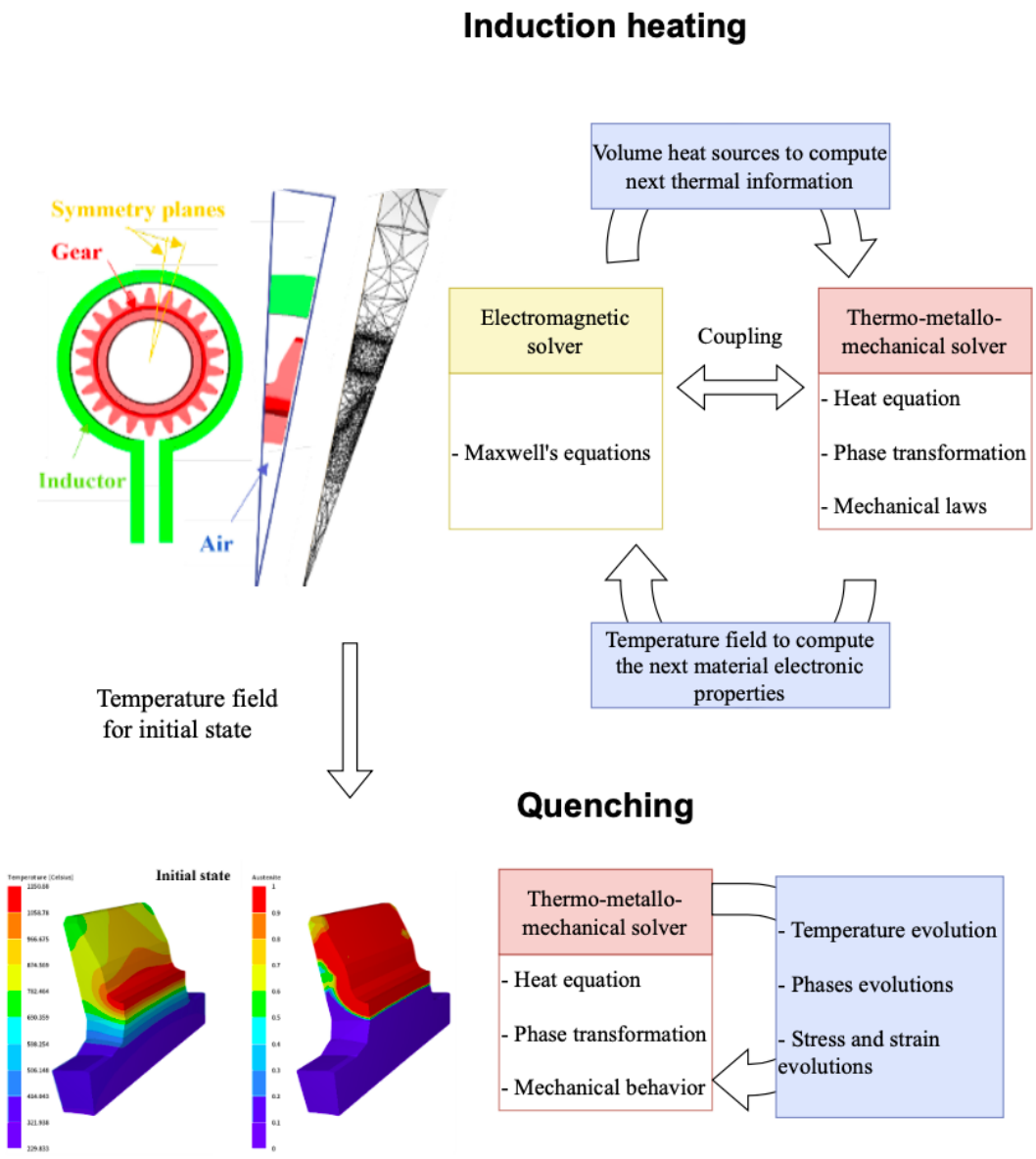

Figure 2.1: Finite element simulation of IH process

A total of 8 heating simulations are carried out with different values of process parameters (frequency, power, and process time). Then, quenching simulations are generated with different heat transfer coefficient (HTC) and times. The design of experiments of heating and quenching steps are illustrated in Table 2.1 and 2.2, respectively.

Table 2.1: Induction heating design of experiment for FE simulation

Run #	Frequency (kH)	Power (kW)	Time (s)
1	19	480	0.37
2	96	68	0.64
3	52	300	0.52
4	36	320	0.8
5	148	200	0.12
6	15	370	0.26
7	118	170	0.5

Table 2.2: Quenching design of experiment for FE simulation

HTC ($W \cdot m^{-2} \cdot K^{-1}$)	Time (s)
2500	12
3000	12
4000	12

2.2 Induction hardening experiments

2.2.1 300M steel cylinders

Experiments are conducted on cylindrical bars made of 300M low alloy steel, with the initial parameters listed in Table 2.3. Samples were rotated around their axis and multiple induction treatments were performed at different positions. The infrared camera verified the absence of interaction effects between inducted sample on the same axis. A ring inductor with a rectangular shape of 2x5mm and an air-gap of 3mm was used to apply the heating phase, while a coaxial ring was used for the subsequent cooling shower of a polymer-water mixture, as shown in Figure 2.2. Temperature measurements on the surface were obtained using a bichromatic pyrometer (see Table 2.3), while FEM (see Figure 2.3) was used to predict the in-depth temperature profile during heating. Micro-hardness Vickers (HV0.3) profiles were conducted in the radial direction of the sample to determine the penetration hardening. These analyses were performed after the induction treatment and performed on a transversal section according to ISO 6507 [121].

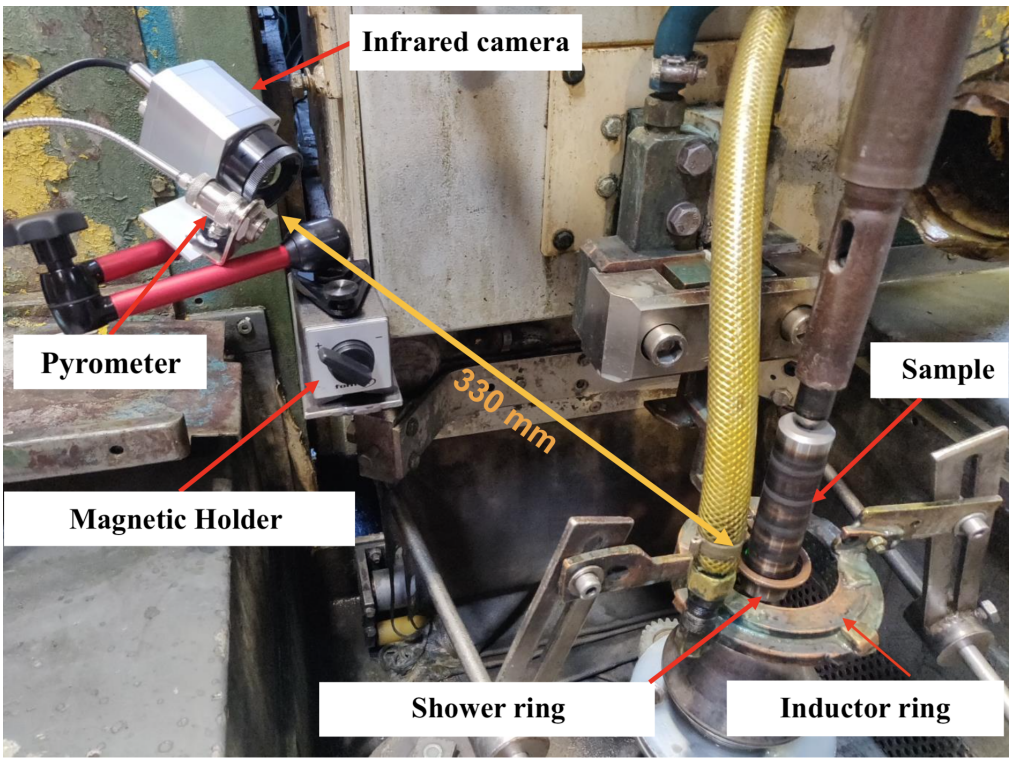

Figure 2.2: Experimental setup utilized during the induction hardening treatment of cylindrical bars under a high single-frequency

Table 2.3: Induction heat treatment conditions for cylindrical samples

Run #	Frequency F (kHz)	Power P (kW)	Time t (s)	Temperature T (°C)
1	224	33	0,15	892
2	224	33	0,2	958
3	224	33	0,3	1008
4	224	33	0,85	1121
5	224	33	1,3	1265
6	224	19	1	927
7	224	19	3.0	1034
8	224	19	3,5	1134
9	224	19	4,5	1277
10	224	49	0,15	1025
11	224	49	0,2	1142
12	224	49	0,08	1085

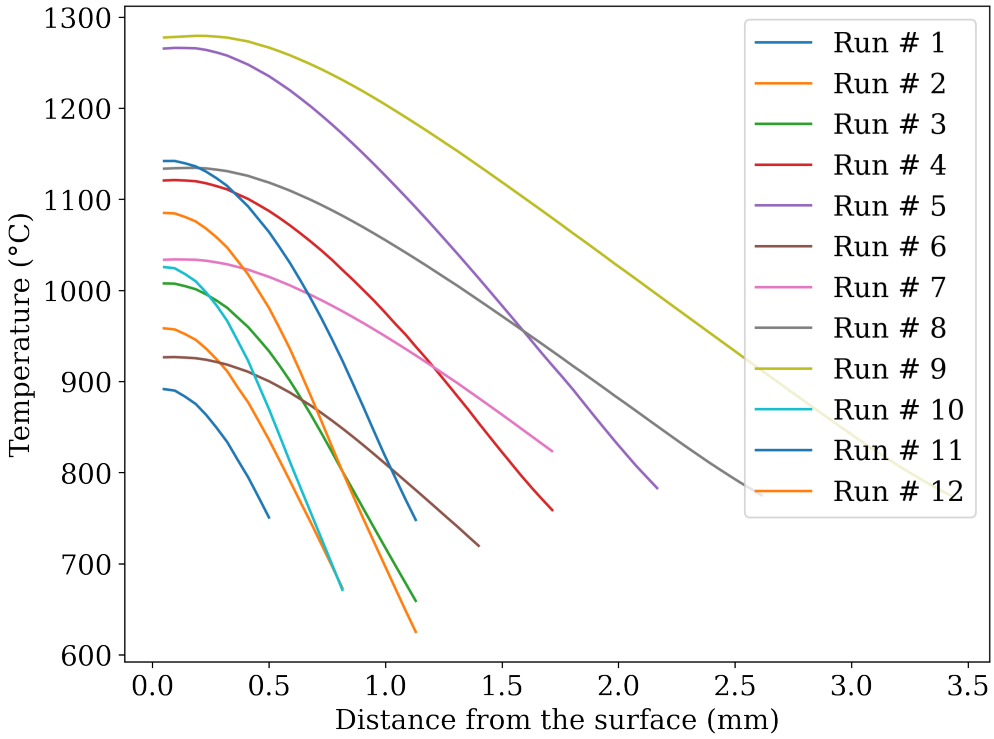

Figure 2.3: Predicted in-depth temperature profiles by FEM for experimental runs

2.2.2 C45 spur-gears

Experiments are conducted on C45 steel spur gears in a second series. The gear geometric data are summarized in Table 2.4, and the process parameters are listed in Table 2.5 and Table 2.6. During the experiments, the gears are mounted on a rotating chuck. A rectangular ring inductor of 12.25x20mm with an air-gap of 2mm is used to conduct the heating phase, while a polymer-water mixture is applied using another coaxial ring for subsequent cooling. An Optris pyrometer is used to measure the temperature on the surface of the tooth root during the treatment. Micro-hardness Vickers (HV0.3) profiles are carried out at the tooth tip and the tooth root in the radial direction of the sample to determine the penetration hardening at these two locations. Figure 2.4 shows the setup for the experiments. These analyses were performed after the induction treatment and performed on a transversal section according to ISO 6507 [121].

Table 2.4: Gear data for double-frequency induction hardening experiments

Gear #	Module	No. of teeth	Width	Addendum circle	Pitch circle	Root circle
1	2.5	22	10 mm	60 mm	55 mm	48.75 mm
2	3	18	10 mm	60 mm	54 mm	46.5 mm

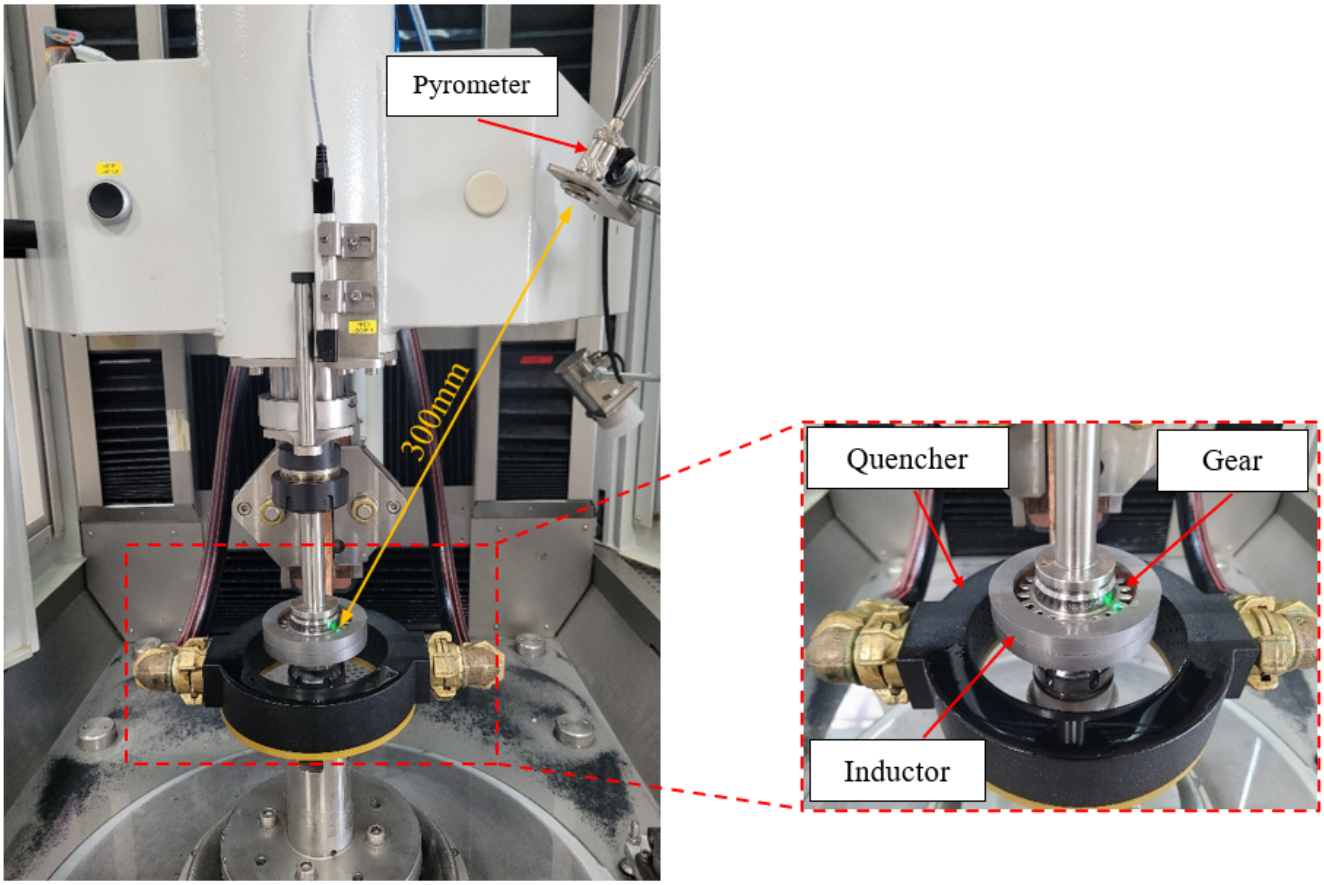

Figure 2.4: Experimental setup utilized during the induction hardening treatment of gears under a double-frequency

Table 2.5: Induction heat treatment conditions for gears with module m=2.5

Run #	Medium Frequency MF (kHz)	High Frequency HF (kHz)	Power of HF P_{HF} (kW)	Power of MF P_{MF} (kW)	Time t (s)	Temperature T (°C)
1	13	256	143	88	0,17	780
2	12	258	225	138	0,17	1080
3	12	258	225	138	0,2	1200
4	12	257	143	113	0,17	835
5	12	258	184	113	0,17	935
6	12	258	225	113	0,17	1005
7	13	257	143	113	0,2	×
8	13	257	184	88	0,2	917
9	13	257	184	138	0,24	1189
10	13	257	143	138	0,2	1059
11	12	257	184	113	0,2	1025
12	13	257	184	88	0,24	1028
13	12	258	225	88	0,2	999
14	13	257	143	88	0,24	925
15	12	258	225	113	0,24	1167
16	12	258	225	88	0,17	900
17	12	257	184	138	0,17	1005
18	13	257	143	113	0,24	1039
19	13	257	143	138	0,24	1145
20	12	258	225	138	0,24	1217
21	12	258	225	88	0,18	884
22	12	258	198	134	0,17	920
23	×	×	238,5	94	0,17	890
24	×	×	247,5	98	0,19	958
25	12	257	202	110	0,17	884
26	×	×	175,5	102	0,19	889
27	12	257	202,5	118	0,17	887
28	×	×	193,5	102	0,19	876
29	×	×	238,5	88	0,19	906
30	×	×	247,5	88	0,19	905
31	×	×	247,5	94	0,17	858

×: missing values

Table 2.6: Induction heat treatment conditions for gears with module m=3

Run #	Medium Frequency MF (kHz)	High Frequency HF (kHz)	Power of HF P_{HF} (kW)	Power of MF P_{MF} (kW)	Time t (s)	Temperature T (°C)
1	12	254	143	88	0,17	800
2	12	256	225	138	0,17	1100
3	12	255	225	138	0,2	×
4	12	254	143	113	0,17	×
5	12	255	184	113	0,17	969
6	12	256	225	113	0,17	992
7	13	254	143	113	0,2	982
8	12	255	184	88	0,2	909
9	13	255	184	138	0,24	1166
10	12	254	143	138	0,2	1075
11	12	255	184	113	0,2	1040
12	12	255	184	88	0,24	1025
13	12	255	225	88	0,2	1025
14	12	254	143	88	0,24	959
15	12	255	225	113	0,24	1197
16	12	256	225	88	0,17	970
17	12	255	184	138	0,17	1045
18	12	254	143	113	0,24	1030
19	12	254	143	138	0,24	1135
20	12	256	225	138	0,24	1293

The frequency ranges from 12 to 14 kHz in MF and from 150 to 350 kHZ in HF. The final measured frequency depends on the torque between the gear and the inductor. So, the measured frequency will not be the same, especially in high frequency. It is clear that the frequencies are not the main variable to describe the system due to their slight variation.

2.2.3 Hardness measurements

The complementary analyses on treated workpieces were carried out by means of hardness filiations. The preparation of the samples is carried out as follows:

- Sampling with a STRUERS metallographic cutter equipped with Al2O3 abrasive discs, 3820rpm, 50m/s
- Hot mounting with a STRUERS press and Durofast epoxy resin (black)
- Mechanical polishing with a STRUERS automatic polishing machine according to the range

described in Table 2.7:

Table 2.7: Polishing steps

Step	Cloths	Category	Lubricant	Time	Velocity	Applied force
1	SiC sheet	120,220,320, 500,800,1200	Water	2-4 min	220	15N
2	STRUERS Cloths	diamond suspension 3µm	ClearBlue STRUERS lubricant	2-4 min	220	15N
3	STRUERS Cloths	diamond suspension 1µm	ClearBlue STRUERS lubricant	2-4 min	220	15N

Measurements on a microdurometer calibrated to 714HV0.3 (±27.9 HV0.3) according to NF-EN-ISO-6507-1:2018 [121]. Vickers hardness measurements are performed on cross sections of the teeth. The equipment used is a Qness 60A+ micro-durometer. The measurement carried out is of type HV0.3, i.e. with a Vickers indenter by applying a load of 2.941N (0.3kgf) during 15s.

To respect the spacing between each measurement specified by the standard, it is necessary to carry out the measurements in a staggered way. The position of the measurement with respect to the surface are listed in Table 2.8

Table 2.8: Hardness filiations Aero 3.6mm

Distance from surface (mm)	Shift in x (mm)
0,03	0
0,06	0,15
0,09	0
0,12	0,15
0,15	0
0,2	0,15
0,25	0
0,3	0,15
0,35	0
0,4	0,15
0,45	0
0,5	0,15
0,55	0
0,6	0,15
0,65	0
0,7	0,15
0,75	0
0,8	0,15
0,9	0
1	0,15
1,1	0
1,2	0,15
1,4	0
1,6	0,15
1,8	0
2	0,15
2,2	0
2,4	0,15
2,6	0
2,8	0,15
3	0
3,2	0,15
3,4	0
3,6	0,15

2.3 Machine learning utilized algorithms

2.3.1 Random Forest

Random forests [122] is a type of machine learning algorithm that is used for both classification and regression tasks. It is called a "forest" because it is made up of multiple decision trees that work together to make a prediction.

2.3.1.1 Decision Tree

Contrary to decision tree [123] for classification using Entropy or Gini impurity as metric of gain of information, the decision tree regressor uses the mean squared error (MSE) to calculate the deviation between prediction and ground-truth, the MSE is calculated for all possible split and for each input variables. The goal is to reduce the MSE at each child from the root. The split is made according to the child with the lowest error. Once all decision trees are built, the final prediction of a random forest is the average of prediction of each tree.

$$MSE = \frac{1}{n}\sum_{i=1}^{n}(y_i - \hat{y}_i)^2 \tag{2.1}$$

where n is the total number of instance, y_i the true point, $\hat{y}_i$ is the predicted point.

Here is an example to better understand the construction of a decision tree with the help of MSE metric. Considering a matrix X with a temperature with respect to the in-depth hardness of a treated workpiece. Figure 2.5 illustrates the result:

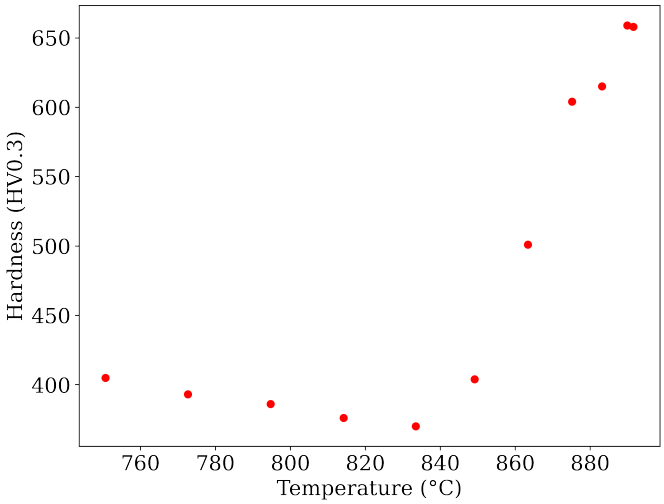

Figure 2.5: Example of data for Decision Tree

The data must be split accordingly of a threshold value, here the temperature is the variable that serves as the split. To obtain the best split leading to the lowest MSE, each possibility must be tested. Practically, in the tree, the data that satisfies the threshold criteria continue their path to the left leaf, and the others to the right leaf. The first one is showed in Figures 2.6, 2.7:

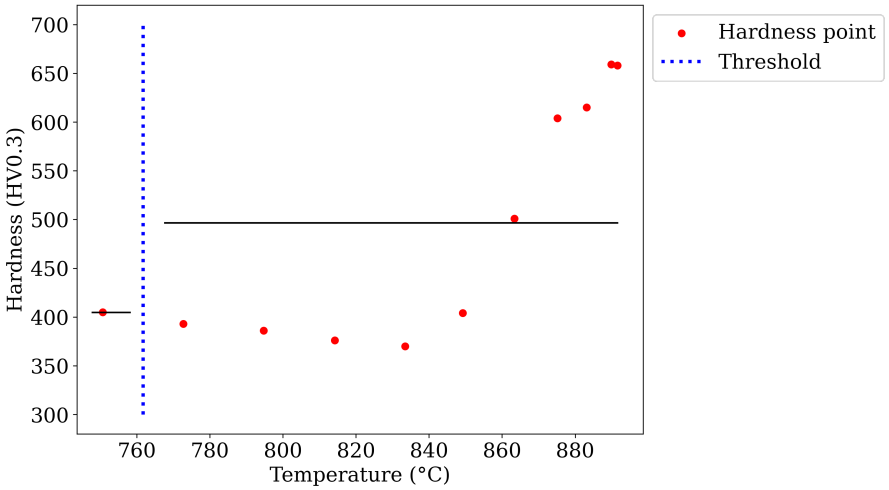

Figure 2.6: Tested split (blue) for decision tree construction with the predictions (black)

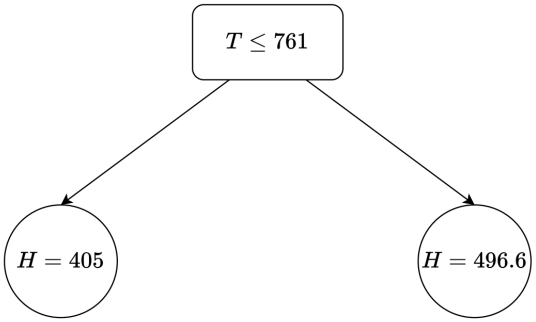

Figure 2.7: Decision tree for tested split

The split value is $T = 750$, the respective black lines are the prediction for each side of the threshold values. Hence it is possible to calculate the MSE between the observed values and the prediction. In this case, $MSE = 14010.84$ which shows that the selected threshold is ineffective for an optimized decision tree.

Every split are tested, and the best one is the one illustrated in Figures 2.8, 2.9:

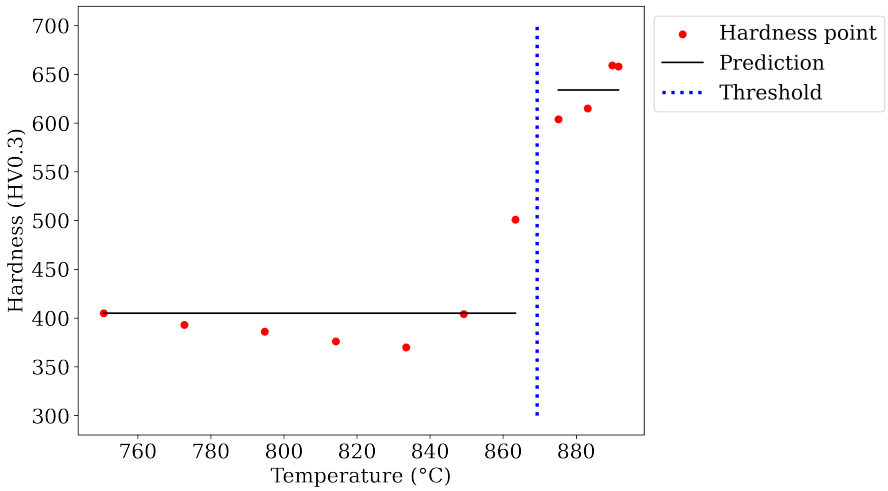

Figure 2.8: Final selected split (blue) for decision tree construction with the predictions (black)

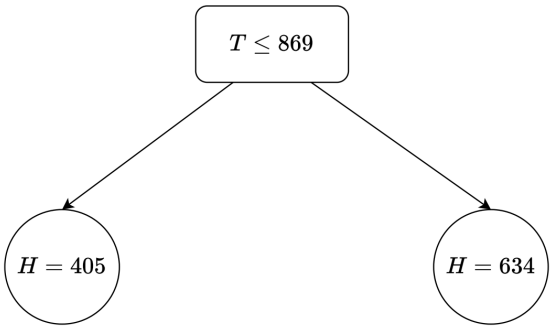

Figure 2.9: Decision tree with selected split

The value of this split is $T = 869$. The error for this tree is $MSE = 1295.4$ which is more relevant than the one previously observed. The decision tree is built deeper, considering the remaining data of each side of the split. The complexity of a decision tree is equal to the number of leaves (final node).

2.3.1.2 Forest of decision trees

Each tree in the forest is trained on a random subset of the data and uses a random subset of the features and are built as presented before. The prediction is the mean of all tree results as illustrated in Figure 2.10

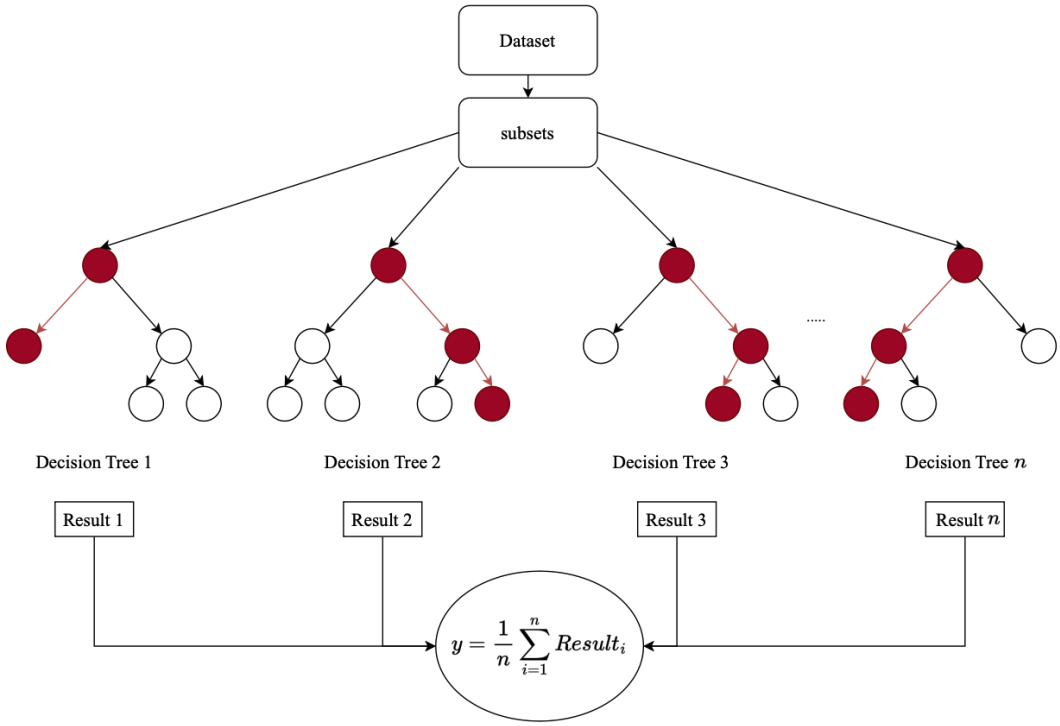

Figure 2.10: Random forest schema with the highlighted path (red) for one instance in the n trees

Random forests strength lies in the ability to capture complex relationships between features and targets by combining many simple decision trees. They also have built-in feature importance measures, which can be used for feature selection or global explicability. Moreover, random forests are not prone to overfitting, which is a common problem in decision trees. However, random forests can be computationally expensive, especially when the number of trees is large or the dataset is very large. They are also not interpretable like a single decision tree, which can make it difficult to understand why a particular prediction was made. Random forests are widely used because they often produce highly accurate results and are relatively easy to use.

2.3.2 XGboost

XGBoost [124, 125] is based on gradient-boosted decision-tree algorithm. In fact, XGBoost build sequentially a forest of gradient boosted decision trees.

To clearly define the XGboost algorithm and its construction, a short example is proposed at the same time as the definitions and equations are given. Hence, Table 2.9 presents a simple matrix defined

to be used along with XGBoost algorithm.

Table 2.9: Example for XGBoost presentation

Index k	Depth d (mm)	Hardness H (HV0.3)
1	0.1	700
2	2	300
3	3	700
4	5.5	600

The first step is to get the initial prediction. If it is the first tree just like here, the value can be set as the mean of the hardness values. The first prediction y_{init} is then:

$$y_{init} = \frac{700 + 600 + 300 + 700}{4} = 575 \tag{2.2}$$

2.3.2.1 Residuals

Each iteration of a tree compute the residuals r_k of each k observed value $y_{obs,k}$ of the dataset with respect to a predicted value $y_{pred,k}$:

$$r_k = y_{obs,k} - y_{pred,k} \tag{2.3}$$

In the example, the first residual should be $r_1 = 700 - 575 = 125$ and all the residuals as illustrated in Figure 2.11 for this first phase are:

$$r = \{125, 25, -275, 125\} \tag{2.4}$$

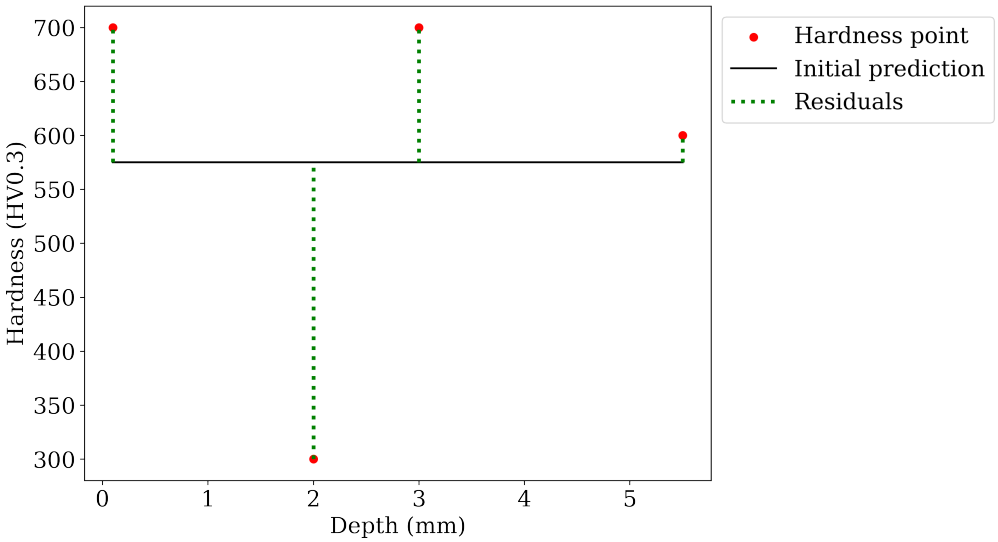

Figure 2.11: Residuals for the first tree

2.3.2.2 Splitting

The residuals are collected in the first leaf of the tree called the root node. The goal is to split considering a threshold condition on a given variable. Each possible split is defined by the average value between two consecutive observed data points. The residuals are used to compute the similarity score S, which is defined as

$$S = \frac{(\sum_{k=1}^{m} r_k)^2}{m + \lambda} \tag{2.5}$$

where m is the number of residuals and λ is the user-defined regulation hyperparameter. Depending on the value of S, the different residuals are set into the right and left leaves given the chosen split, making new similarity scores. In fact, S score of the root node and the left and right leaves are used to calculate the gain G such as:

$$G = S_{left} - S_{right} - S_{root} \tag{2.6}$$

The split inducing the highest gain G is kept. Then, splits can be made again on the latest nodes. A branch with a negative gain should be removed as the tree is pruned.

Chapter 3

Scientific contribution

This chapter groups different academic papers associated to the accomplished researches and represents the global contribution of the thesis.

3.1 Article 1 : Data-driven modelling for multi-physics parametrized problems - Application to induction hardening process

Khouloud Derouiche, Sevan Garois, Victor Champaney, Monzer Daoud, Khalil Traidi and Francisco Chinesta. Published in Metals in 2021.

Data-driven modelling provides an efficient approach to compute approximate solutions for complex multi-physics parametrized problems such as induction hardening (IH) process. Basically, some physical quantities of interest (QoI) related to IH process will be evaluated under real-time constraint, without any explicit knowledge of the physical behavior of the system. Hence, computationally expensive finite element models will be replaced by a parametric solution, called meta-model. Two Data-driven models for temporal evolution of temperature and austenite phase transformation, during induction heating, were first developed by using the proper orthogonal decomposition based reduced-order model followed by a non-linear regression method for temperature field, and a classification combined with regression for austenite evolution. Then, data-driven and hybrid models were created to predict hardness, after quenching. It is shown that the results of artificial intelligence models are promising and provide good approximations in the low-data limit case.

Keywords: Data-driven modelling; Induction hardening; Meta-model; Proper orthogonal decomposition; Artificial intelligence; Hybrid model.

3.1.1 Introduction

The aeronautical and automotive industries would eventually like to lighten the mechanical structures in order to meet the relative environmental concerns to carbon dioxide emissions and fuel economy while maintaining optimal mechanical properties and performances. The heat treatment provides a valuable solution to give the material its optimal microstructures and mechanical properties, corresponding to the various predefined performance criteria [126]. However, for many applications, only superficial layer material properties play an important role. In this context, surface treatments of industrial components by mechanical, thermal or thermochemical means are particularly suitable [127, 128]. These techniques are mainly used to improve the fatigue strength and the resistance to the imposed external mechanical loads by changing the properties of the critical zones.

Induction hardening (IH) is one of the most appealing surface heat treatment processes widely employed in automotive and aerospace industries [129, 16]. Two main steps are at the origin of IH: an electromagnetic induction heating and subsequent quenching. It has the advantage of providing a very short surface heat-up time, a good fatigue performance, a precise control of the treated zone, a good reproducibility, and an operating mode compatible with severe environmental requirements, unlike thermochemical treatments such as carburizing and carbonitriding [130]. In the published literature,

many research works based on analytical and numerical methods were carried out on the IH process [131, 132, 133, 134]. From the industrial point of view, the challenges behind the development of such methodologies are:

- Reducing development time;
- Reducing costs by "doing it right the first time" (Reduction of the NRC "Non Recurring Costs" such as the costs of tools and prototypes and the RC "Recurring Cost" such as production costs)
- Understanding the involved physical mechanisms for better controlling of the influencing parameters and thus be able to better define the characteristics to be controlled;
- Anticipating the management of non-quality risks (eg: being able to reinforce the critical zones predicted by the calculations, anticipate possible defects, etc.)

The main difficulty behind the process control and the optimization in terms of time and cost is the multidisciplinarity of the process since it combines multi-physics (electromagnetism, metallurgical, thermal, and mechanical fields) in addition to the large number of process parameters; owing to the advanced numerical simulation tools such as FORGE®, which is used in this study, modelling the IH process and solving the physical equations behind it is possible by using some conventional discretization methods such as the well-known and largely experienced finite element (FE) method [135]. However, passing through those methods to solve multi-physics parametrized problems is often regarded as a key issue. In practice, the need to evaluate multiple configurations (choices of parameters) before converging to an adequate result that optimizes the process performance, may make the optimization procedure very time consuming and computationally expensive since each configuration takes several hours between preparing the data setting and executing the simulation.

In order to alleviate such issues, a data-driven parametric meta-modelling approach for IH process simulation constitutes an appealing alternative to standard discretization techniques given the interesting compromise in terms of execution speed, computational cost, and results accuracy. This approach enables computing the parametric-based solution from sampled data collected from FE simulation codes. The main challenge behind this work is to succeed on building a robust meta-model for some physical quantities of interest (thermal and metallurgical history as well as the hardness), by using a reduced amount of data.

3.1. ARTICLE 1 : DATA-DRIVEN MODELLING FOR MULTI-PHYSICS PARAMETRIZED PROBLEMS - APPLICATION TO INDUCTION HARDENING PROCESS

This paper is decomposed into two main parts; in the first part, two models were created to predict the temporal evolution of temperature and austenite phase transformation in a spur gear of C45 steel, during induction heating and under the effect of process parameters, in almost real-time. Hence, the goal is to replace the initial physical models implemented in the FE simulation code FORGE® by a meta-model with a sufficient accuracy and a short computational time. To achieve this goal, two different approaches were considered for each quantity of interest (QoI), however, a common point between them is the fact that both techniques rely only on data (synthetic data provided by the high-fidelity multi-physics simulation) and do not require any knowledge of the full-order formulation or intervention in the numerical FE codes. It is worth pointing out that synthetic data was collected at some sparse points in the space domain and for different values of input parameters associated with the Latin Hypercube Sampling. For the temperature evolution, the POD-based reduced order model [136] was used and then followed by a non-linear regression model. For the austenitic phase evolution, a classification combined with a regression model was applied.

The second part of this work focuses on the quenching process. Choosing a full data-driven approach, the goal is to predict the hardness at the final state of the process. Therefore, a classic machine learning pipeline to select variables and create new ones based on the evolution of the temperature of the system was applied. By using XGboost [125], a tree-boosted model was made and was able to predict - in a local way - the hardness. A second approach is the hybrid model where the obtained austenite phase ratio was considered to increase the knowledge for a better prediction of hardness since they seem to be well correlated. This new precision allowed to predict the hardness in the whole gear, in a global way, and to suggest that the hybrid approach may be the solution in any field with a lack of data and having complex systems.

The rest of the paper is organized as follows: Section 2 presents the data-driven modelling for induction heating. In this section, the process and the data generation will be first presented. Then, the applied methods, the model results and discussions for temperature and austenite phase evolution will be illustrated. Section 3 highlights the modelling for hardness prediction with both hybrid and fully data-driven approach and Section 4 addresses the main conclusions.

3.1.2 Data-driven modelling for induction heating process

3.1.2.1 Process and data

Induction heating is becoming one of the preferred heating technologies at the industrial scale [137] due to its numerous advantages. Basically, it consists in applying an alternating current (AC) to a copper coil surrounding a conducting workpiece, the magnetic field generated by the AC induces an eddy current and consequently heating by Joule effect of the workpiece. Induction heating combines electromagnetic and thermal fields in addition to the phase transformation associated with an increase in temperature. These physical phenomena can be simulated by several FE codes, in which physical models described by partial differential equations (PDE) are solved. In this paper, the workpiece is C45 steel spur gear of module 4 and 22 teeth, as shown in Figure 3.1.

Figure 3.1: Spur gear of C45 steel

In order to optimize and improve induction heating performances applied to the workpiece, multiple parameters can be taken into consideration such as material behavior, process parameters, and geometrical features. As a first step of this study, two important process parameters were considered while the other ones were kept constant. The selected parameters and their lower and upper limits are shown in Table 3.1.

Table 3.1: Input parameters and their lower and upper limits

Input parameters	**Lower limit**	**Upper limit**
Frequency (kHz)	10	250
Power (kW)	50	600

Changing these input parameters could highly impact the process results. In order to evaluate this effect, two important physical quantities such as temporal evolution of temperature and austenitic

phase transformation are taken into consideration.

Particularly, a model for each one of these quantities will be constructed. To achieve this objective, a set of precomputed high-fidelity solutions (called snapshots) are collected by solving the original full-order model for different values of input parameters using the commercial finite element software FORGE®. It is worth mentioning that the model has two symmetry planes and hence only half of the gear tooth was modeled to improve the computational efficiency. The implemented material properties of C45 were taken from literature and JmatPro database [138, 139, 140, 141, 142]. To simulate heating, FORGE® uses two coupled solvers. The electromagnetic solver solves Maxwell's equations and consequently gives rise to a heating power. This latter is applied to the thermal solver to obtain the temperature field by solving the heat equation. More details can be found in [143]. Several FE simulations were carried out according to the Latin Hypercube Sampling (LHS) design of experiments [144]. Despite generating a quasi-random sampling distribution, LHS guarantees a good coverage of each dimension space. According to the LHS, a total of 20 simulations have been generated as shown in figure 3.2. Therefore, it is worth seeing how well the applied non-linear regression technique performs with a reduced number of data.

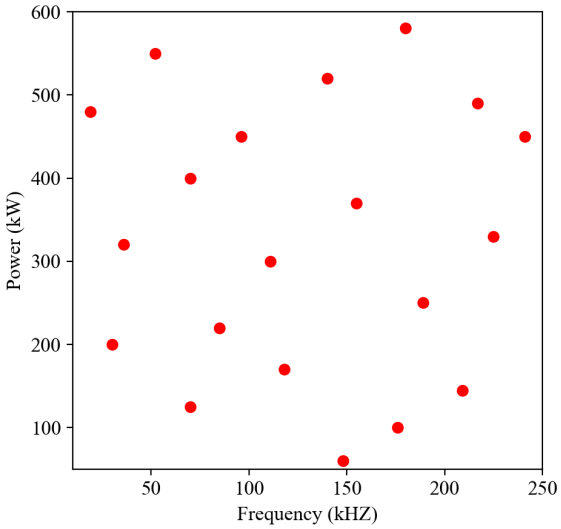

Figure 3.2: Latin Hypercube Sampling design of experiments

As mentioned above, all process parameters except frequency and power were kept constant during heating. Therefore, process time which is one of the most important parameters was first chosen to be

equal to 1 second for all snapshots, where 1 second is considered enough for such rapid heating process. However, higher values of power and frequency give rise to higher temperature (more than 1000 °C) which can be reached very fast. Hence, such process time induces the divergence of the numerical computation even before reaching the final time step. To alleviate such issue, different process times were considered in order to reach an acceptable level of temperature.

For this part of the work, the temperature and austenite evolutions were extracted at 14 specific points representing the main heat-affected zones as shown in Figure 3.3. A model for each spatial point was constructed.

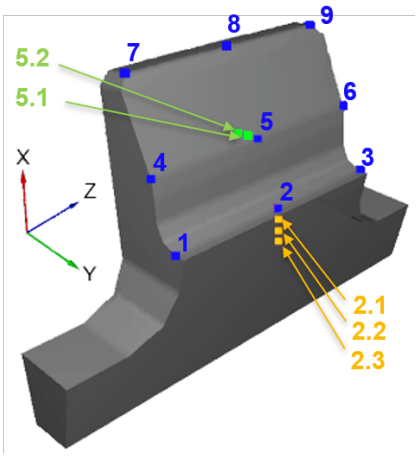

Figure 3.3: Measurement points (sensors)

3.1.2.2 Modelling the time evolution of temperature

3.1.2.2.1 Methodology Based on the set of computed snapshots, collected at some sparse points in the space domain and for different values of frequency and power, a dimensionality reduction approach based on proper orthogonal decomposition (POD) [136] followed by a machine learning algorithm for regression was applied in order to create an approximate solution for the temperature field evolution. However, different data-lengths were obtained by using different process times. First, a normalization and a uniform discretization with respect to the final process time for each snapshot were applied in order to transfer all quantities (time, temperature, austenite, etc.) into the same discretization, however, this method introduced pollution in the regression. To overcome this issue, all the data was truncated when reaching a constant temperature and noting that the temperature evolution is monotonic, the role of time and temperature was inversed. Therefore, the time was modelled as a

function of the temperature, where the maximum value of the latter was kept the same for all the experiments. Basically, a constant final temperature was chosen exclusively for each measurement point depending on its position. Despite having a constant final temperature, all the data doesn't have the same length, therefore a uniform discretization was applied to data. Once the new datasets for time as a function of the temperature are established, the POD-based reduced order model is applied, followed by a non-linear regression technique.

As a first step, a POD reduced basis was built, onto which the initial FE solution was projected and consequently a much lower dimension of the initial problem was obtained. To achieve this dimensionality reduction, consider the set of the N_s snapshots ($N_s = 20$) collected at S measurement points (S = 14), $\boldsymbol{t}^{j_i} = \boldsymbol{t}^j(F_i, P_i)_{i=1,...,N_s;j=1,...,S} \in \mathbb{R}^N$, and computed by solving the full-order FE model for different values of the input parameters, where F, P, and N are the frequency, the power, and the number of time-temperature points, respectively. The snapshot matrix $\boldsymbol{M} \in \mathbb{R}^{N\times N_s}$ for each measurement point is defined such that $\boldsymbol{M}^j = [\boldsymbol{t}_1^j \boldsymbol{t}_2^j \dots \boldsymbol{t}_{N_s}^j]$. To obtain the reduced basis, the singular value decomposition (SVD) is applied to $\boldsymbol{M}^j$ as follows:

$$\boldsymbol{M}^j = \boldsymbol{U}^j \boldsymbol{\Sigma}^j \boldsymbol{V}^{jT} \quad \text{for } j = 1, \dots, S \tag{3.1}$$

where $\boldsymbol{U}^j \in \mathbb{R}^{N\times N}$ and $\boldsymbol{V}^j \in \mathbb{R}^{N_s\times N_s}$ are orthogonal matrices containing the left and right singular vectors of $\boldsymbol{M}^j$, respectively. $\boldsymbol{\Sigma}^j \in \mathbb{R}^{N\times N_s}$ is a rectangular diagonal matrix containing the singular values of $\boldsymbol{M}^j$ sorted in a decreasing order. The reduced POD basis, $\boldsymbol{B}^j = [\boldsymbol{\phi}_1^j, \boldsymbol{\phi}_2^j, ..., \boldsymbol{\phi}_R^j]$, is defined as the first R left singular vectors of $\boldsymbol{M}^j$ (i.e. first R columns of $\boldsymbol{U}^j$) corresponding to the R largest singular values. Thus, singular values provide a quantitative guidance to choose the size of the POD basis. In practice, POD provides an efficient representation of the snapshot data in a low-dimensional subspace of dimension R, much lower than N, such that

$$\boldsymbol{t}_i^j \approx \sum_{k=1}^{R} \boldsymbol{\phi}_k^j \alpha_{ki}^j = \boldsymbol{B}^j \boldsymbol{a}_i^j \quad \text{for } j = 1, \dots, S \quad i = 1, \dots, N_s \tag{3.2}$$

where $\boldsymbol{\phi}_k^j$ and α_{ki}^j are called POD modes and POD modal coefficients, respectively. In matrix form, $\boldsymbol{B}^j \in \mathbb{R}^{N\times R}$ and $\boldsymbol{a}_i^j = (\boldsymbol{B}^j)^T \boldsymbol{t}_i^j$ where $\boldsymbol{a}_i^j \in \mathbb{R}^R$. Now, instead of using N_s snapshots $\boldsymbol{t}_i^j$ of dimension N to fit a model to the data, the low-dimensional representation of the initial snapshots was considered. Then, the reconstruction of the solution was achieved using Equation 3.2.

Then, as a second step, the reduced state vectors of the snapshots data, the so-called POD modal coefficients, were considered and a non-linear regression method called sparse Proper Generalized Decomposition (sPGD) [145], based on the separated representation approach enabling quite rich approximations for high dimensional problems in a low-data limit [146], was used to fit the low dimensional POD modal coefficients. More details about sPGD can be found in Appendix A.

3.1.2.2.2 Results and discussion The POD modes and modal coefficients are computed at each measurement point as mentioned before. The left singular vectors of the snapshot matrices are truncated to the two first singular vectors which correspond to the POD modes. This choice is made in accordance with the singular values decay as shown in Figure 3.4. As it can be seen, more than 90% of the variance is retained with two singular values.
It is worth pointing out that only results for points (#1, #5, #7, and #2.2) in reference to Figure 3.3 are shown for the sake of clarity.

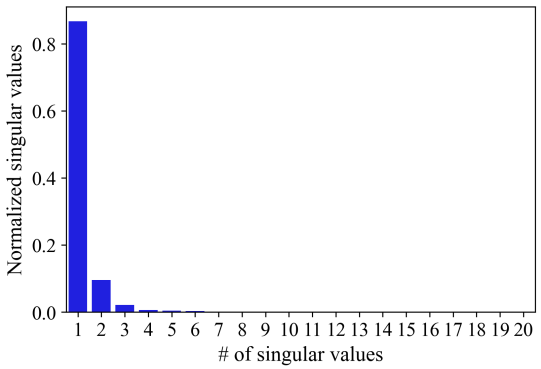

(a) measurement point #1

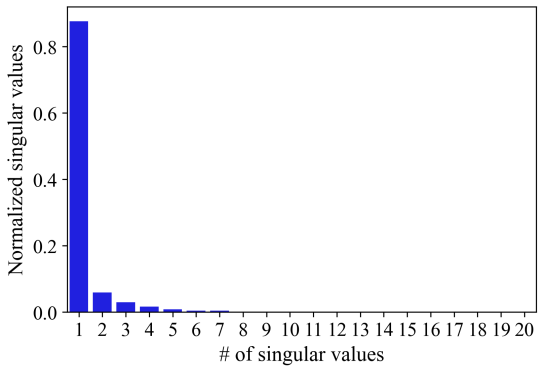

(b) measurement point #5

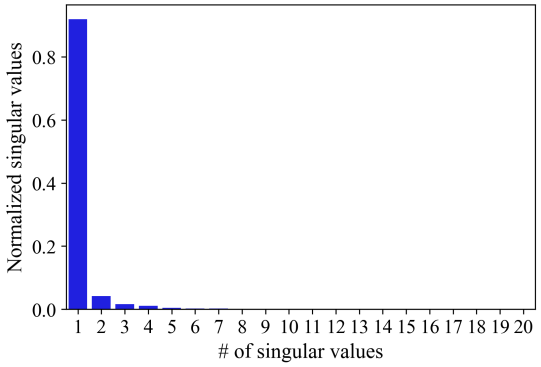

(c) measurement point #7

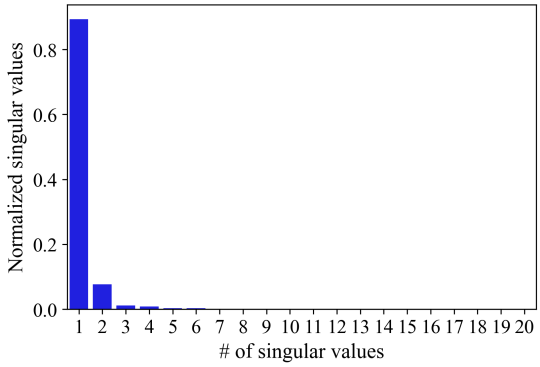

(d) measurement point #2.2

Figure 3.4: Normalized singular values of the thermal field for 4 snapshot matrices

After computing the modal coefficients, a model for each one of them and for each measurement point was constructed. It is commonly known that time is inversely proportional to frequency and electric power, as a result, the inverse of the input parameters were considered when constructing the parametric regression of the modal coefficients. Besides, the standardization of the input parameters was applied to avoid problems related to units and different scaled variables, then the datasets were split into training and testing subsets (75% of data is used to build the models and 25% to evaluate the prediction accuracy). Figure 3.5 shows the real versus the predicted values of modal coefficients for points (#1, #5, #7, and #2.2) using sPGD regression model. The red points correspond to the data used to build the model while the blue ones correspond to the data used to evaluate its accuracy. When points are close to the black line, the model provides a good fit to data. Indeed, the dispersion of these points with respect to the black line gives a visual indicator of error.

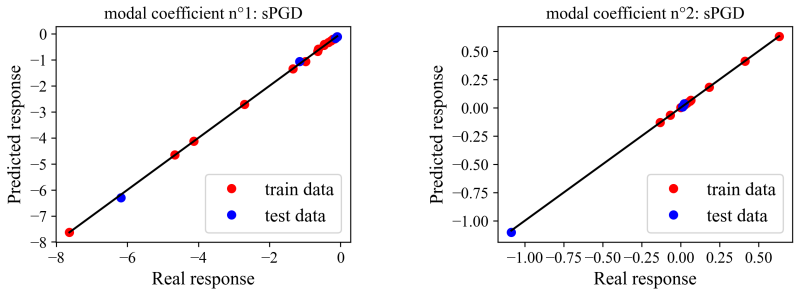

(a) measurement point #1

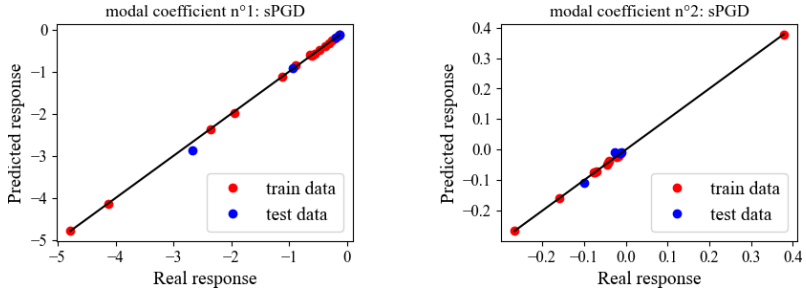

(b) measurement point #5

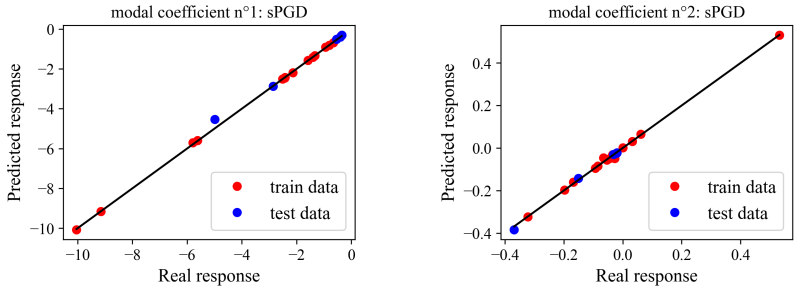

(c) measurement point #7

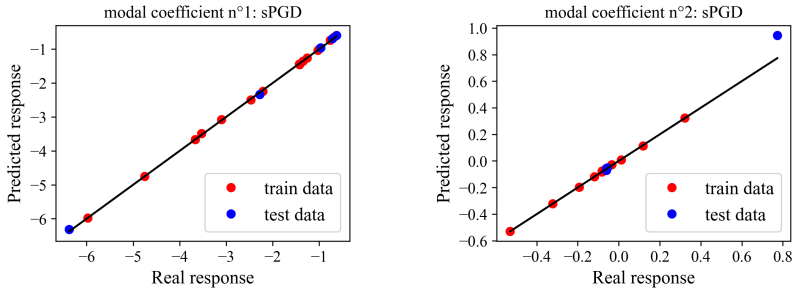

(d) measurement point #2.2

Figure 3.5: Real versus predicted response for 4 measurement points

Figure 3.6 shows the time evolution of the temperature obtained by the full model, and the sPGD

regression model (i.e. using Equation 3.2 with the predicted values of modal coefficients as a function of the frequency and power). It can be seen that the real curves obtained by the full order FE model (black curves) and the predicted ones by sPGD model (dashed red curves) show the same trend and they are almost overlapped for both training and testing datasets and for the four measurement points as well.

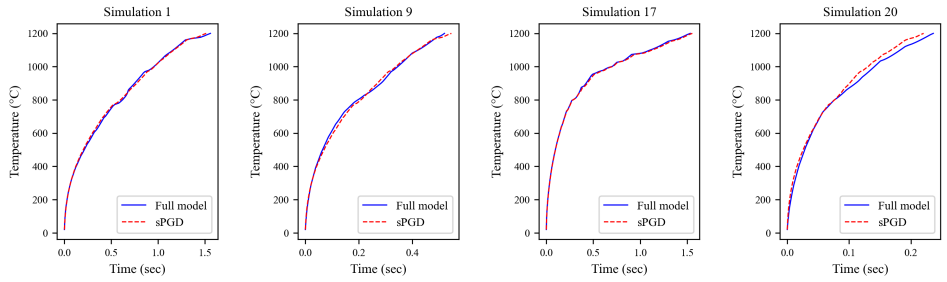

(a) measurement point #1

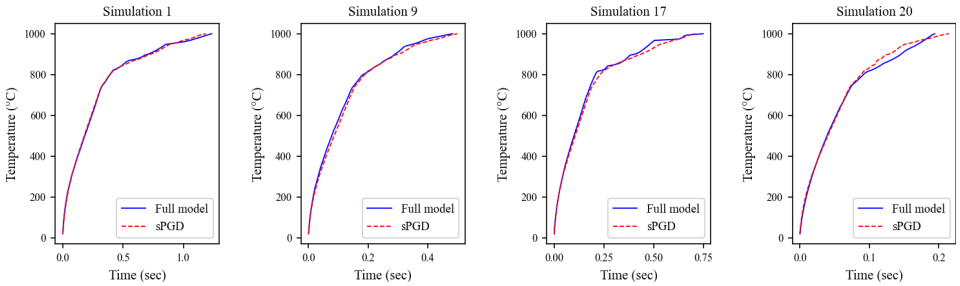

(b) measurement point #5

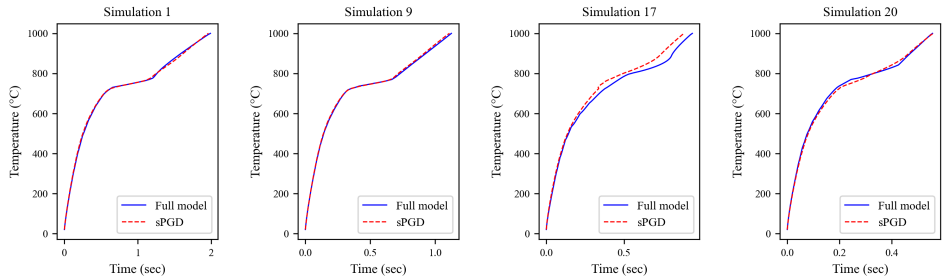

(c) measurement point #7

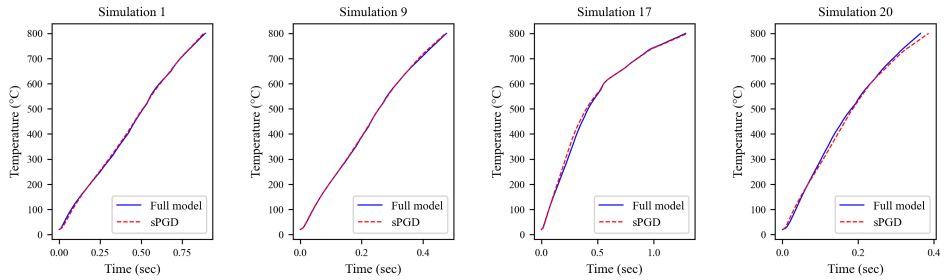

(d) measurement point #2.2

Figure 3.6: Comparison of the time evolution of temperature between the reference full model and the sPGD regression model (with the predicted values of modal coefficients) for 4 measurement points: simulations #1 and #9 are used to create the regression model and simulations #17 and #20 are used to check the regression model accuracy

Additionally, the relative error to measure the prediction accuracy for training and testing datasets is presented in Table 3.2, where the computed error is defined as:

$$Error(\%) = \frac{1}{n}\sum_{i=1}^{n}\left(\frac{1}{t_{true}^{max}}\sqrt{\frac{1}{T^{max}-T^{min}}\int(t_{true}-t_{pred})^2 dT}\right)\times 100 \tag{3.3}$$

where n, t_{true}^{max}, t_{true}, t_{pred}, T^{max}, T^{min} are the number of data points, the maximum value of time, the real response values, the predicted response values, the maximum and minimum values of temperature, respectively. The obtained results prove that the approximation is quite good.

Table 3.2: Relative errors of time evolution using sPGD model

	point #1	**point #5**	**point #7**	**point #2.2**
$Error_{train}$	2.8%	2.6%	2.1%	1.6%
$Error_{test}$	6.5%	3.4%	4.1%	2.5%

A model to predict the time related to each temperature value in a given interval was created while keeping a constant final temperature value for all snapshots. The applied POD enables building a basis with only two modes, and the sPGD model created for the two POD modal coefficients provides an excellent prediction accuracy and a good approximate solution is obtained, even with a small amount of data.

3.1.2.3 Modelling the temporal evolution of austenite

3.1.2.3.1 Methodology During heating, austenitization consists in transforming the different metallurgical phases present at low temperature into austenite. The austenite phase provides a better comprehension of how the system evolves during heating and it will be widely considered in the second part of this paper. Several models for the characterization of phase transformation kinetics can be found in the literature, the Johnson-Mehl-Avrami (JMA) [147, 148, 149, 150] model is one of the most commonly used model and it is implemented in FORGE® for induction heating process. However, it is worth reminding that only data generated by FORGE® is needed in this work and the knowledge of the models is not required.

Besides, depending on the input parameter changes, austenitic phase evolution can be observed in three different states as shown in figure 3.7.

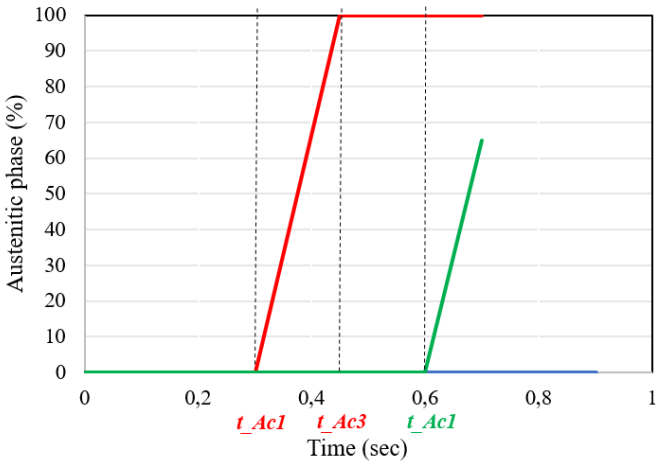

Figure 3.7: Three possible states of austenite phase evolution

As can be seen, the phase transformation starts at time t_Ac1 and austenitization is completed at time t_Ac3. These instants are associated to the characteristic temperatures $Ac1$ and $Ac3$ which correspond to the start and end transformation temperatures, respectively. In some cases, due to a short processing time or low values of process parameters, austenite phase evolution does not reach a complete austenitization (green curve) or does not even start its transformation (blue curve). Therefore, a methodology based on classification followed by regression to avoid dealing with different shaped curves, was developed as follows:
First, the snapshots for each measurement point, were classified into two classes:

- Class 1: no austenitic phase transformation was produced, austenite phase remains at zero until the end of the process (blue curve in Figure 3.7);
- Class 2: there is an austenitic phase transformation; two cases are envisaged:
  - 100% of austenite is reached at the final time step (red curve in Figure 3.7);
  - less than 100% of austenite was obtained after heating (green curve in Figure 3.7)

Then, a constraint was imposed in order to deal only with the data in class 2.

Finally, t_Ac1 and t_Ac3 (if complete austenitization is reached) were collected from the data in class 2 and the non-linear regression model sPGD was then applied to build a model of this two quantities. It is worth pointing out that the inverse of frequency and power were considered to fit a model to t_Ac1 and t_Ac3.

3.1.2.3.2 Results and discussion A standardization of the input parameters was first applied and then the datasets were divided into training and testing subsets (75% of data was used to build the models and 25% to evaluate their prediction accuracy). Figure 3.8 shows the real versus the predicted values of t_Ac1 for points (#1, #5, #7 and #2.2) using sPGD regression model and for both training and testing datasets. It can be noticed that the predicted values are in good agreement with the real ones, proving the excellent performance of the sPGD regression model.

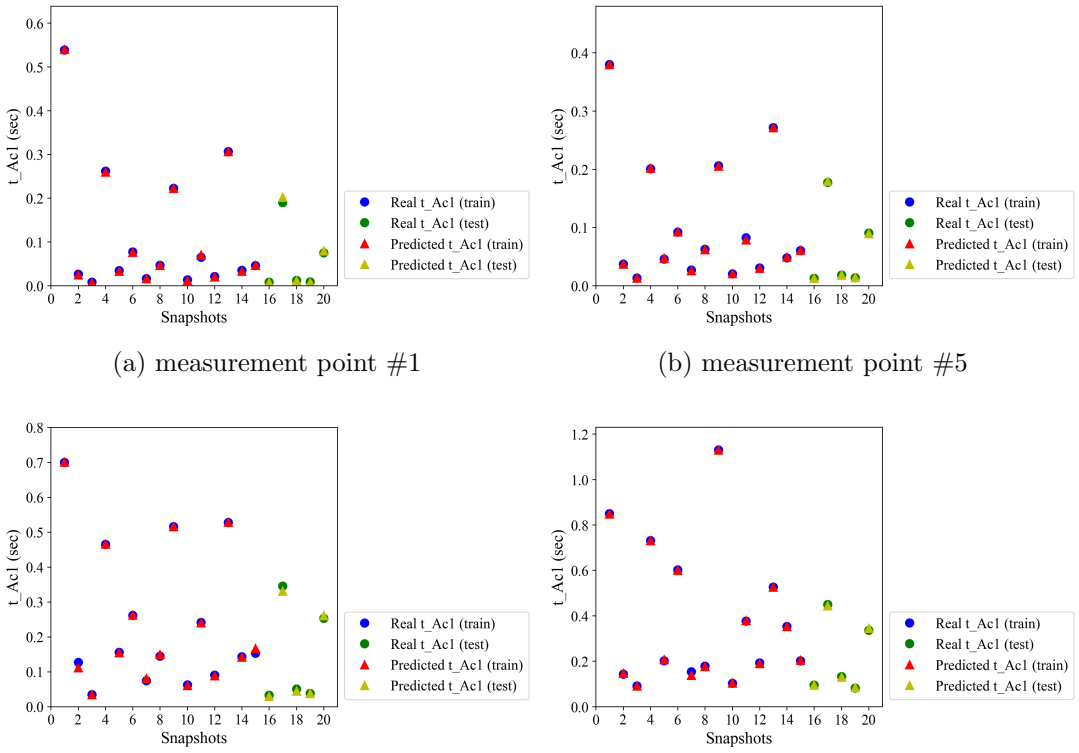

(a) measurement point #1

(b) measurement point #5

(c) measurement point #7

(d) measurement point #2.2

Figure 3.8: Real versus predicted values of t_Ac1 for 4 measurement points

In order to measure the prediction accuracy, the mean arctangent absolute percentage error (MAAPE) [151] was applied, because of its capacity to deal with a zero or close-to-zero true values, which is the case in this study since t_Ac1 and t_Ac3 evolve between zero and two seconds. MAAPE is defined when predicting a quantity y as:

$$MAAPE = \frac{1}{n}\sum_{i=1}^{n} \arctan\left(\left|\frac{y_{true} - y_{pred}}{y_{true}}\right|\right) \times 100 \tag{3.4}$$

where y_{true} is the real response value, y_{pred} is the one predicted by the model, and n is the total number of data points.

The MAAPE for the training and testing datasets is shown in Table 3.3. As it can be noticed, the error is acceptable for all measurement points and does not exceed 6%.

Table 3.3: MAAPE for t_Ac1 using sPGD model

	point #1	**point #5**	**point #7**	**point #2.2**
$MAAPE_{train}$	2.3%	1.5%	2.7%	1.4%
$MAAPE_{test}$	5.2%	1.5%	5.7%	1.9%

By using the same rationale, Figure 3.9 shows the real versus the predicted values of t_Ac3 for points (#1, #5, #7 and #2.2) using sPGD model and for both training and testing datasets. Again, an excellent approximation for t_Ac3 is observed.

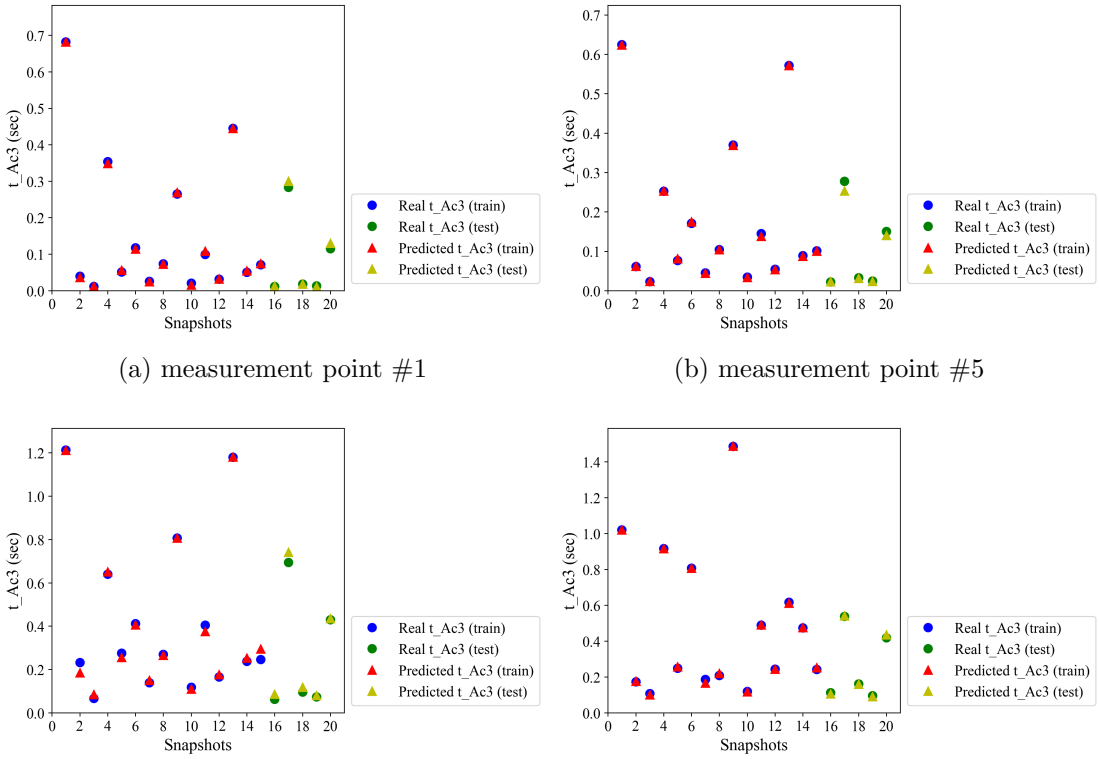

(a) measurement point #1

(b) measurement point #5

(c) measurement point #7

(d) measurement point #2.2

Figure 3.9: Real versus predicted values of t_Ac3 for 4 measurement points

The MAAPE for the training and testing datasets is shown in Table 3.4. The obtained error is acceptable, even if the error of 14.8% is obtained at the tooth tip (measurement point #7).

Table 3.4: MAAPE for t_Ac3 using sPGD model

	point #1	**point #5**	**point #7**	**point #2.2**
$MAAPE_{train}$	5.0%	2.0%	7.5%	2.3%
$MAAPE_{test}$	8.8%	5.6%	14.8%	3.7%

In summary, models for t_Ac1 and t_Ac3 were created. They provide a complete approximation of the austenite phase transformation history as follows:

- 0% of austenite phase was obtained for all $t < t\_Ac1$ which means that no phase transformation was initiated yet;
- 100% of austenite phase was obtained for all $t > t\_Ac3$ which means that a complete austenitization was reached;
- the austenite phase evolves linearly between 0% and 100% for all $t\_Ac1 < t < t\_Ac3$

The methodology was successfully applied for 14 sparse measurement points in the space domain, a good approximation was provided, and a quite good performance of sPGD was shown as well.

3.1.3 Data-driven and hybrid modelling for hardness during quenching

3.1.3.1 Input analysis and data pre-processing

Consider the gear shown in Figure 3.3, at the end of the heating. Then, after a short elapsed time, a powerful quenching applies in order to cool the workpiece and induce its surface hardening. The workpiece is equipped with several measurement points (sensors), most of them located on the outer surface of the gear. Therefore, several simulations using FORGE® software were carried out to generate different datasets during the quenching step where the input configurations were the final state of heating. The set of the considered input variables to describe the system, the so-called feature space F, reads:

$$F = \left\{ k, t, \theta_{init}, (\theta_i)_{i\in[1;5]} \right\}, \tag{3.5}$$

where k is the simulation step, t is the total time of the quenching process, θ_{init} is the initial temperature at the quenching stage, $(\theta_i)_{i\in[1;5]}$ are the different temperature values collected at different times uniformly distributed on the quenching time interval t such that:

$$\forall i \in [1;5],\ \theta_i = \theta\left(t_i = \frac{t \times i}{5}\right), \tag{3.6}$$

Using these 5 temperatures provides the model a reasonable amount of information about the temperature history to describe the hardness. Using more temperature values would make the feature space too large for this low-data setting.

First preliminary predictions using naive models (simple models without optimization) showed a lack of accuracy which could be explained by a lack of information to describe the hardening process with respect to the considered variables. Hence, it was decided to define new variables from the temperature itself. Therefore, the space and time gradients of the temperature were chosen to complete the feature space F as they are expected having a significant influence on the material hardening [2]. The temporal temperature gradient reads

$$C_i = \frac{\theta_{init} - \theta_i}{|t_0 - t_i|}, \tag{3.7}$$

where $t_0 = 0$.

In order to compute the gradient in space, it was necessary to associate a distance to ensure the frame indifference of the learned model. The proposed solution considers the distance to the surface, that is: $\forall x,\ d(x, x_s)$ represents the Euclidian distance from a point x in the gear to its nearest point on the gear surface x_s. Therefore, the space gradient of the temperature field is expressed as follows, if $x \neq x_s$:

$$D_{i,x} = \frac{\theta_{i,x_s} - \theta_{i,x}}{d(x, x_s)} \tag{3.8}$$

The available data allows computing that gradient at the measurement point located in the bulk material, the sensor 2 in Figure 3.10. At the other measurement points located on the outer gear surface, the spatial temperature gradient cannot be calculated.

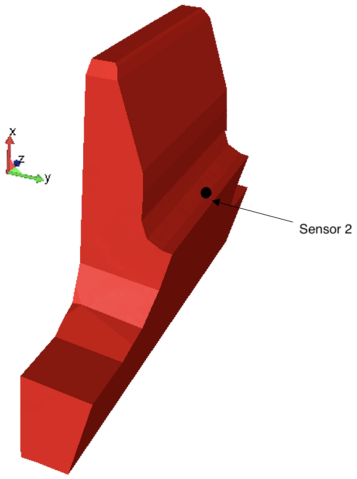

Figure 3.10: Location of sensor 2 in the gear

Therefore, the initial feature space is enriched with the considered temperature gradients in (3.7) and (3.8) at the sensor 2 location, according to:

$$F = \left\{\theta_{init},\ (\theta_i)_{i\in[1;5]},\ (D_{i,x_2^j})_{i\in[1;5]},\ (C_i)_{i\in[1;5]},\ d(x,x_2)\right\}, \tag{3.9}$$

where D_{i,x_2^j} is the space gradient at time i of points x_2^j in the neighboorhod of x_2, point at which sensor 2 is located on the outer surface, as illustrated in Figure 3.11.

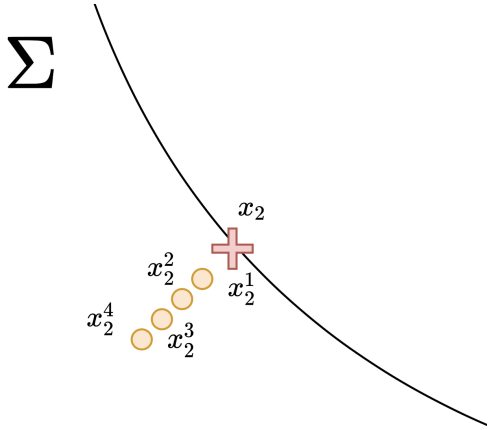

Figure 3.11: Schematic representation of the sensor 2 (x_2) and the associated measurement points x_2^j in the gear Σ.

The next step consists of splitting the data into the training and testing subsets. One of the most common techniques used in the field of machine learning is the K-Fold Cross Validation [152] which consists in choosing the best fold to be tested by the regression model. Nevertheless, since data distribution is not well balanced, it brings a huge bias in the results. It can be noticed that the hardness H shows three different trends. These trends are $H < 268$, $268 < H < 721$ and $H = 721$ as shown in Figure 3.12.

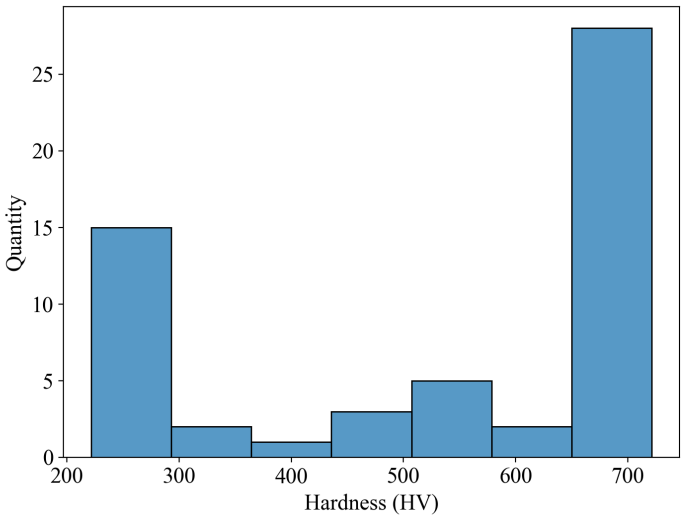

Figure 3.12: Hardness points Histogram

Therefore, it was not possible to apply a K-Fold Cross Validation on these imbalanced datasets because the model performs very well on the largely represented data, but lacks robustness [153]. In order to have a balanced distribution in the testing dataset, in absence of considering richer samplings, it was decided to cluster data into 3 classes with the K-means algorithm [154] and define a testing dataset in each cluster. Now, each trend of the distribution is represented in the testing dataset and the performance is no longer biased.

The next step is to select variables in the feature space previously defined. Considering the low number of data points, it was necessary to reduce the number of input variables [155]. The adopted technique is a statistical method called F-test. Two models are considered, M_1 and M_2, one with a selected variable and a constant and the other one with just a constant. The F-test analyses the least square error between M_1 and M_2 to check if it is significant or not. It leads to the F-score which is

basically the significance of a variable according to the model. Then, the F-score is used to select the features. After the selection, the new space reads:

$$F_{selected} = \left\{\theta_{init}, D_{2,x_2^j}, \theta_1, D_{1,x_2^j}, D_{0,x_2^j}, C_1, d(x, x_2), \theta_2\right\}, \tag{3.10}$$

3.1.3.2 Modelling the hardness

The type of regression model was chosen accordingly to the needs of the studied problem. The complexity of the system excluded simple models such as linear regression. Then, the lack of data avoided the use of a classical neural network like the multilayer perceptron. Therefore, the considered model in this work was the gradient boosting algorithm [125] implemented in the XGBoost library which has recently become one of the most widely used machine learning techniques [156, 157]. Parameters of this model were optimized using a random search to avoid excessive computation time and the associated issues [122]. The starting search space was defined arbitrarily with basic and *foolproof* hyperparameters.

3.1.3.2.1 Data-driven model There are 56 data points registered at sensor 2 and its neighboor measurement points after the simulations. Therefore, the proposed datasets are small compared to the usual standards in machine learning. In fact, the more points a dataset has, the more efficient each training step is. Basically, applying machine learning algorithms to such a complex system was regarded as a challenge. This is why, it was important to proceed with variables extraction, selection, and optimized hyperparameters search to maximize the performance of the model.

It is well known that models learned from data are efficient to interpolate but fail to extrapolate. Therefore, when a testing point is located in a region outside the training region of the parametric space, the error usually increases. Two points were removed from the testing dataset since there was no point close to them in the training dataset.

To avoid overfitting, part of the training dataset was also used as an evaluation set to stop when reaching a relevant score. Moreover, another stopping criterion was set to break the loop with a chosen number of iterations [158]. This number was chosen to ensure the smallest test error.

In order to evaluate the prediction accuracy, Root Mean Squared Error (RMSE) and Root Mean

Squared Percentage Error (RMSPE) were used. They are defined as follows:

$$RMSE = \sqrt{\frac{1}{n}\sum_{i=1}^{n}(y_{pred} - y_{true})^2}, \tag{3.11}$$

$$RMSPE = \sqrt{\frac{1}{n}\sum_{i=1}^{n}(\frac{y_{pred} - y_{true}}{y_{true}})^2} \times 100, \tag{3.12}$$

where y_{true} and y_{pred} are the real hardness and the predicted one, respectively.

The advantage of RMSPE compared to RMSE is that it shows a percentage which is more significant than an arbitrary quantity. Therefore, after fitting the regression model and testing the dedicated set on it, the results are given in Table 3.5.

Table 3.5: Errors of the XGBoost and Random Forest models to compare as a simple baseline to predict hardness with *sensor 2* dataset

Model	**XGBoost with Austenite**	**XGBoost without Austenite**
$RMSE_{train}$	0.264	30.629
$RMSE_{test}$	77.319	151.494
$RMSPE_{train}$	**0.08%**	8.30%
$RMSPE_{test}$	**12.58%**	25.42%

It is clear that the models still have trouble generalizing on new data but those results are still relevant and give perspective to reach a better accuracy using more sampling points. The position of the predicted data with respect to the real data was illustrated in Figure 3.13. It can be noticed that the trend is well described. The visualisation of the numerical results shows that the training dataset has been well predicted as it is almost impossible to distinguish green points (true ones), i.e. they are overlapped with the blue ones. On the other side, the testing dataset does not have the best results so far, but it would surely be possible to improve them with more data. Moreover, the fact that the maximal hardness is reached with a low temperature ($\theta_{init} = [700, 750]$ (°C) for $H = 721$ (HV)) could lead to question the considered variables. However, it is common in data science to get a large scope of different data to make the model learn on a complete profile in order to describe every behavior. Indeed, it allows to trust the results if someday an uncommon prediction is required and to avoid extrapolation which makes the prediction harder for a model learnt on small datasets.

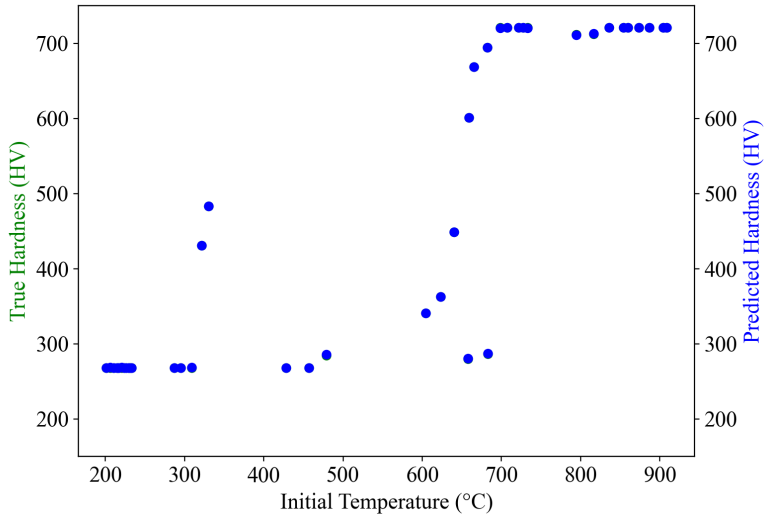

(a)

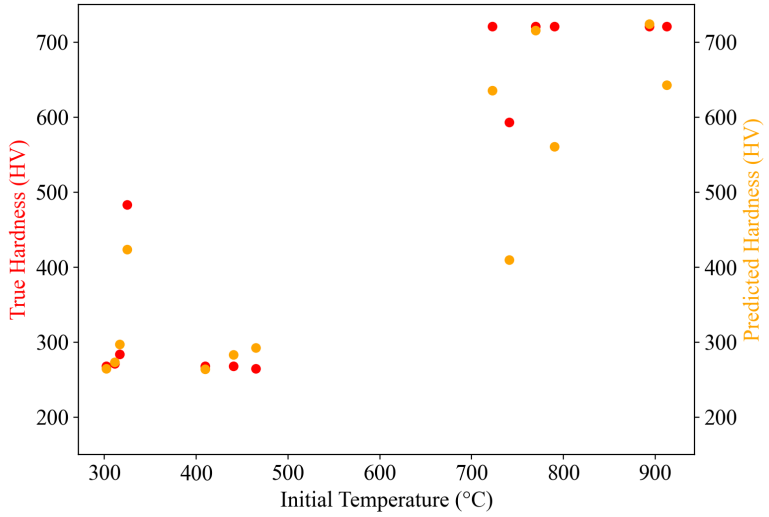

(b)

Figure 3.13: Comparison between the true and predicted hardness of the sensor 2 dataset: **(a)** training dataset with the predicted hardness (blue) over the ground truth (green). **(b)** testing dataset with the predicted hardness (yellow) over the ground truth (red). Both with respect to the initial temperature of the system.

3.1.3.2.2 Hybrid model The lack of data, due to the high computational costs or the difficulty to collect experimental data, makes difficult the construction of efficient models. A hybrid framework [42] could constitute an appealing compromise to ally accuracy and data frugality. Indeed, physical laws represent a valuable knowledge of the system even if in general reality is a bit more complex. Data should be used to enrich models instead of replacing them.

It is well known that the austenite ratio before quenching is highly correlated with the hardness as shown in Figure 3.14. Hence, the prediction of the austenite ratio at every point of the gear at the end of the heating (before quenching starts) can be used as a new input variable, represented by the variable α, to better describe the hardness.

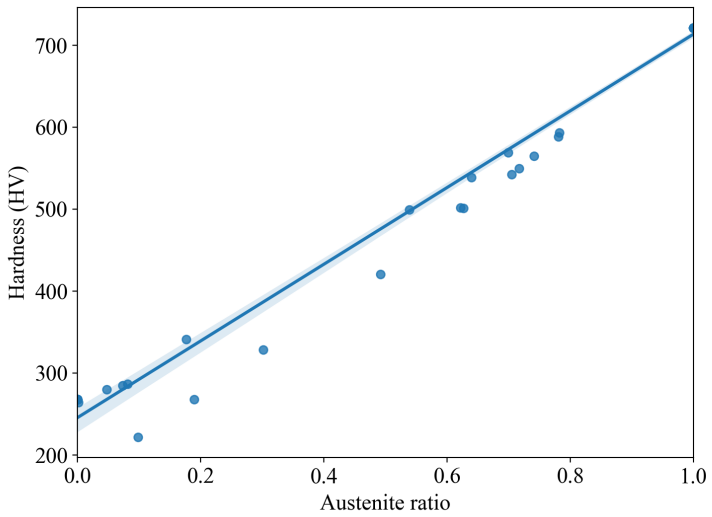

Figure 3.14: Regression plot of the austenite ratio with respect to the hardness

Considering α, the pipeline described before in Section 3.1.3.1 is used again with a new selection of variables and model optimization. The new feature space reads:

$$F = \{\theta_{init}, \theta_1, \theta_2, \theta_3, \theta_4, \theta_5, \alpha, C_1, C_2, C_4, C_5\}, \tag{3.13}$$

The knowledge provided by the austenite ratio offers the possibility to avoid the use of the space temperature gradients that simplifies the data collection. Results are shown in the Figure 3.15 as well as grouped in Table 3.6.

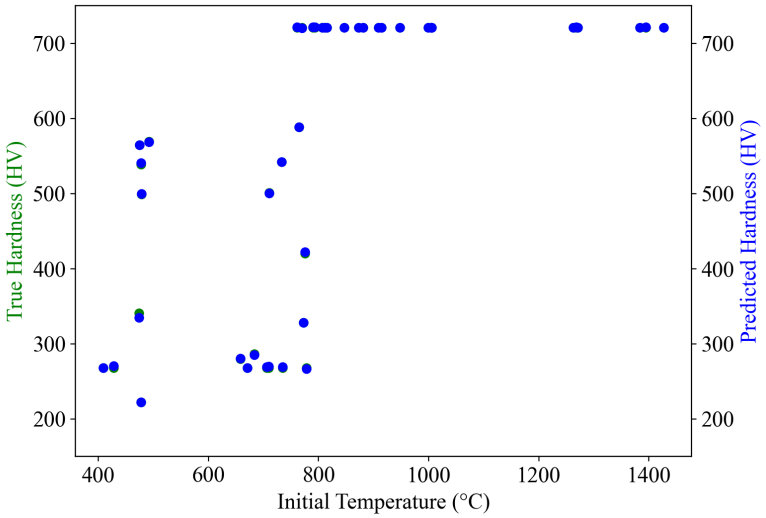

(a)

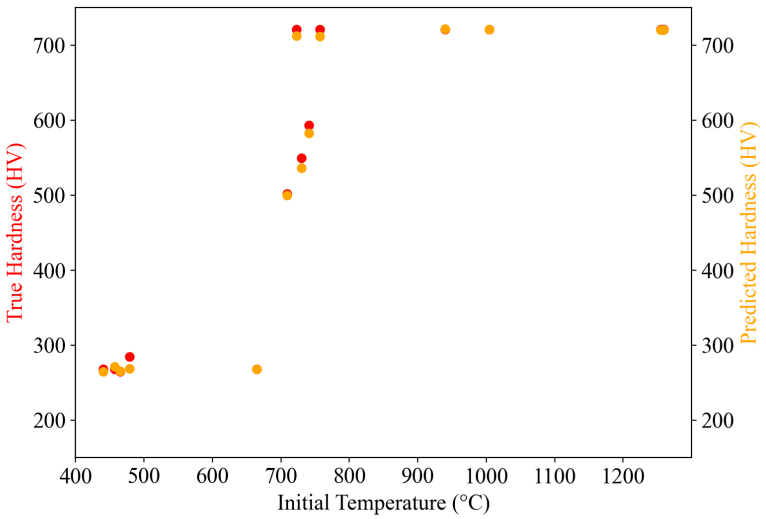

(b)

Figure 3.15: Comparison between the true and predicted hardness of the global dataset: **(a)** training dataset with the predicted hardness (blue) over the ground truth (green). **(b)** testing dataset with the predicted hardness (yellow) over the ground truth (red). Both with respect to the initial temperature of the system.

Table 3.6: Prediction error of the hardness computed with the XGBoost model, with and without the austenite ratio as a feature with the global dataset

Model	**XGBoost with Austenite**	**XGBoost without Austenite**
$RMSE_{train}$	1.502	0.668
$RMSE_{test}$	7.249	106.229
$RMSPE_{train}$	**0.44%**	0.17%
$RMSPE_{test}$	**1.82%**	21.62%

3.1.3.3 Discussion

Predicting hardness at any point after induction hardening process is an important gear validation procedure for industrial applications. It was proved in this work that a gradient-boosted tree-based model with features selection could perform satisfactorily in complex settings. However having access to those variables (e.g. temperature gradients) seems technically a tricky issue and the lack of data combined with the high non-linearity of the system suggest the need of introducing existing knowledge into the learning procedure. Here, the austenite ratio was considered because it could be provided by a validated reduced model, and it is a variable that exhibits a correlation with the hardness.

3.1.4 Conclusions

In this paper, the multi-physics parametrized induction hardening process was studied, and parametric meta-models was developed to predict three physical quantities: temperature and austenite phase evolution during heating as well as the workpiece hardness after quenching. First, an approach, based on dimensionality reduction by POD coupled with a regression technique to fit a model to the POD modal coefficients, was first proposed to compute the time evolution as a function of temperature. The approach was successfully applied for 14 sparse measurement points in the space domain, in which a basis with two modes was built and consequently two POD modal coefficients were used for creating the prediction model. A good approximation was provided using the sPGD regression.

Second, a methodology, based on classification combined with the sPGD regression model, was applied where only data with phase transformation were considered and a model for start and complete austenitization time instants was created. A good approximation was provided using sPGD even with a small amount of data. Since these models were built for some sparse points in the space domain, the solution will be extended to address the whole space domain using interpolation techniques.

Finally, as far as the hardness is concerned, the prediction was carried out by using tree-based gradient boosted data-driven models with two approaches. On the one hand, a fully data-driven model with the extraction of new variables based on the temperature profile. It is located in the bulk material because of lack of data but with encouraging performance. On the other hand, a physic-enhanced model with the austenite ratio available thanks to a reduced model. This one is global i.e. in the whole gear with great performance. However, more data are required to enhance prediction accuracy of data-driven model for predicting the hardness. The hybrid modelling could be improved by enforcing a thermodynamical consistency.

Appendix A: Sparse proper generalized decomposition sPGD

sPGD is a non-linear regression model which provides a quite rich approximation for multidimensional and parametric problems with a small amount of sparse data. For ease of explanation, let's consider a parametric problem where the studied QoI lives in $\mathbb{R}^2$, $u(P1, P2)$ where $P1 \in \Omega_1$ and $P2 \in \Omega_2$ are the considered parameters and u is known for certain values of P1 and P2. In order to calculate the approximate solution $\tilde{u}(P1, P2)$ of $u(P1, P2)$, the Galerkin projection is first applied such that:

$$\int_{\Omega_1 X \Omega_2} w^*(P1, P2)(\tilde{u}(P1, P2) - u(P1, P2))\, dP1\, dP2 = 0 \tag{3.14}$$

where w^* is an arbitrary test function. Then, following the Proper Generalized Decomposition (PGD) rationale, the approximate solution $\tilde{u}(P1, P2) \approx \tilde{u}^N(P1, P2)$ is expressed in the separated form:

$$\tilde{u}^N(P1, P2) = \sum_{i=1}^{N} M_i^1(P1).M_i^2(P2) \tag{3.15}$$

The determination of the precise form of pairs $M_i^1(P1).M_i^2(P2)$ is done by first projecting them on a finite element basis, as shown in equation 3.16, and by employing a greedy algorithm such that the N^{th} order term is calculated once the approximation up to order $N-1$ is known

$$\begin{aligned} M_i^1(P1) &= \sum_{k=1}^{N} N_i^k(P1).\alpha_i^k \\ M_i^2(P2) &= \sum_{k=1}^{N} N_i^k(P2).\beta_i^k \end{aligned} \tag{3.16}$$

where N_i^k, α_i^k, and β_i^k represent the FE shape functions and the degrees of freedom of the chosen approximation, respectively. the choice of basis in which each one of the one-dimensional function was

expressed is made based on the studied problem. A choice ensuring accuracy and avoiding spurious oscillations consists of using interpolants based on Kriging techniques. It is worth mentioning that the product of the test function w^* times the objective function $u(P1, P2)$ is only evaluated at some points corresponding to the available sampled data. Since information is just known at sampling points, so instead of using the test function in a finite element context, it is expressed as a set of Dirac delta distributions collocated at the sampling data (denoted by S) such that:

$$w^*(P1, P2) = \tilde{u}^*(P1, P2) \sum_{i=1}^{S} \delta(P1_i, P2_i) \tag{3.17}$$

By combining the all equations presented above, a nonlinear system of equations is derived, due to products of terms. The alternate direction scheme is used to linearize the problem and to solve it.

3.2 Article 2 : Data-driven modeling for residual stress prediction after induction treatment process of C45 steel

Sevan Garois, Khouloud Derouiche, Monzer Daoud, Khalil Traidi and Francisco Chinesta. Presented in ICRS11 in 2022.

Induction heating followed by quenching is one of the surface heat treatment processes widely employed in automotive and aerospace industries to enhance the fatigue life of critical components, such as gears, by introducing compressive surface residual stress fields. These fields are mainly impacted by the selection of the process parameters. In this work, an approach based on artificial intelligence technique coupled with finite element modeling of the induction treatment process was developed to predict the residual stress profile within a gear-shaped workpiece. To conduct such a study, a 3D-periodic symmetry finite element model was employed to perform several finite element (FE) simulations using Latin Hypercube Sampling design of experiments. Data-driven model based on XGboost library was then developed. It was found that the developed model predicts with good agreement the residual stress profiles and can be used in induction treatment process optimization.

Keywords: Induction treatment; Residual stresses; Artificial intelligence technique; Data-driven model; XGBoost; Finite element modeling

3.2.1 Introduction

Induction hardening is a process that has been major for the last years to reinforce the durability of steel gears in the whole industry such as aeronautical and automotive fields. This process is divided into two parts, the first one is a very fast and powerful heating, the second is a quenching that can be achieved thanks to water or a polymerized solution. The heat treatment changes the microstructure and mechanical properties of the material so it becomes optimal to fit many performances criterion. These techniques are used to increase the resistance of the mechanical gears by changing the properties of their critical zones. As it imposes on the gear a fundamental change on the material microstructures, it obviously leads to residual stresses. To keep an industrial quality, this impact needs to be evaluated and quantified as part of the certification of the validity of the treated gear. Today experimental data have a certain cost. This requires expensive machines, advanced materials and measuring instruments and experts to handle them. In order to compensate for this lack of experimental data, the literature and industry have turned to simulation, which, even if it is not the reality, gives a more than acceptable approximation with more and more accurate software's like FORGE®. The simulation is based on the Finite Element Modeling (FEM) which has been proven reliable and accurate for this kind of system. Nevertheless, data from simulation have a high computational cost and need HPC machines. Thus, the aim of this work is to replace FEM with the power of artificial intelligence (AI). It is about using

machine learning techniques with an induction hardening system as input and predict the final residual stress efficiently. It is good noticing that similar work has been conducted for hardness prediction with relevant results [159]. The challenge for this work is to produce an effective model with little data available, which is often a major issue in AI applied to other fields when data is expensive or not available. The computational power needed for the model training may also be discussed, but it is actually negligible in comparison to that required for the FEM.

This work is divided into two distinct parts, the first goal of this work is to make a FEM to generate accurate and relevant data which are the input of the further AI model. Then, the data need to be treated in order to be injected in a machine learning pipeline and all of its optimization process. Because of the natural lack of data in this field, everything needs to be optimized to make the model need less data to train precisely. In the end, different profiles will be highlighted to show the results with respect to the FEM data with different input parameters of simulation.

3.2.2 Methodology for residual stress prediction

3.2.2.1 Finite element simulation

The finite element modeling (FEM) represents an efficient way to solve the equations describing the physical phenomena that appeared in the induction treatment (IT) process, where the system is discretized in space and time and partial differential equations are solved. In this work, several finite element (FE) simulations were carried out for the IT process by using the commercial FE software FORGE®. A gear-shaped workpiece of C45 steel having a module of 2.5 and 22 teeth was studied. In all simulations, only one-half of the gear tooth was modeled, and two symmetry planes were imposed to improve the computational efficiency. The implemented material properties of C45 steel were taken from the literature [160, 161, 162, 163, 164, 165].

The IT process is based on two main steps; the induction heating step and the quenching step. During the first step, electromagnetic and thermal fields in addition to the metallurgical phase transformation associated with the temperature evolution are combined. In this step, FORGE® uses two coupled solvers. The electromagnetic solver where the workpiece, the inductor, and the surrounding air are introduced and a tetrahedral global mesh is created such that a fine mesh of 0.2 mm is defined around the gear tooth interface and the inductor and increases while going far from the common interface. Indeed, the electromagnetic solver solves Maxwell's equations and consequently gives rise

to a heating power. The calculated heating power is then applied to the thermal solver to obtain the temperature field by solving the heat equation. The workpiece with a tetrahedral mesh of 0.2 mm on the studied zones is defined for this solver.

In the quenching step, a thermo-metallo-mechanical solver is used, where a strong coupling between these latter physical fields is insured. FORGE® takes the last state of the heating step and gives rise to the hardness in addition to the stresses and strains. In this work, the mesh of the heating part is kept for the quenching step. Figure 3.16 shows the IH simulation and the coupling between the different physical fields.

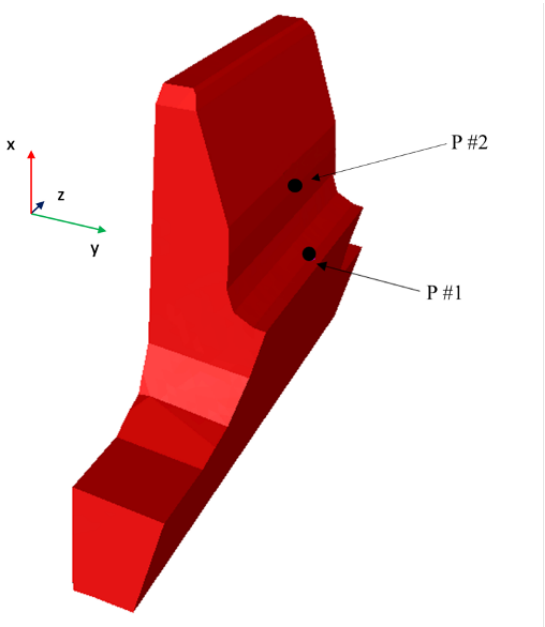

Figure 3.16: Finite element simulation of IH process.

In this work, a parametric solution for the residual stresses obtained after quenching was proposed based on synthetic data collected from the high-fidelity FE simulations. To achieve this goal, a total of 8 heating simulations were first carried out for different values of process parameters (frequency, power and process time). Then, quenching simulations were generated with different cooling rates and times and by using the obtained results from heating. The heat transfer coefficient (HTC) is defined by the quotient between heat flux and with the thermal difference. The design of experiments is illustrated in Table 3.7 and Table 3.8.

Table 3.7: Induction heating design of experiment for FE simulation

Run #	Frequency (kH)	Power (kW)	Time (s)
1	19	480	0.37
2	96	68	0.64
3	52	300	0.52
4	36	320	0.8
5	148	200	0.12
6	15	370	0.26
7	118	170	0.5

Table 3.8: Quenching design of experiment for FE simulation

HTC ($W \cdot m^{-2} \cdot K^{-1}$)	Time (s)
2500	12
3000	12
4000	12

3.2.2.2 Artificial intelligence technique

3.2.2.2.1 Residual stress data As mentioned above, the residual stress profiles used in this investigation were obtained based on FEM results. Only the residual stresses in the axial direction σ_{ZZ} (z direction according to 3.17) at two positions ($P\#1$ and $P\#2$, both in surface) within C45 steel were considered in this work. The two positions were chosen according to the interest to put in-depth sub-sensors during the simulations. Hence, there are the only positions of which it is possible to extract in-depth information and evolution of the variables.

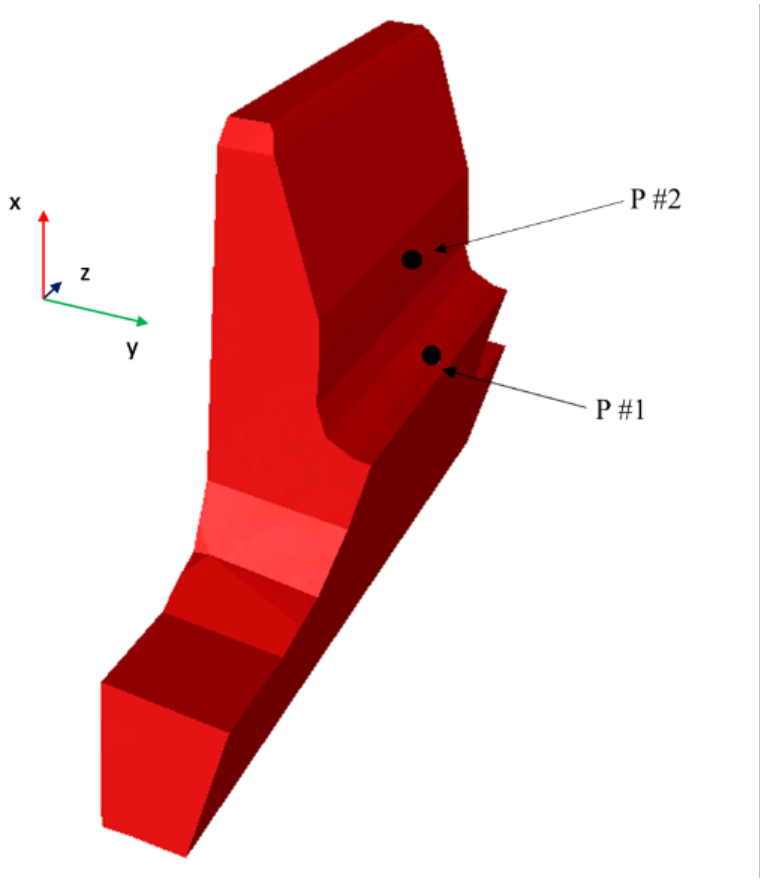

Figure 3.17: Schema of the gear presenting the 2 main positions of interest.

3.2.2.2.2 Data Analysis The set of the considered input variables to describe the system, the so-called feature space X, is composed of the following quantities: the initial temperature θ_{init} , the history of temperature through time $(\theta_i)_{(i\in[1;5])}$, all θ_i taken at fixed moments during each quenching process such as the moments are isochronous, splitting the process into 5 identical portion of time, providing a homogeneous profile, the austenite ratio γ, the heat transfer coefficient (HTC) h, the mean cooling rate $(C_i)_{i\in[1;5]}$ given by

$$\forall i \in [1,5], C_i = \frac{\theta_{init} - \theta_i}{t_0 - t_i} \tag{3.18}$$

It is worth mentioning that the incremental step of simulation k will be not considered. This is because it has no physical meaning compared to others [2].

Therefore, the feature space is expressed as:

$$X = \{\theta_{init}, (\theta_i)_{(i\in[1;5])}, \gamma; (C_i)_{(i\in[1;5])}\} \tag{3.19}$$

It is possible to make a correlation matrix to highlight if the information given by the variables are related or not to the target quantity (σ_{ZZ}). The obtained matrix is given in Figure 3.18. The darker blue and red show a strong negative and positive correlation, respectively, while the white (near 0) shows a poor correlation.

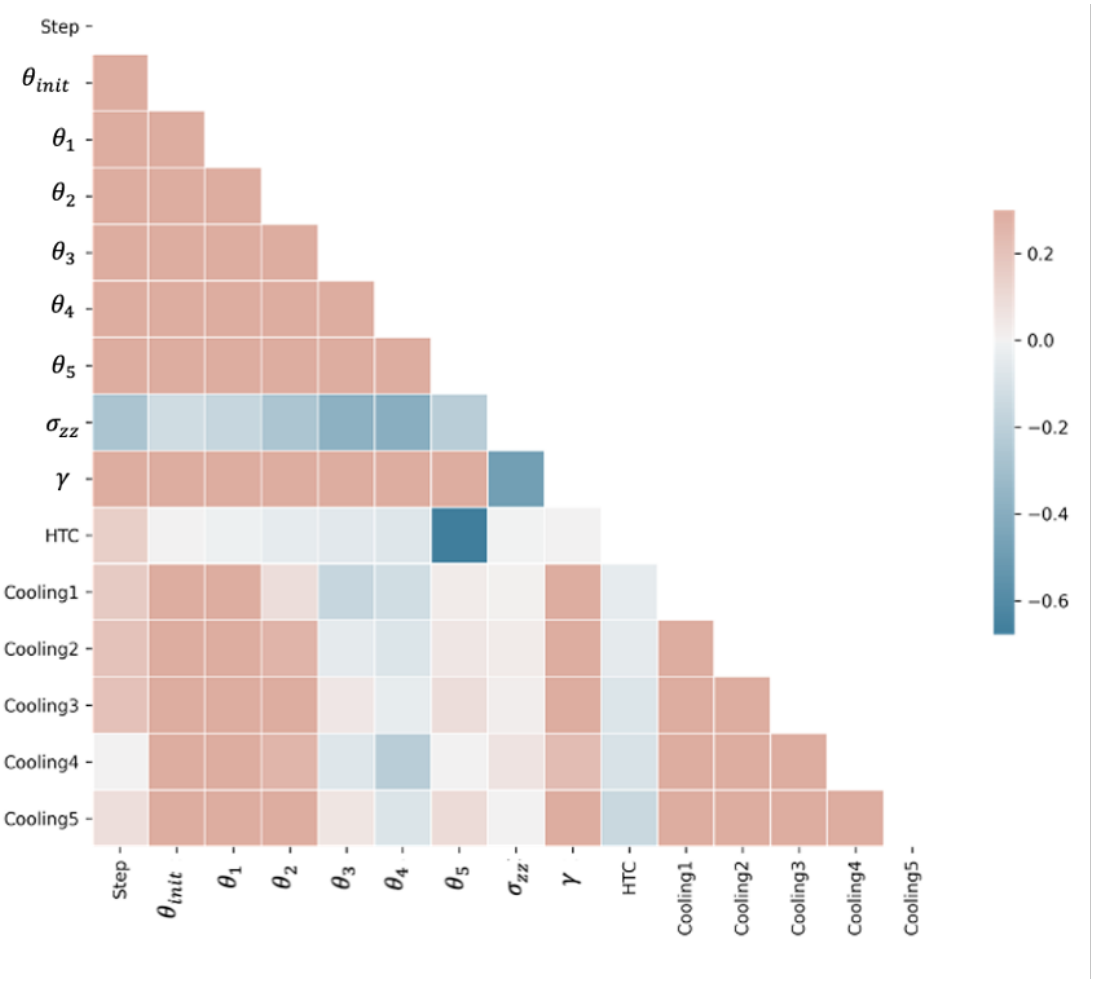

Figure 3.18: Correlation matrix

It is clear that there is no variable more correlated to σ_{ZZ} than another one. However, it is known that all these variables are physically related to the target quantity [10]. It is possible to observe some consistency such as the HTC negatively correlated to θ_5 being the last recorded temperature of the

process. Also, the different temperatures are a little correlated between them as it is supposed to be a profile and so they depend on each other. However, the cooling rate are not particularly correlated with σ_{ZZ}, so they can perhaps have some information as an ensemble of features, but as a single feature, they can't describe residual stresses. The feature space needs to be reduced as there is a few amounts of data and feature selection techniques are known to increase the accuracy [155]. Thus, a simple F-test has been conducted to statistically detect which variable according to the further model has more impact to predict σ_{ZZ}. The F-test is used to evaluate the relationship between each feature and the target variable, by comparing the variance including the feature, to the variance without taking the feature in account, for each input feature. A higher F-test score indicates that the feature is more strongly related to the target variable and should be included in the model, while a lower score indicates that the feature is less important and may be removed from the model. After the test, the reduced feature space is now expressed as:

$$X' = \{\theta_{init}, \theta_1, \theta_2, \theta_3, \theta_5, \gamma, C_1, C_2, C_4\} \tag{3.20}$$

3.2.2.3 Data-driven modeling

In this work, data-driven model was developed based on XGBoost library [125]. Indeed, the tree-based gradient-boosted algorithm from this library is known to be highly efficient even for complex systems. Moreover, it is easily and quickly trainable with small datasets unlike neural networks [166]. The main principle is a model building trees sequentially with the residual gradient error computed for to help training the next tree. A Random Search on the hyperparameters has been made to find the most effective ones. The depth of the trees is more likely to be deep because of the complexity of the system.

As there is an experimental uncertainty of ± 20 MPa related to X-ray diffraction technique [167], it is used here in this work as an indicator to see from which score an error is acceptable. Counting this already existing uncertainty, an error of ± 50 MPa is satisfying. Therefore, the model was optimized to reduce this error as much as possible. The error metrics used in this work are the RMSE and the RMSPE as a percentage is more interpretable. Both metrics are defined in Eq. 3.21 as follows:

$$RMSE = \sqrt{\frac{1}{n}\sum_{i=1}^{n}(y_{pred} - y_{true})^2}$$
$$RMSPE = \sqrt{\frac{1}{n}\sum_{i=1}^{n}(\frac{y_{pred} - y_{true}}{y_{true}})^2} \times 100 \quad (3.21)$$

where y_{pred} and y_{true} are the predicted and true residual stresses, respectively.

The results of the final optimized model are given in Table 3.9:

Table 3.9: Errors of the XGBoost model to predict residual stresses σ_{ZZ} (the lower the better)

Model	XGBoost
$RMSE_{train}$	9.47
$RMSE_{test}$	48.69
$RMSPE_{train}$	**1.61%**
$RMSPE_{test}$	**9.26%**

On the first hand the training error is very low, it indicated a good specification of the model, on the other hand the testing error is lower than the fixed threshold and it proves the capacity of the model to generalize to a certain extent. Because of the satisfying criteria the results and the model are accepted. Figure 3.19 and Figure 3.20 show the residual stress profiles obtained by FEM and XGBoost model at the two positions of interest ($P\#1$ and $P\#2$).

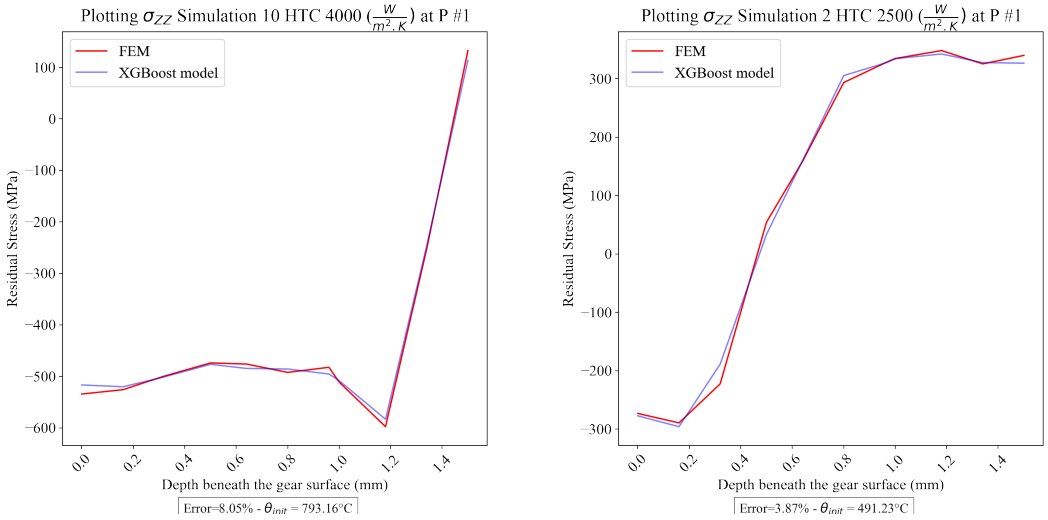

Figure 3.19: Comparison between the XGBoost model and the FEM one of in-depth residual stress profiles (σ_{ZZ}) at position $P\#1$

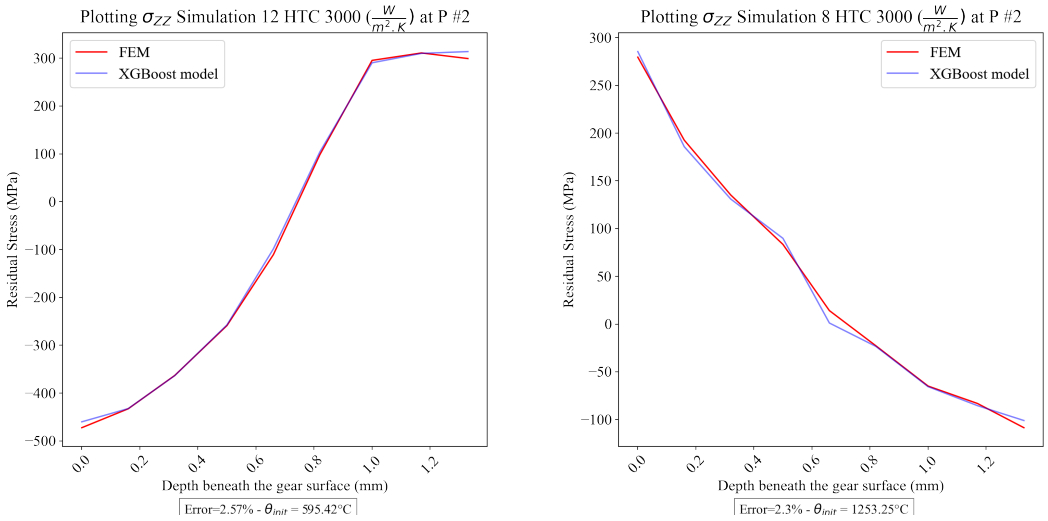

Figure 3.20: Comparison between the XGBoost model and the FEM one of in-depth residual stress profiles (σ_{ZZ}) at position $P\#2$

It is clear that the residual stress profiles predicted by the XGBoost model follow the finite element ones accurately for different process parameters. Thus, it confirms the numerical results shown in Table 3.9.

3.2.3 Conclusion

In this work, a predictive model was developed to predict the in-depth residual stress profile within a gear-shaped workpiece of C45 steel. The capability of this model was evaluated and discussed. The main conclusions were as follows:

- Data-driven model was developed based on XGBoost library, a tree-based gradient-boosted machine learning model.
- Several finite element simulations were conducted using 3D-periodic symmetry model
- The low value of RMSPE found indicated that the XGBoost model could adequately predict the residual stress profiles.
- Results showed that the XGBoost model predictions were in good agreement with the finite element ones at the positions of interest.

It is worth outlining that it is possible to reduce the variable space, considering every temperature and not only 5 ones thanks to a proper orthogonal decomposition (POD) method and the associated mods. Even if the obtained results are satisfying, it is worth noticing that they can be improved with further and more sophisticated features or model optimization. Moreover, with more data, the predictions could be more accurate and provide a higher threshold of confidence. In the light of the obtained results, the proposed modeling can be used in induction treatment process optimization and extended to predict other mechanical multiaxial fields.

3.3 Article 3 : Artificial intelligence modeling of induction contour hardening of 300M steel bar and C45 steel spur-gear

Sevan Garois, Monzer Daoud, Khalil Traidi and Francisco Chinesta. Published in Internation Journal of Material Forming in April 2023.

Induction hardening is a heat surface treatment technique widely employed for steel components in order to improve their fatigue life without affecting the metallurgy of the bulk material. The control of the treated components goes through the prediction and the optimization of the induction hardening process parameters. The aim of this work is to propose an approach based on artificial intelligence technique to predict the in-depth hardness profile. For this purpose, experimental tests were first carried out on 300M steel bar and C45 steel spur-gear under single and double frequencies, respectively. Intermediate variables were then generated to be used as input data. Data-driven model based on XGBoost library was finally developed. It was found that the proposed approach predicts with good agreement the hardness profiles and can be used in induction treatment process optimization.

Keywords: Induction hardening ; Hardness ; Artificial intelligence technique ; Data-driven model ; XGBoost

3.3.1 Introduction

Induction hardening is a multi-physics process which is widely employed to enhance the fatigue behavior of many critically loaded mechanical workpieces in automotive and aerospace industries. During the process, redthe ferrous components such as steel grades are rapidly heated to a very high temperature (heating phase), then quickly cooled to room temperature (quenching phase) [168]. As a result, a fine-grain martensite phase [12, 13] as well as a compressive residual stress field [2] are induced in the superficial layer which enhance fatigue life of engineering components [9, 10]. Industries use more and more this process because it provides a high quality over time, good repeatability, fast, and clean processing for precise heating of the interested zones without affecting the metallurgy of the bulk material. [16, 126].

The main process parameters are the frequency, power level of the employed source currents, and heating time. Depending on how the frequency is applied, there are two usual heating approaches that can impact the heating phase. The former is induction with a single-frequency and the latter one consists of combining two different frequencies, medium and high frequencies, applied simultaneously or sequentially. These two approaches have been employed in numerical and experimental investigations. It is worth mentioning that these two approaches have differences in terms of precision and quality of the treatment[17]. In fact, the use of a double-frequency induction heating allows a full hardening of the superficial layer of a complex geometry, which can be incomplete with the single-frequency heating

[18].

In practical applications, an appropriate selection of the process parameters is highly important to carry out a desired contour free of cracks. Many experimental investigations have been carried out to study this induction surface hardening process. These investigations have focused on the influence of process parameters on the induced residual stresses of hardened cylindrical specimens [169], the relationship between the change in mechanical properties and the microstructure of 45 steel bars [170], the effects of different quenching parameters on distortion of cylindrical parts [171], the influence of different grinding parameters on residual stress results [172], the effects of spray cooling for gearwheel induction [173], the consequences of the variation of initial hardness level of discs on the distortion and hardening depth [174]. However, experimental approach is not only time consuming but requires significant experimental tests for a restricted validation range. More promising approach for orienting and optimizing the experimental activity is provided by numerical techniques such as the finite element method (FEM). It has proven to be highly efficient for dealing with multiphysics-based parametrized problems thanks to the advanced numerical simulation codes [175]. Consequently, a large number of research works has focused on the use of FEM to analyze the hardness [176, 159], the temperature field [177, 178], the residual stress fields [44] and the microstructure [159, 179].

Although the different mechanical and microstructural fields are predicted, 3D-FEM still suffers from some drawbacks. To name a few, they are high computational cost, supporting the use of multiple frequencies, and data exchange between solvers [180, 181].

Several analytical models have been proposed and used mainly to describe the phenomena involved during the induction hardening process [33, 34, 31, 32, 35]. However, these models are very limited by the geometry of the inductor and the workpiece. This made way to integrate analytical models to the FEM to solve the coupled electromagnetic-thermomechanical problem [182, 183]. The computational time, however, is still too high.

In recent years, the rise of different machine learning algorithms, coupled with more efficient optimization techniques, allows a relevant alternative for this type of analyses [184, 95, 185]. Machine learning represents different techniques such as Artificial Neural Network (ANN), Random Forest (RF) or Gradient-Boosted Trees (GBT). The classical machine learning pipeline (sequence of actions) for modeling is used to analyze the data, treat the variables, split them into train and test sets, fit and construct the model, predict the results with testing data, and compare the model predictions with

the ground truth to quantify the result error. ANN are regularly involved in metallurgy analysis under induction heating [94], surface hardness in carburizing quenching [93] and in laser hardening [92], and various mechanical properties in metal rolling [186]. ANN appears to be one of the most suitable technique here. Also, machine learning algorithms from the XGBoost library [125] are recognized of being efficient in some challenges while being convenient in the use and optimization [187]. Despite the relative well-known lack of data in the field of metallurgy, it is possible to propose reliable models. In fact, XGBoost has been used with success for predicting some mechanical properties like hardenability [86] and tensile strength, compressive strength, and elongation of hot-rolled strips [43] using small and big datasets, respectively.

The literature review shows a particular interest on both single and double-frequency induction hardening experiments [188] either to validate results obtained by modeling in FEM [189] or to optimize the process parameters [190]. Studying both of them should be interesting anyway.

This work aims at proposing an approach based on artificial intelligence technique to build more predictive fast running models of the induced hardness profile within a cylindrical bar of 300M steel alloy and spur-gear of C45 steel during the induction heating process. To conduct such a study, experimental data under single and double frequencies are presented in Section 2. Section 3 concerns the development of data-driven model based on XGBoost library to predict the hardness profile under the effect of the process parameters. The obtained results are presented and discussed in Section 4. The main conclusions and the relevancy of the work are exposed in Section 5.

3.3.2 Experimental procedure

3.3.2.1 Induction hardening of cylindrical bars

The first series of experiments were conducted on a cylindrical bar made of 300M low alloy steel. The process parameters are listed in Table 3.10. During these experiments, samples rotated around a vertical axis and each one was used to carry out several induction treatments at different positions sufficiently spaced to avoid any eventual interaction effects which was verified by the infrared camera. The heating phase was carried out by a ring inductor encircling the sample and having a rectangular shape of 2x5mm and an air-gap of 3mm while the subsequent cooling shower of a polymer-water mixture was applied by another coaxial ring as shown in Figure 3.21. During heating, temperature measurements on surface were obtained using a bichromatic pyrometer (see Table 3.10) while the

in-depth temperature profile was predicted based on FEM (see Figue 3.22). Micro-hardness Vickers (HV0.3) profiles were carried out in the radial direction of the sample in order to determine the penetration hardening. These analyses were performed after the induction treatment and performed on a transversal section according to ISO 6507 [121].

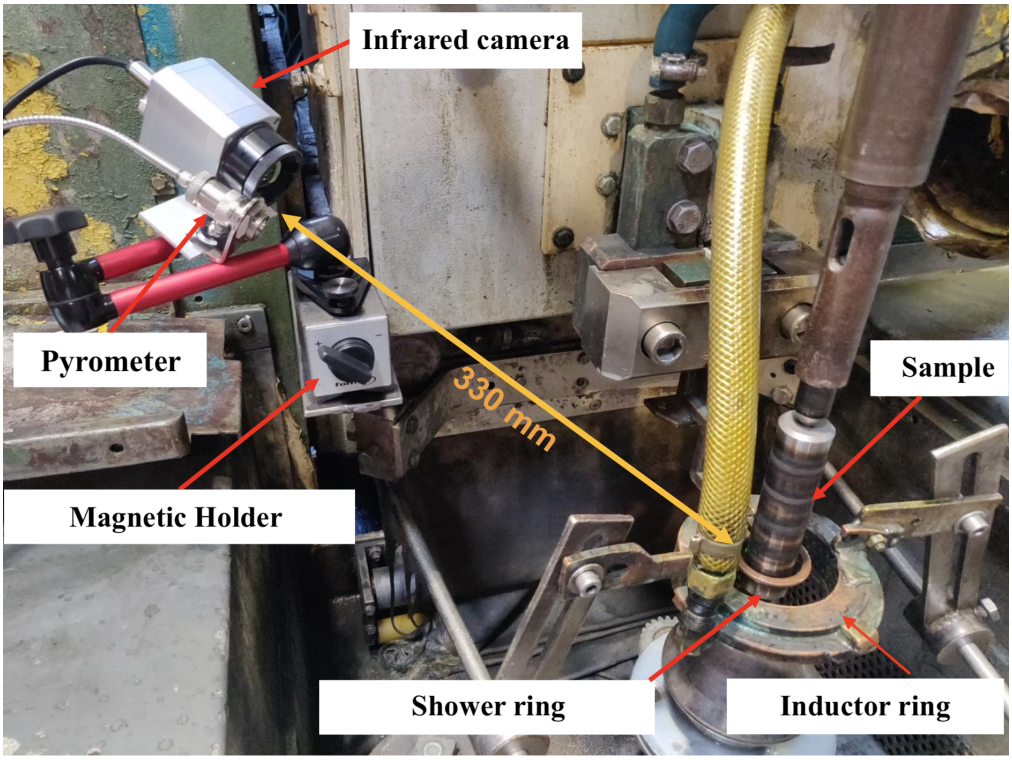

Figure 3.21: Experimental setup utilized during the induction hardening treatment of cylindrical bars under a high single-frequency

Table 3.10: Induction heat treatment conditions for cylindrical samples

Run #	Frequency F (kHz)	Power P (kW)	Time t (s)	Temperature T (°C)
1	224	33	0,15	892
2	224	33	0,2	958
3	224	33	0,3	1008
4	224	33	0,85	1121
5	224	33	1,3	1265
6	224	19	1	927
7	224	19	3.0	1034
8	224	19	3,5	1134
9	224	19	4,5	1277
10	224	49	0,15	1025
11	224	49	0,2	1142
12	224	49	0,08	1085

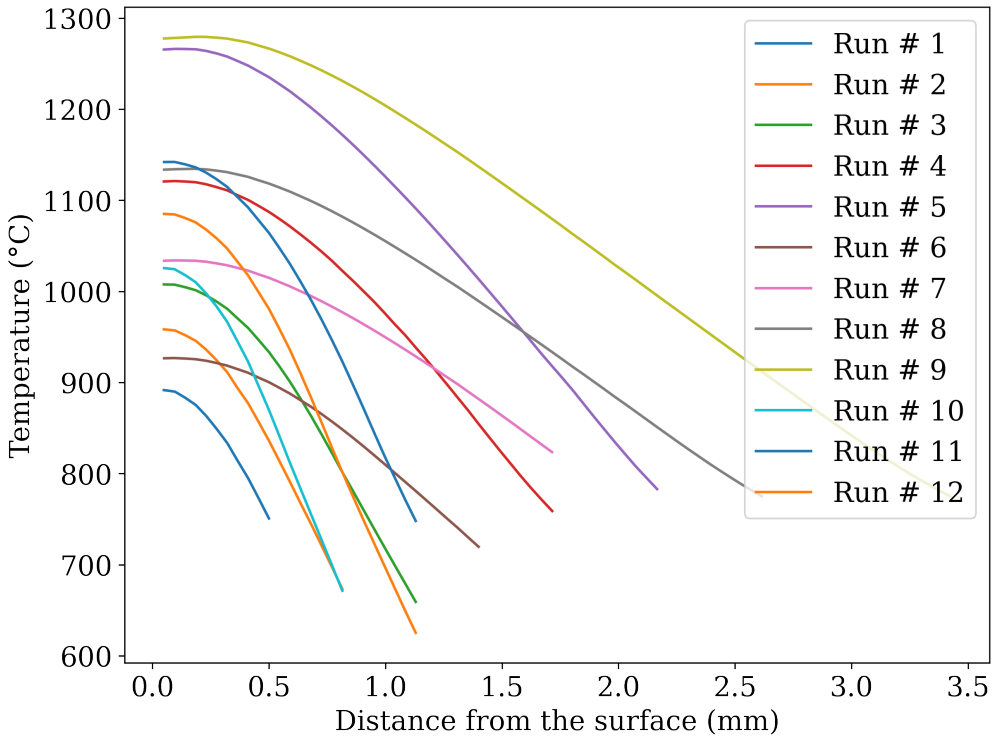

Figure 3.22: Predicted in-depth temperature profiles by FEM for experimental runs

3.3.2.2 Induction hardening of gears

The second series of experiments were carried out on C45 steel spur gears. The main gear data were summarized in Table 3.11 while the process parameters were listed in Table 3.12 and Table 3.13. For these experiments, gears were mounted on a rotating chuck during the process. An Optris pyrometer was used to measure the temperature on surface at the tooth root during the treatment. The heating phase was conducted with ring inductor encircling the sample having a rectangular shape of 12.25x20mm and an air-gap of 2mm while the subsequent cooling shower of a polymer-water mixture was applied by another coaxial ring as shown in Figure 3.23. Micro-hardness Vickers (HV0.3) profiles were carried out in the radial direction of the sample at the tooth tip and the tooth root in order to determine the penetration hardening on these two locations. These analyses were performed after the induction treatment and performed on a transversal section according to ISO 6507 [121].

Table 3.11: Gear data for double-frequency induction hardening experiments

Gear #	Module	No. of teeth	Width	Addendum circle	Pitch circle	Root circle
1	2.5	22	10 mm	60 mm	55 mm	48.75 mm
2	3	18	10 mm	60 mm	54 mm	46.5 mm

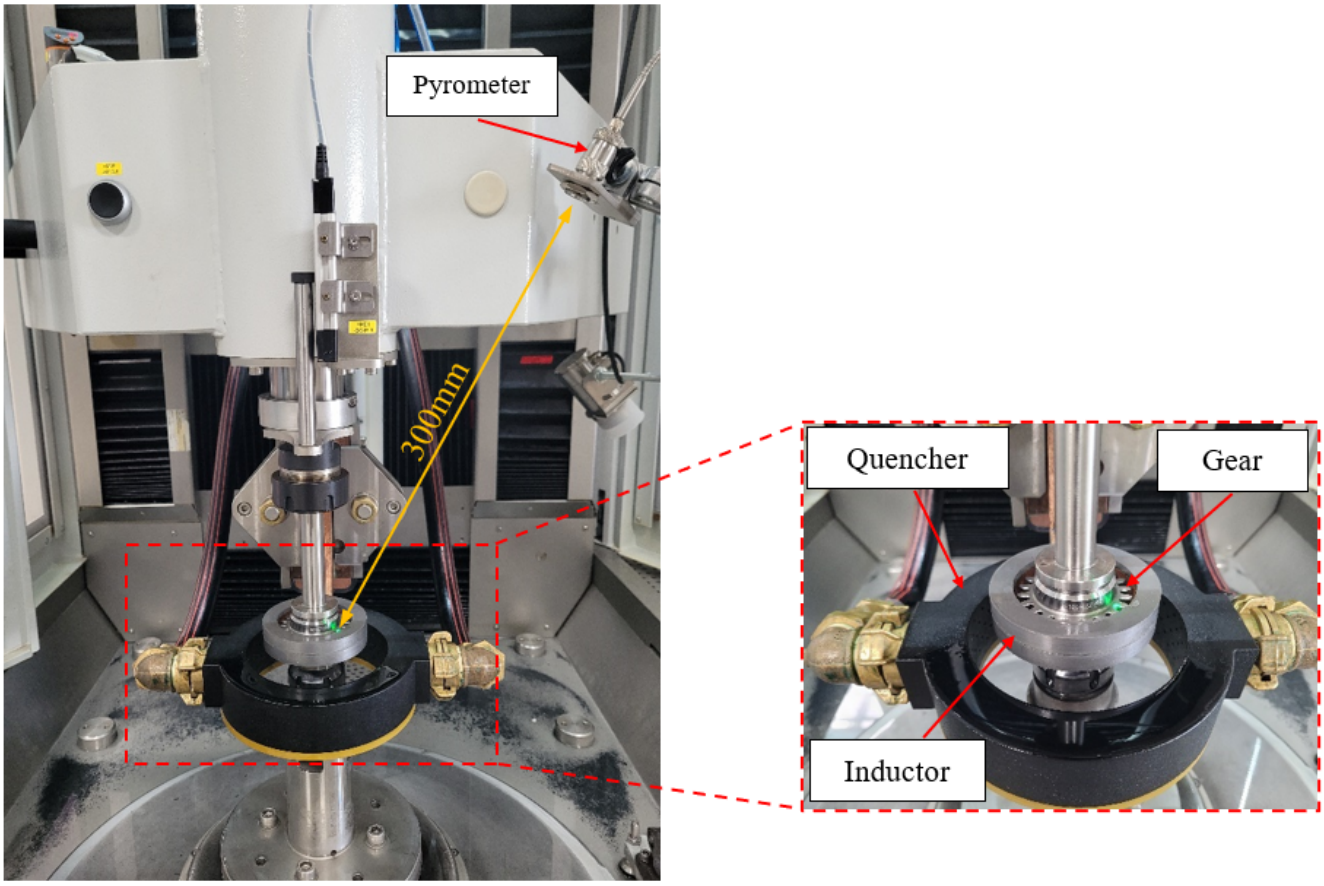

Figure 3.23: Experimental setup utilized during the induction hardening treatment of gears under a double-frequency

Table 3.12: Induction heat treatment conditions for gears with module m=2.5

Run #	Medium Frequency MF (kHz)	High Frequency HF (kHz)	Power of HF P_{HF} (kW)	Power of MF P_{MF} (kW)	Time t (s)	Temperature T (°C)
1	13	256	143	88	0,17	780
2	12	258	225	138	0,17	1080
3	12	258	225	138	0,2	1200
4	12	257	143	113	0,17	835
5	12	258	184	113	0,17	935
6	12	258	225	113	0,17	1005
7	13	257	143	113	0,2	×
8	13	257	184	88	0,2	917
9	13	257	184	138	0,24	1189
10	13	257	143	138	0,2	1059
11	12	257	184	113	0,2	1025
12	13	257	184	88	0,24	1028
13	12	258	225	88	0,2	999
14	13	257	143	88	0,24	925
15	12	258	225	113	0,24	1167
16	12	258	225	88	0,17	900
17	12	257	184	138	0,17	1005
18	13	257	143	113	0,24	1039
19	13	257	143	138	0,24	1145
20	12	258	225	138	0,24	1217
21	12	258	225	88	0,18	884
22	12	258	198	134	0,17	920
23	×	×	238,5	94	0,17	890
24	×	×	247,5	98	0,19	958
25	12	257	202	110	0,17	884
26	×	×	175,5	102	0,19	889
27	12	257	202,5	118	0,17	887
28	×	×	193,5	102	0,19	876
29	×	×	238,5	88	0,19	906
30	×	×	247,5	88	0,19	905
31	×	×	247,5	94	0,17	858

×: missing values

Table 3.13: Induction heat treatment conditions for gears with module m=3

Run #	Medium Frequency MF (kHz)	High Frequency HF (kHz)	Power of HF P_{HF} (kW)	Power of MF P_{MF} (kW)	Time t (s)	Temperature T (°C)
1	12	254	143	88	0,17	800
2	12	256	225	138	0,17	1100
3	12	255	225	138	0,2	×
4	12	254	143	113	0,17	×
5	12	255	184	113	0,17	969
6	12	256	225	113	0,17	992
7	13	254	143	113	0,2	982
8	12	255	184	88	0,2	909
9	13	255	184	138	0,24	1166
10	12	254	143	138	0,2	1075
11	12	255	184	113	0,2	1040
12	12	255	184	88	0,24	1025
13	12	255	225	88	0,2	1025
14	12	254	143	88	0,24	959
15	12	255	225	113	0,24	1197
16	12	256	225	88	0,17	970
17	12	255	184	138	0,17	1045
18	12	254	143	113	0,24	1030
19	12	254	143	138	0,24	1135
20	12	256	225	138	0,24	1293

It is worth noting that the frequency ranges from 12 to 14 kHz in MF and from 150 to 350 kHZ in HF. The final measured frequency depends on the torque between the gear and the inductor. So, the measured frequency will not be the same, especially in high frequency. It is clear that the frequencies are not the main variable to describe the system due to their slight variation. This point will be investigated in next sections.

3.3.3 Hardness modeling

3.3.3.1 XGBoost algorithm

In the present work, the EXtrem Gradient Boosting (XGBoost) algorithm was chosen because it is one of the most effective boosting tree algorithms for gradient boosting machine (GBM) and highly efficient for machine learning prediction problems with a few pre-processing requirements [191, 192]. It has the advantage of being convenient and easy to test and manipulate because there is no need to search and optimize an architecture like neural networks: only a few hyperparameters related to the

trees such as the maximum depth or the number of estimators. Moreover, it has been proven that the XGBoost is robust enough [193, 194] while requiring a satisfying training time. Finally, it is worth mentioning that the largest available dataset in the present work is the combined data from the two studied gears which has only 2000 data points: it is not large enough for deep learning algorithms but represents an interesting amount of data for the use of XGBoost algorithm. XGBoost is based on gradient-boosted decision-tree algorithm. In fact, XGBoost build sequentially a forest of gradient boosted decision trees.

Each iteration of a tree compute the residuals r_k of each k observed value $y_{obs,k}$ of the dataset with respect to a predicted value $y_{pred,k}$:

$$r_k = y_{obs,k} - y_{pred,k} \tag{3.22}$$

The residuals are collected in the first leaf of the tree called the root node. The goal is to split considering a threshold condition on a given variable. Each possible split is defined by the average value between two consecutive observed data points. The residuals are used to compute the similarity score S, which is defined as

$$S = \frac{(\sum_{k=1}^{m} r_k)^2}{m + \lambda} \tag{3.23}$$

where m is the number of residuals and λ is the user-defined regulation hyperparameter. Depending on the value of S, the different residuals are set into the right and left leaves given the chosen split, making new similarity scores. In fact, S score of the root node and the left and right leaves are used to calculate the gain G such as:

$$G = S_{left} - S_{right} - S_{root} \tag{3.24}$$

The split inducing the highest gain G is kept. Then, splits can be made again on the lastest nodes. A branch with a negative gain should be removed as the tree is pruned. The output value of the full tree is expressed as:

$$y_{output} = \frac{\sum_{k=1}^{m} r_k}{(m + \lambda)} \tag{3.25}$$

The predicted value of the tree $\hat{y}_n$ using the previous one $\hat{y}_{n-1}$ and the output y_{output} of the built tree is obtained as follows:

$$\hat{y}_n = \hat{y}_{n-1} + \eta \cdot y_{output} \tag{3.26}$$

where η is the learning rate. If $n = 1$, y_0 is a default value. Now a single tree is built and the predicted values $\hat{y}_n$ are involved for the calculation of the residuals of the next tree. The goal is to minimize the

residuals to a value close to 0. When all trees are built it is possible to compute a final and accurate prediction $\hat{y}$, it is defined as a weighted sum of trees output and can be written as:

$$\forall i \in [1; n], \quad \hat{y} = \sum_{i=1}^{n} \eta \cdot y_{output,i} \tag{3.27}$$

where n is the final number of trees. The final ensemble of trees can be summarized in Figure 3.24.

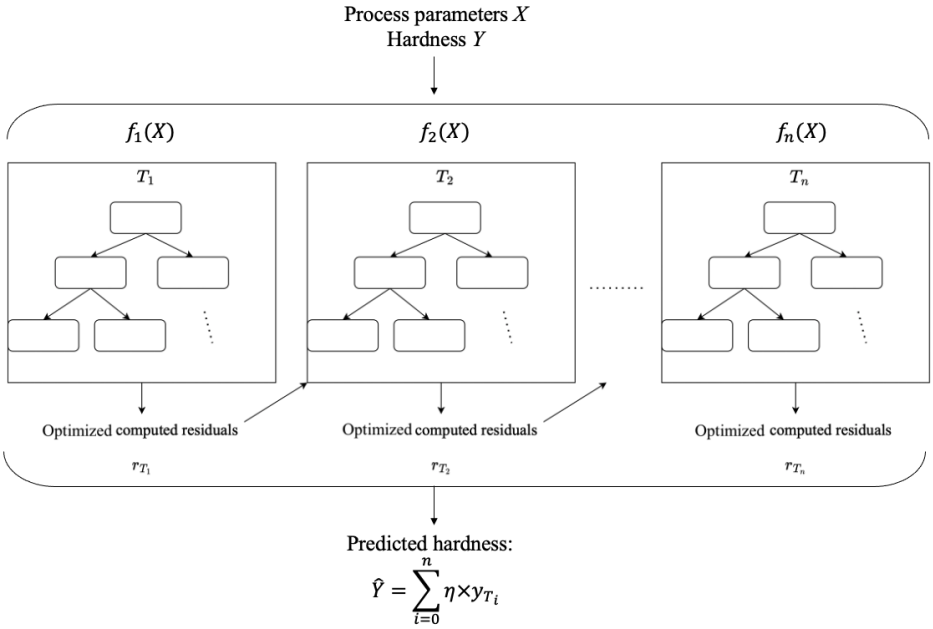

Figure 3.24: Ensemble of the XGBoost trees

3.3.3.2 Extraction of intermediate parameters

Extraction of intermediate parameters of any system for the training phase is highly important. This is because, in the present work, the temperature profiles and the surface temperature for cylindrical bars and gears, respectively, were considered as an important parameter to describe the hardness. In fact, preliminary analysis have shown that first results lacked of accuracy without it. The temperature is not a machine parameter and requires a particular system (pyrometer of thermocouple) to be measured which is not present in the industrial case. Therefore, the temperature was predicted to be used as input for hardness modeling. Predictions were carried out using XGBoost algorithm using the process parameters previously listed in Table 3.12 as input without any further optimization. Figures 3.25 and 3.26 show the comparison between the real and the predicted heating temperature for cylindrical bars and gears, respectively. The test error for both predictions was found to be 1.5%

and 0.24%, for cylindrical bars and gears, respectively. These results indicated that the XGBoost algorithm gave a good prediction of the heating temperature.

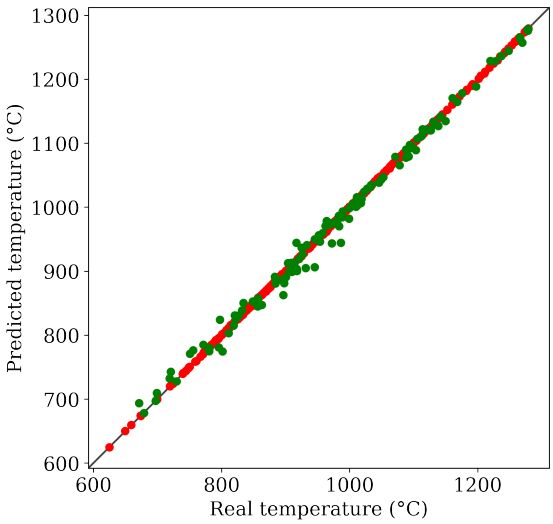

Figure 3.25: Predicted versus real in-depth temperatures for cylindrical bars showing training (red) and testing (green) data points

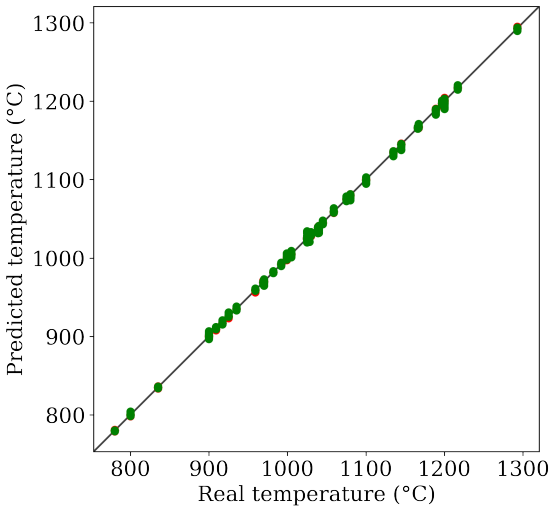

Figure 3.26: Predicted versus real surface temperatures for gears showing training (red) and testing (green) data points

3.3.3.3 Determination of space of variables for different cases

In order to use all the collected data with some missing ones, it is necessary to consider several cases.

3.3.3.3.1 Experiments carried out on cylindrical bars The space of variables for the induction hardening of cylindrical bars is expressed as:

$$X_{1f} = \{F, P, T, d, t\} \tag{3.28}$$

where F is the frequency; P is the generator power; T is the in-depth temperature; d is the depth at which the hardness was measured and t is the heating duration.

3.3.3.3.2 Experiments carried out on gears In general, the space of variables for the induction hardening of gears could be expressed as:

$$X_{2f} = \{MF, HF, P_{MF}, P_{HF}, T, d, t\} \tag{3.29}$$

where MF and HF are the medium and high frequency respectively; P_{MF} and P_{HF} are their respective generator powers; T is the temperature measured at the side surface close to the tooth root; d is the depth at which the hardness was measured, and t is the heating duration.

Case 1: Cloud of points-based dataset from both modules The space of variables could be expressed as:

$$X_{C1} = \{MF, HF, P_{MF}, P_{HF}, T, t, d\} \tag{3.30}$$

The dataset is composed of two subsets of 20 runs each for each gear module. In this first case, the two subsets are merged to make a greater dataset allowing to verify if there is a significant difference of the hardness measured between the two gear modules data. This dataset contains a total of 2215 randomly mixed data points. Usually, and in the rest of this work, 70% of the dataset is considered for training, leaving 30% to the testing phase. Here, it represents 1697 training points versus 518 testing points

Case 2: Cloud of points-based dataset added from module 2.5 gear The second case brings new data concerning the gear with module 2.5 with 4 extra runs added to the initial induction heat treatment conditions. The space of variables remains as case 1:

$$X_{C2} = \{MF, HF, P_{MF}, P_{HF}, T, t, d\} \tag{3.31}$$

In this case, 1058 points were considered for training, leaving 322 to the testing phase.

Case 3: Cloud of points-based dataset with frequencies taken off In this case, the modeling was carried out without frequencies and hence the space of variables is given as:

$$X_{C3} = \{P_{MF}, P_{HF}, T, t, d\} \tag{3.32}$$

In this case, 1426 points were considered for training, leaving 434 to the testing phase.

Case 4: Profiles-based dataset without frequencies In this case, data points were aggregated into profiles with respect to their run. Therefore, 24 profiles were considered for training, leaving 7 profiles to the testing phase.

3.3.3.4 Data smoothing and experimental variation area

Experimental data are noisy because of the intrinsic physical variability and the uncertainty of measurements. Therefore, it is interesting to smooth the data to increase model training ease. The data to be smoothed are the hardness profiles. There are several statistical methods for reducing output noise. For this work, the method of Kernel Regression [195] was chosen because it implies a conditional expectation. Figure 3.27 shows the smoothed in-depth hardness profile.

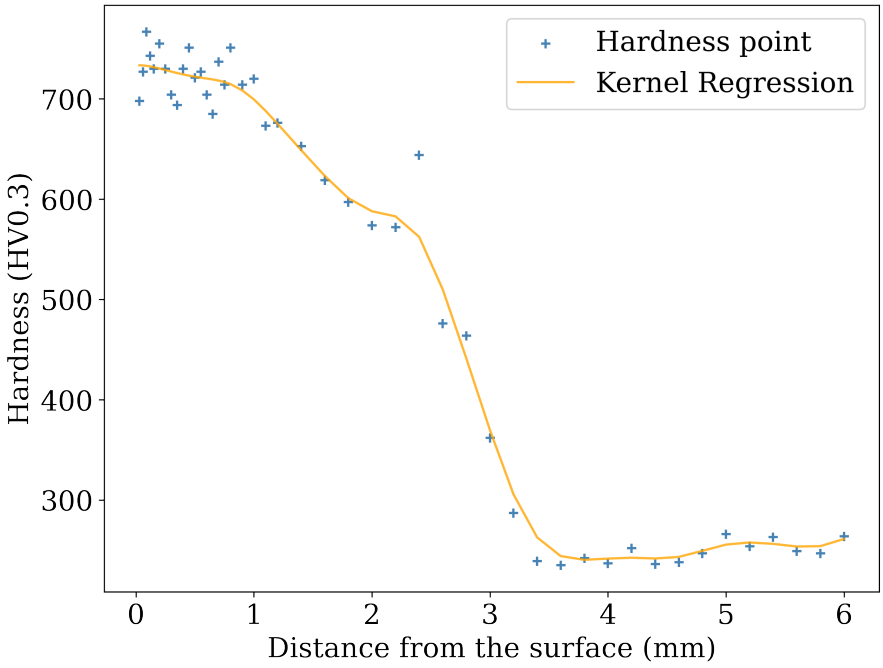

Figure 3.27: Smoothed in-depth hardness profile using Kernel regression

Moreover, after applying Kernel Regression to smooth the data, the noisy nature of the data was taken into account by integrating an experimental variation area. Each smoothed point has a higher and lower hardness point defining the experimental variation area. This area was considered up to ±5% of the smoothed hardness as set by industrial practice and will be illustrated in the next Figures as a light-red zone.

3.3.3.5 Optimized data selection

Specifically for the case 4, because each run belongs to only one set, either train or test, the number of different values for each variable is restricted in each. Hence, the train test split stage has particularly a large impact on the final result because all patterns are not necessarily represented in the training set. To have the most suitable patterns in the training set, a selection is made for the training set based on the test results so the predictions could be more accurate. This allows to avoid extrapolation and to take data that are more likely to train the model.

3.3.4 Results and discussion

3.3.4.1 Hardness profile prediction in the cylindrical bar

A Random Forest (RF) regressor as well as the XGBoost model were used for a comparative investigation. The metrics used to evaluate the results are the Root Mean Squared Error (RMSE) and the Root Mean Squared Percentage Error (RMSPE) which is a relative error. They are defined as follows in Eq 3.33.

$$\begin{aligned} RMSE &= \sqrt{\frac{1}{n}\sum_{i=1}^{n}(y_{pred} - y_{true})^2} \\ RMSPE &= \sqrt{\frac{1}{n}\sum_{i=1}^{n}(\frac{y_{pred} - y_{true}}{y_{true}})^2} \times 100 \end{aligned} \tag{3.33}$$

where y_{true} and y_{pred} are the real hardness and the predicted one, respectively. As can be seen in Table 3.14, although the RF shows good results, the XGBoost gives better prediction with smaller relative errors. It is worth mentioning that even though this problem involves complex multi-physical behavior, the geometry being a simple cylinder makes it relatively easy to treat. Hence, it is clear that the results are good enough and that the RF could be considered as an alternative approach.

Table 3.14: XGBoost and Random Forest results for hardness prediction for cylindrical bars

Model	XGBoost	Random Forest
$RMSE_{train}$	5.57	11.14
$RMSE_{test}$	28.64	32.73
$RMSPE_{train}$	**0.93%**	**2.17%**
$RMSPE_{test}$	**5.42%**	**6.37%**

Figure 3.28 shows the predicted and experimental in-depth hardness profiles. As shown in this figure, three zones could be identified from the surface: a hardened zone, a transition zone where the hardness drops drastically, and the core of the workpiece unaffected by the induction treatment. Although the predicted profile exceeds the experimental variation area at certain zones, it appeared that the predicted profiles gave the same trends and the same type of hardness level at surface as the measured ones.

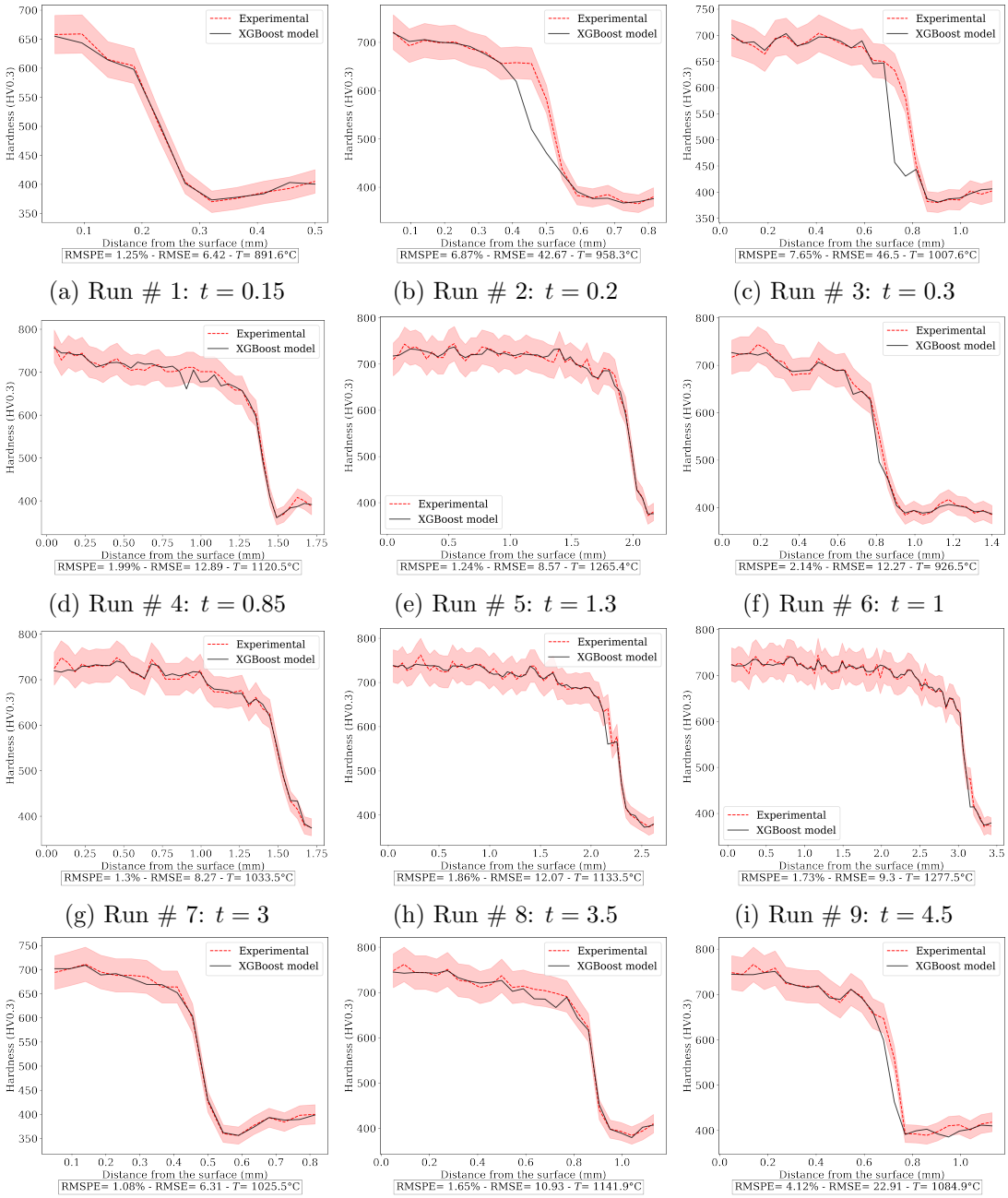

(a) Run # 1: $t = 0.15$ (b) Run # 2: $t = 0.2$ (c) Run # 3: $t = 0.3$

(d) Run # 4: $t = 0.85$ (e) Run # 5: $t = 1.3$ (f) Run # 6: $t = 1$

(g) Run # 7: $t = 3$ (h) Run # 8: $t = 3.5$ (i) Run # 9: $t = 4.5$

(j) Run # 10: $t = 0.15$ (k) Run # 11: $t = 0.2$ (l) Run # 12: $t = 0.08$

Figure 3.28: Comparison of the XGBoost model with the experimental hardness for the cylindrical bars treated under single frequency. T represents the measured surface temperature.

3.3.4.2 Hardness profile prediction in the gear

All the errors obtained after modeling each of the different cases presented in Section 3 are analyzed and listed in Table 3.15. Firstly, for each cases the tooth tip seems to be easier to predict than the tooth root. This could be explained by the fact that there is comparatively more data in the tooth tip. However, it is noticeable that this tendency is reversed in the case of indivisible profiles. This could be explained by the fact that the profiles in the tooth are comparatively less diversive than in the tooth tip.

Secondly, it is interesting to see that whatever the case studied: different modules, different frequencies and powers, with or without frequency and profile-based dataset, the results remain more or less always precise. Therefore, there is a certain global efficiency to describe different cases for a global overview, despite some differences in the inputs.

In any case, the error being always lower than 10%, it is reasonable to say that the numerical results are encouraging and satisfying.

Table 3.15: Training and testing errors of the XGBoost models at the tooth tip and the tooth root for different cases

Case #	XGBoost Error	Tooth root	Tooth tip
1	$RMSE_{train}$	5.75	3.13
	$RMSE_{test}$	24.43	17.92
	$RMSPE_{train}$	**1.37%**	**0.80%**
	$RMSPE_{test}$	**6.93%**	**4.73%**
2	$RMSE_{train}$	7.53	2.4
	$RMSE_{test}$	24.75	19.27.
	$RMSPE_{train}$	**1.90%**	**0.57%**
	$RMSPE_{test}$	**6.44%**	**4.58%**
3	$RMSE_{train}$	7.97	3.21
	$RMSE_{test}$	28.90	18.73
	$RMSPE_{train}$	**2.02%**	**0.78%**
	$RMSPE_{test}$	**8.21%**	**4.84%**
4	$RMSE_{train}$	0.52	2.26
	$RMSE_{test}$	28.22	35.46
	$RMSPE_{train}$	**0.1%**	**0.54%**
	$RMSPE_{test}$	**6.07%**	**8.2%**

For the sake of clarity, only few results were presented in Figures 3.29,3.30 and 3.31. Nonetheless, more testing runs of the case 4 will be displayed because it is considered as a validation case. Finally,

it is worth mentioning that data from gear with module 3 are not modeled after case 1 because the results obtained in that case prove that it is possible with the data merged from both of these gears to have a relevant hardness prediction. Moreover, data from gear with module 2.5 has more and complete available data. Therefore, it was chosen for further modeling.

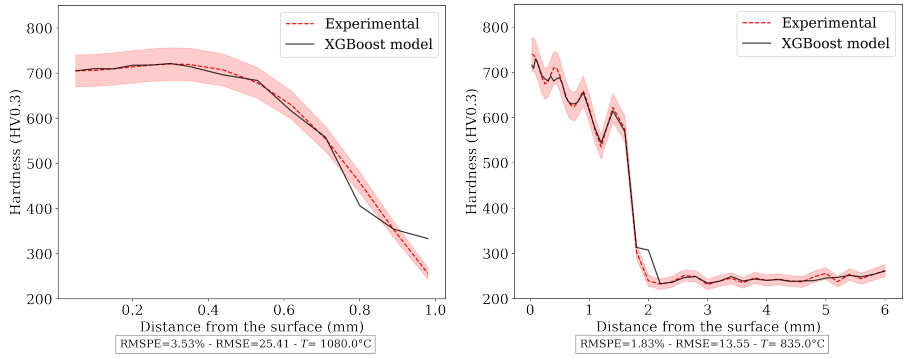

(a) Run # 2: toot root - module 2.5

(b) Run # 4: tooth tip - module 2.5

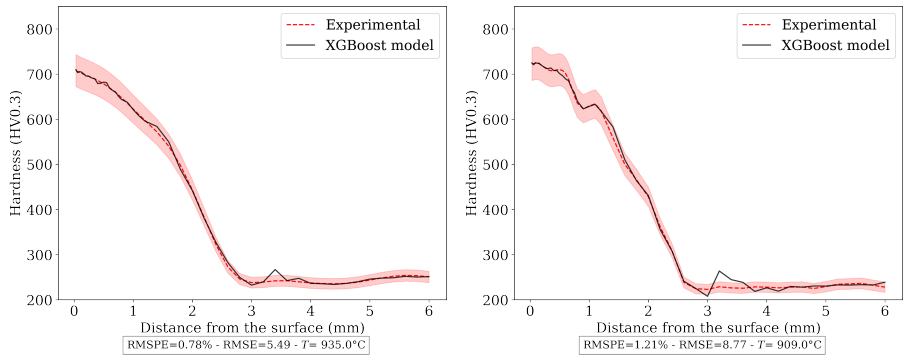

(c) Run # 5: toot tip - module 2.5

(d) Run # 8: tooth tip - module 3

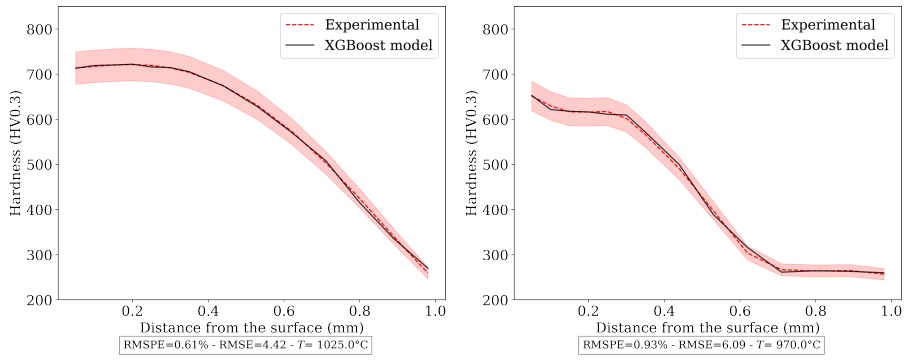

(e) Run # 11: toot root - module 2.5

(f) Run # 16: tooth root - module 3

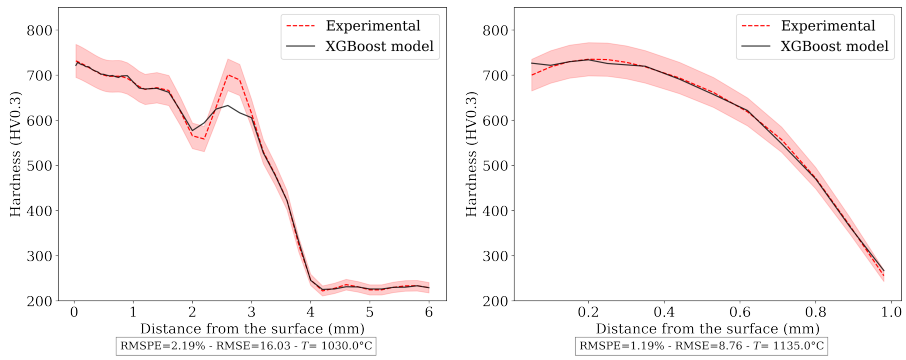

(g) Run # 18: tooth tip - module 3

(h) Run # 19: tooth root - module 3

Figure 3.29: Comparison of the XGBoost model with the experimental hardness for the gear treated under double frequency - Case 1. T is the measured surface temperature

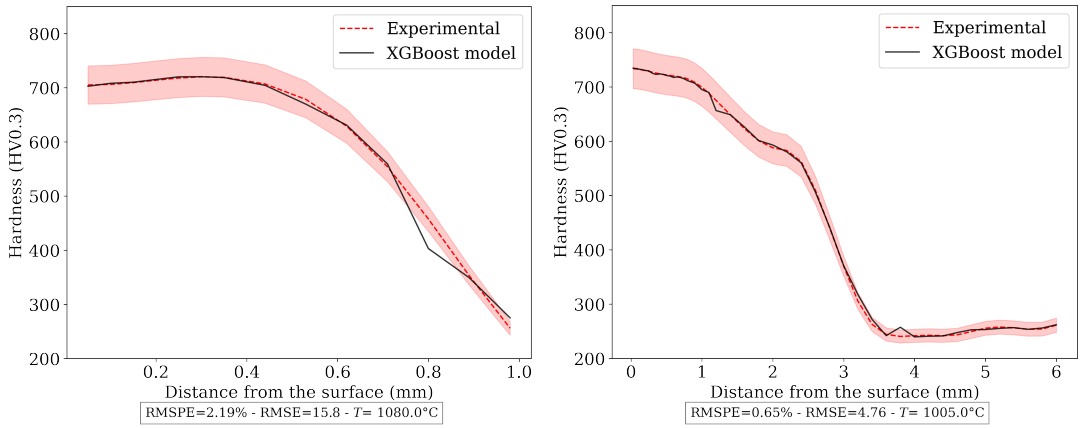

(a) Run # 2: tooth root

(b) Run # 6: tooth tip

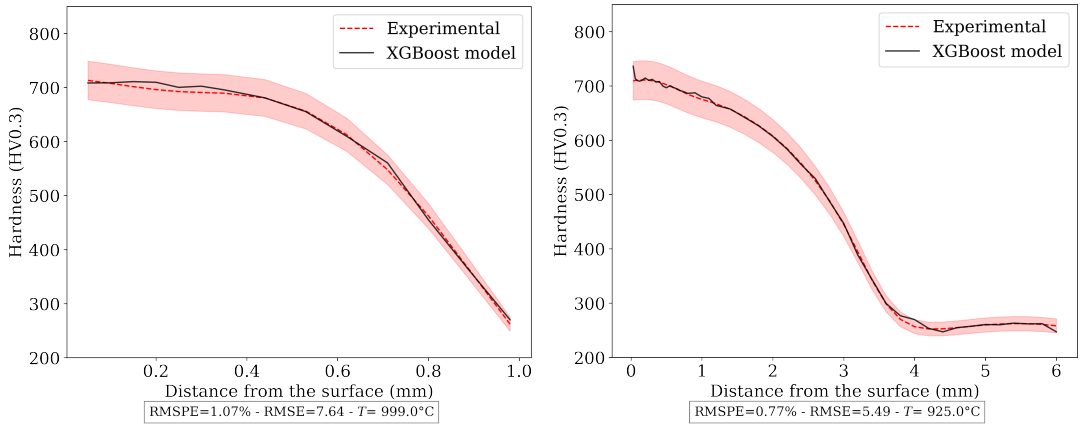

(c) Run # 13: tooth root

(d) Run # 14: tooth tip

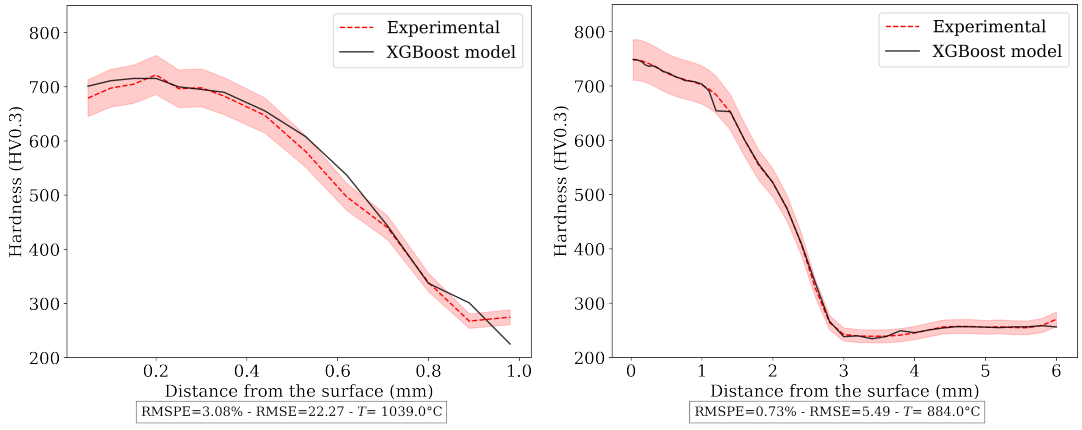

(e) Run # 18: tooth root

(f) Run # 23: tooth tip

Figure 3.30: Comparison of the XGBoost model with the experimental hardness for the gear treated under double frequency - Case 2. T is the measured surface temperature

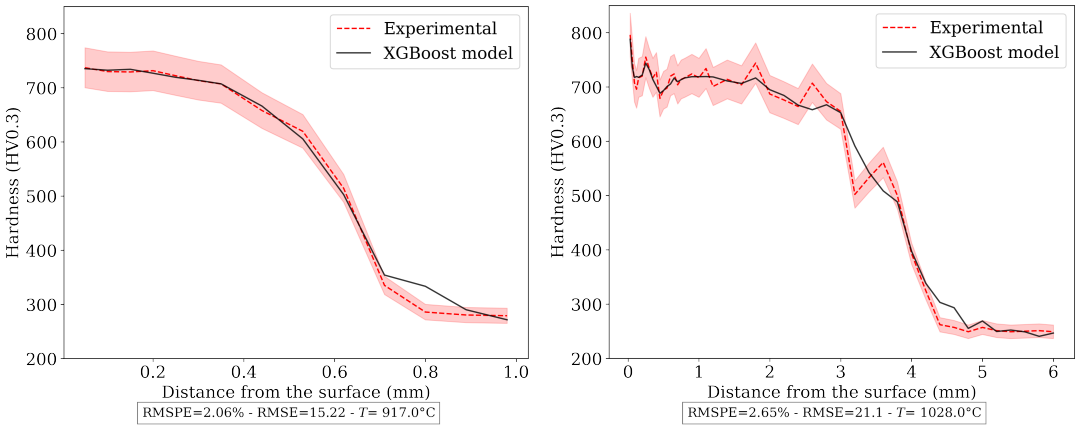

(a) Run # 8: : tooth root

(b) Run # 12: tooth tip

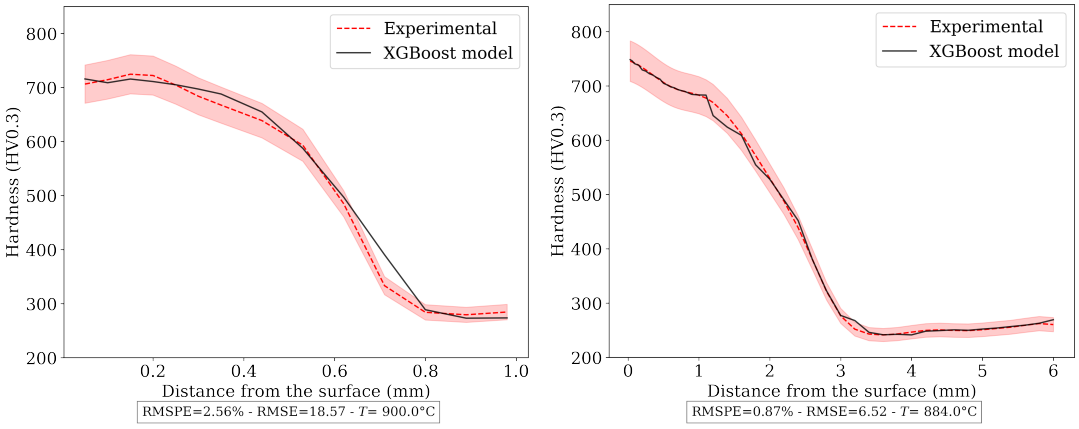

(c) Run # 16: : tooth root

(d) Run # 21: tooth tip

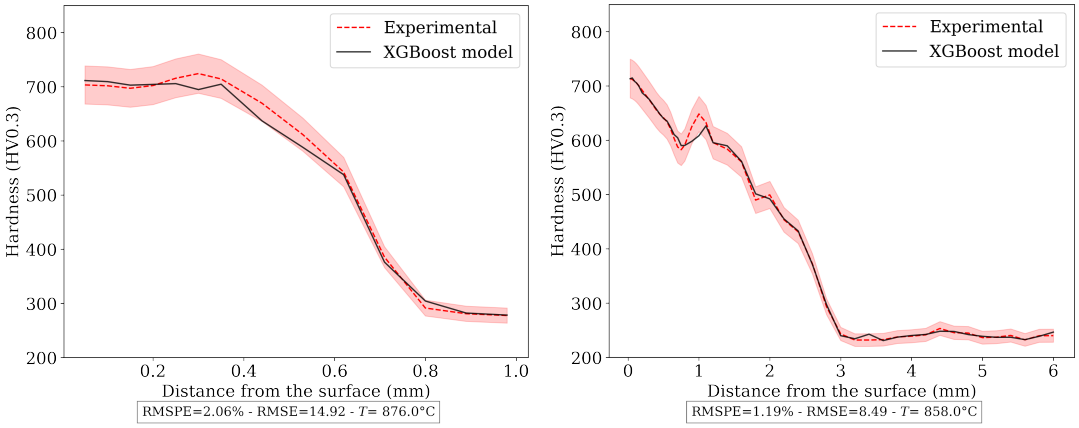

(e) Run # 28: tooth root

(f) Run # 31: tooth tip

Figure 3.31: Comparison of the XGBoost model with the experimental hardness for the gear treated under double frequency - Case 3. T is the measured surface temperature

It is clear that for each case, regardless of the illustrated run, The XGBoost predictions were in

good agreement with the experimental results.

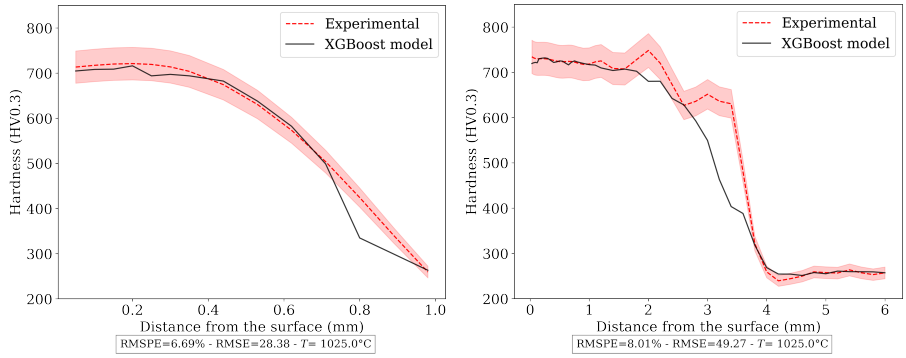

(a) Test Run # 11: tooth root

(b) Test Run # 11: tooth tip

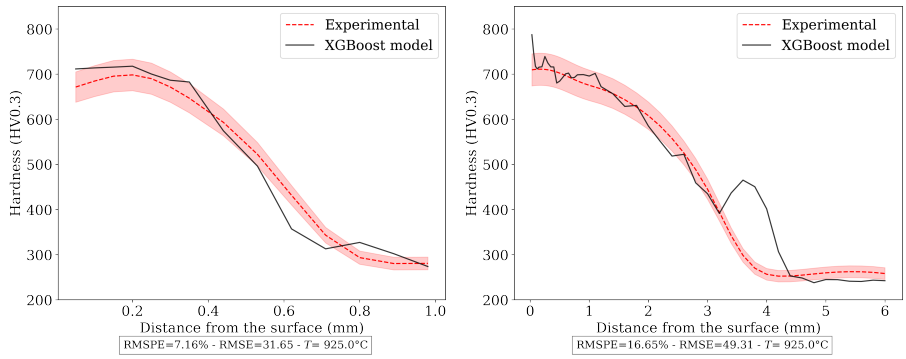

(c) Test Run # 14: tooth root

(d) Test Run # 14: tooth tip

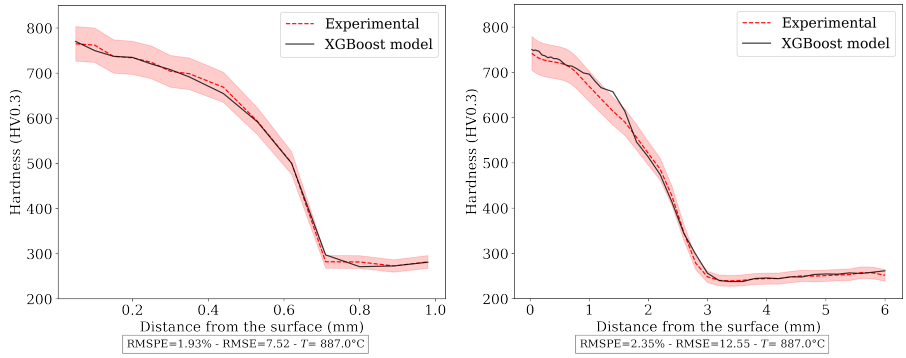

(e) Test Run # 24: tooth root

(f) Test Run # 24: tooth tip

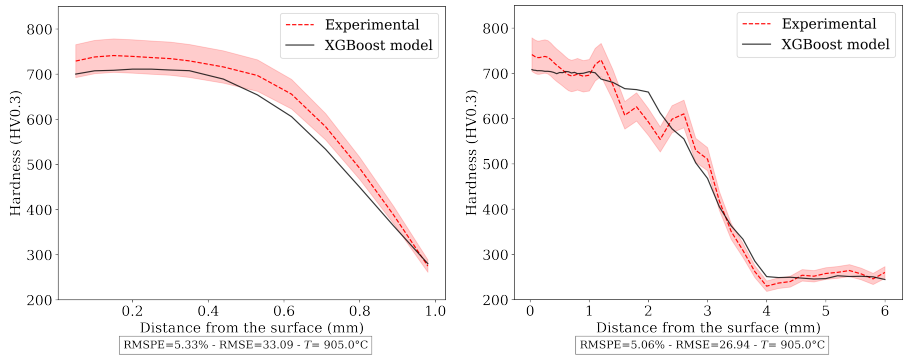

(g) Test Run # 30: tooth root

(h) Test Run # 30: tooth tip

Figure 3.32: Comparison of the XGBoost model with the experimental hardness for the gear treated under double frequency - Case 4. T is the measured surface temperature

Although some errors appear more remarkable than in the previous cases, as in Figure 3.32 (b), the XGBoost results are still in good agreement with the experimental hardness profiles and none of them is unconsistent. This case serving as a global validation of the ability of an XGBoost model to describe the hardness of an hardened gear, the model presented is quite efficient and accurate.

3.3.5 Conclusion

In this work, an approach based on artificial intelligence technique was developed to predict the in-depth hardness profile within 300M steel bar and C45 steel spur-gear. The capability of this approach to get a representative induction hardening treatment was evaluated and discussed. The main conclusions were as follows:

- Two experiments were carried out on cylinder bars and gears with single and double-frequency induction hardening, respectively. Data-driven models were developed based on XGBoost library, a tree-based gradient-boosted machine learning model.
- The low value of RMSPE and the accurate predicted profiles found indicated that the XGBoost model could adequately predict the hardness profiles.
- The space of variables did not have a significant impact on the training nor the testing results.
- Results showed that the XGBoost model predictions were in good agreement with experimental measurements in each case studied.

It is worth outlining that it is possible to improve the space of variables, considering in-depth temperature for the gear case and not only the surface temperature: it could be easier to describe the hardness. Even if the obtained results are satisfying, it is worth noticing that they can be improved with more runs considering more different process parameters. The predictions could be more accurate and provide a higher threshold of confidence. According to the obtained results, the proposed modeling can be used in induction treatment process optimization and extended to other geometries or treatments.

3.4 Article 4 : Explaining Hardness Modeling with XAI of C45 Steel Spur-gear Induction Hardening

Sevan Garois, Monzer Daoud and Francisco Chinesta. Submitted in Internation Journal of Material Forming in March 2023.

This work presents an interpretability study with XAI tools to explain an XGBoost model for hardness prediction in the simultaneous double-frequency induction hardening. Experiments were carried out on C45 steel spur-gear. In order to explain the model, firstly, the built-in tool of the XGBoost library was used to interpret the feature importance. Then, a more advanced approach with the SHAP library was employed to highlight local and global explanations. Finally, the implementation of an interpretable surrogate model allowed to illustrate rules for prediction, making the explanation, although approximate, clear. This study proposes a relevant approach of AI to explain the results obtained by black box models which is currently a major element for the industry allowing to justify the quality of the results in a clear way. It is concluded that the model is consistent with physical principles.

Keywords: XAI ; explicabilty ; machine learning ; induction hardening ; C45 steel ; spur-gear

3.4.1 Introduction

Induction hardening (IH) is one of the most compelling surface heat treatment processes widely employed in aerospace and automotive industries to enhance the fatigue behavior of many critically loaded mechanical workpieces [129, 16]. Two main stages defines IH: an electromagnetic induction heating and a subsequent quenching. Its advantages are providing a very short surface heating time, a precise check of the treated zone, a good reproducibility, and an operating mode compatible with environmental claims contrary to thermochemical treatments such as carburizing and carbonitriding [130]. As a result of the treatment, a fine-grain martensite phase [12, 13] as well as a compressive residual stress field [2] are induced in the superficial layer which enhance fatigue life of engineering components [9, 10]. These industries could want to highlight the mechanical structures in order to meet the relative environmental concerns to carbon dioxide emissions and fuel economy while maintaining optimal mechanical properties and performances. The heat treatment provides a valuable solution to give the material its optimal microstructures and mechanical properties, corresponding to the various performance criteria [126]. However, these criteria must be quantified to validate the the proper functioning of the treatment. Different approaches have been used to model this system with relevant results such as analytical modeling or finite element modeling (FEM) [131, 132, 133, 134]. However, in the terms of computational time it has been chosen to model the critical quality parameters of IH with machine learning algorithms. Because this process is a multi-physic system and need complex

and black box algorithms to be precisely modeled. Nowadays, there is a need to explain the results of these black-boxes, to interpret the AI.

In fact, interpretability of artificial intelligence models appears today to be a major issue in the sector of machine learning and AI [196]. A few years ago the accuracy of the models was the main goal, it is now essential to be able to explain the results of the models and understand their decision making. This field is called eXplainable Artificial Intelligence (XAI). Although the field of XAI is young and seldom made available in the literature, it has been much studied and standardized in theory, semantics, taxonomy, ... There are machine learning models capable of explaining themselves because their operation is basic or intuitive. It is the case of decision trees to name one [197]. However, with the increased complexity of models with neural networks at the forefront, models are no longer as easily explained. Therefore, it is necessary to find techniques to prevent the black box effect from persisting on the given model. This is the type of black model considered in the present work. It is possible to either explain the black-box model or take a model that is a white-box [198]. According to the literature [100, 199, 200], the problem of explaining a black-box can be divided into three distinct problems. The first one is called Explaining the model. The method consists in giving a global explanation of the black box model through an interpretable and transparent model. The idea is that this model can mimic the behavior and results of the former by an approximation while being understandable by the user. This predictor is assumed to be derived from the black-box model. Therefore the concept is to make two models in parallel that have the same goal and to make the interpretable be an approximation of the black-box predictor to understand what is going on by a kind of mirror effect. The second one is explaining the output. The problem of explaining the output is the same as explaining the model but at the local level. The idea is not to explain the entire logic of the model but a single result. This method is possibly more interesting than the first one, it allows to have a more local vision which could be simpler to implement while avoiding having two models for the same results. The final problem is the inspection of the model. The definition of the model inspection is such that a black-box model b with X the input data. The goal is to look for a representation r such that $r = f(b, X)$. Model inspection can also be a graphical representation of the most important variables with respect to the predictions.

XAI coupled with machine learning has been used on different domains to explain the logic behind black box models. Consequently, many works have been carried out with the scope of interpretability

such as the forecasting of NO_2 for air quality [201], the mapping of urban vegetation using images [202], the model of natural hazard like spatial drought [203], a machining variable visualization [204] and concerning austenite-grain growth [205], to name a few. In this work, the XAI was applied to the induction hardening process modeling. The authors believe that the IH process has not been studied yet in the scope of XAI. This work is about explaining black box models used for an hardness prediction with experimental data [206] using specifically an XGBoost model [124] presented in Section 2. The XAI methods for the three different problem evoked before in the introduction are presented in Section 3. Then, Section 4 is dedicated to the presentation and analysis of the results of the use of these tools in the context of XGBoost modeling for IH results using these tools.

3.4.2 Hardness modeling with XGBoost algorithm

In the present work, data-driven model based on experimental results and XGBoost library was developed to predict the in-depth hardness profile of C45 spur gear under the effet of the induction process parameters. The utilized gear data are shown in Table 3.16. To conduct such a modeling, a series of experiments (see Table 3.17) were carried out.

Table 3.16: Gear data for double-frequency induction hardening experiments

Module	No. of teeth	Width	Addendum circle	Pitch circle	Root circle
2.5	22	10 mm	60 mm	55 mm	48.75 mm

Table 3.17: Induction heat treatment conditions for gear

Run #	Medium Frequency MF (kHz)	High Frequency HF (kHz)	Power of HF P_{HF} (kW)	Power of MF P_{MF} (kW)	Time t (s)	Temperature T (°C)
1	13	256	143	88	0,17	780
2	12	258	225	138	0,17	1080
3	12	258	225	138	0,2	1200
4	12	257	143	113	0,17	835
5	12	258	184	113	0,17	935
6	12	258	225	113	0,17	1005
7	13	257	143	113	0,2	×
8	13	257	184	88	0,2	917
9	13	257	184	138	0,24	1189
10	13	257	143	138	0,2	1059
11	12	257	184	113	0,2	1025
12	13	257	184	88	0,24	1028
13	12	258	225	88	0,2	999
14	13	257	143	88	0,24	925
15	12	258	225	113	0,24	1167
16	12	258	225	88	0,17	900
17	12	257	184	138	0,17	1005
18	13	257	143	113	0,24	1039
19	13	257	143	138	0,24	1145
20	12	258	225	138	0,24	1217
21	12	258	225	88	0,18	884
22	12	258	198	134	0,17	920
23	×	×	238,5	94	0,17	890
24	×	×	247,5	98	0,19	958
25	12	257	202	110	0,17	884
26	×	×	175,5	102	0,19	889
27	12	257	202,5	118	0,17	887
28	×	×	193,5	102	0,19	876
29	×	×	238,5	88	0,19	906
30	×	×	247,5	88	0,19	905
31	×	×	247,5	94	0,17	858

×: missing values

During these experiments, gears were kept rotating around their axes and the heating phase was carried out by a ring inductor encircling the sample and having a rectangular shape of 12.25x20mm and an air-gap of 2mm while the subsequent cooling shower of a polymer-water mixture was applied by another coaxial ring as shown in Figure 3.33.

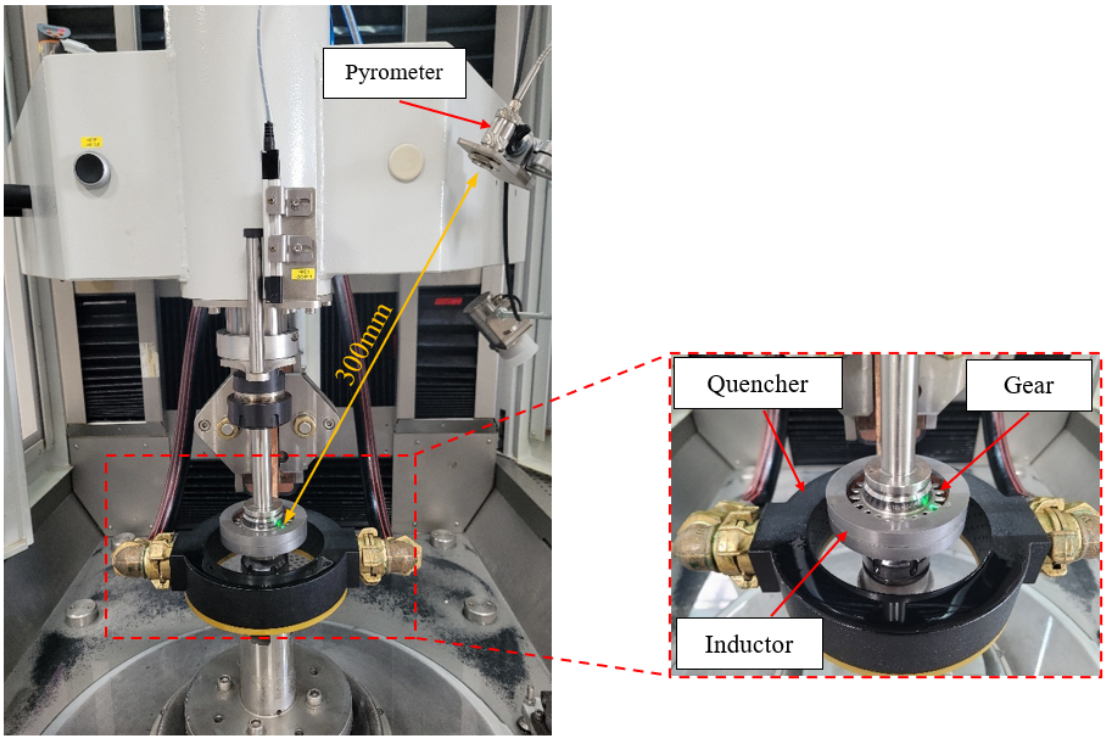

Figure 3.33: Experimental setup utilized during the induction hardening treatment of gears under a double-frequency

During heating, temperature measurements on surface at the tooth root was obtained using an Optris pyrometer. This temperature is considered on surface for simplicity for the rest of this work. Micro-hardness Vickers (HV0.3) profiles were carried out in the normal direction to the surface of the sample in order to determine the penetration hardening. These analyses were performed after the induction treatment and performed on a transversal section according to ISO 6507 norm [121].

The data are then collected and treated for further machine learning approach. The space of variable is defined as X

$$X = \{MF, HF, P_{MF}, P_{HF}, T, d, t\} \tag{3.34}$$

where MF and HF are the medium and high frequency respectively; P_{MF} and P_{HF} are their respective generator powers; T is the temperature measured at the side surface close to the tooth root; d is the depth at which the hardness was measured, and t is the heating duration.

The precise case used in this study is with frequencies taken off because as illustrated, both

frequencies being almost constant. Hence, the studied space of variables reduces to:

$$X = \{P_{MF}, P_{HF}, T, d, t\} \tag{3.35}$$

The data was agglomerated as profiles, and each of them is dedicated wheter to the training or the testing phase according to the usual 70/30% splitting. This makes the evaluation more relevant on the robustness of the model and avoid some bias.

Thanks to the data measured experimentally, it was possible to use a XGBoost algorithm to predict the hardness with a low time and computational cost while having a relatively low prediction error. However, the use of a black-box model involves the necessity of explanation of the results. To get a precise overview of the explanation, 3 analyses were conducted using 3 different methods. These methods are presented in the next section.

3.4.3 Methods to conduct XAI analysis

3.4.3.1 XGBoost built-in tool

The most common tool used for explaining the results of a model is the importance of input variables. In fact, the feature (or variable) importance is a relevant machine learning technique to check the impact of the variables using F-Score [207, 208]. Therefore, it is possible to take off those that could be ineffective and lead to biases or noise in the predicted results. There are three metrics to interpret the feature importance in the built-in tool of the XGBoost library. The first one is based on weights. It is the most basic metric of feature importance. It is the percentage representing the relative number of times that a particular variable is used as a splitting threshold across all trees. The second one is based on gain. It is the relative contribution of the corresponding variable to the model obtained by taking the contribution of each variable for each tree in the model. The final one uses the coverage. It is based on the number of times that a variable is used to split the data across all trees weighted by the number of training data points that go through those splits. For the 3 different metrics, the greater the score is, the more important the variable is. The weights are usually used for estimating the importance of the features, hence it can be used as a metric for a first sight. In order to check a binary variable, the coverage and gain are more interesting because the number of split for this type of variable is low. Moreover, the gain is the metric of improving the tree prediction, therefore involving this metric could be relevant. In the end, it is interesting to check all of these metrics to

have a good overview of how the different variables have an impact on tree training.

3.4.3.2 SHAP

3.4.3.2.1 SHAP values There are several external tools and librairies to explain models like Local Interpretable Model-agnostic Explanation (LIME) [209] or Local Rule-based Explanations (LORE) [210]. However the SHapley Additive exPlanations (SHAP) was used in the current work because it is more suitable to explain XGBoost models [211, 104]. In fact, by using SHAP in machine learning problems, it is possible to quantify the contribution of each feature for each prediction which means it can be used eiter for a local or global explanation of the model. The calculation of SHAP values relies on a powerset which is all the subsets S of a set X, including the empty set $\varnothing$ and X itself. Assuming, a powerset F, its cardinal is as:

$$card(F) = 2^n \tag{3.36}$$

where n is the number of variables i.e. $card(X)$. The goal is to train a predictive model f on every variable subset S of F such as $S \subseteq F$.

In order to evaluate the impact of a variable i on a model, the difference between the output of a model with i as input and a model that excludes i must be calculate. Therefore, the model, including the i variable as input, is noted as $f_{S\cup\{i\}}$. The same model without the variable in the subset is noted f_S. The SHAP value is defined as the weighted difference of the prediction with and without the variable under study:

$$\phi_i = \sum_{S\subseteq F\setminus\{i\}} \frac{|S|!(|X|-|S|-1)!|}{|X|!}(f_{S\cup\{i\}}(x_{S\cup\{i\}}) - f_S(x_S)) \tag{3.37}$$

where $|S|$ and $|X|$ are respectively the cardinal of S and X. Therefore, the SHAP values represent the impact of a variable on a prediction. It is worth noting that this study with SHAP can be very expensive in terms of calculation if there is a large number of variables. However, this is not the case here as the variable space is defined by the power in high and medium frequency P_{MF}, P_{HF}, the time t, the depth d, and the surface temperature T (Equation 3.35).

3.4.3.2.2 SHAP plots SHAP has a large number of different plots to deeply analyze the SHAP values and their distribution among all predicted values for each variable involved. A small and simple

matrix A was considered to generate the further plots to illustrate them. It is possible to obtain a global analysis by taking into account all the SHAP values of all the variables in a single graph. It is called the summary plot and has two ways to be displayed. The first one with the bars, illustrated in Figure 3.34, shows the absolute value of the SHAP values. In this plot, there is no information about the nature of the impact (if it is positive or negative and hence if it results in an increase or a decrease of the predicted value, respectively). This plot shows that the depth has higher SHAP value as compared to the temperature SHAP value. There is a high gain in precision for the model by taking into account the depth. Based on this type of plot, the depth should be considered before the temperature.

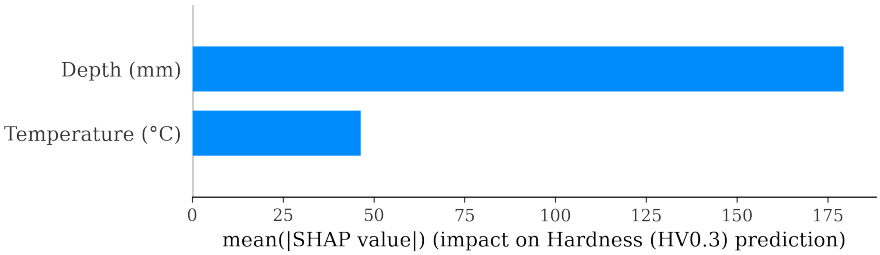

Figure 3.34: SHAP summary plot with bars

On the contrary, the other summary plot brings more precision of the value of the variable and their respective SHAP values. This plot is illustrated in Figure 3.35. The scale on the extreme right shows the value of the feature, either high (red) or low (blue). This plots display the SHAP values according to the values of the feature, each point being one SHAP value for a variable. For each variable, overlapping points are spread out in y-axis direction to have a sense of the distribution of the SHAP values of each variable. This gives a relevant overview of the impact of a variable on the prediction depending on the value of this variable.

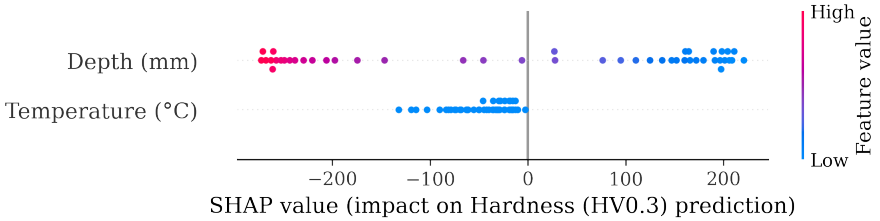

Figure 3.35: SHAP summary plot

It is also possible to use force plot to focus on one single instance x and to analyze locally the SHAP values. An instance is a row i.e. the input parameters for one hardness value. An example is displayed in Figure 3.36 and the data of the instance is listed in Table 3.18. This example is interesting as it shows the difference between local and global analysis: it is presented in Figure 3.34 that the depth is the most important variable globally, but in this example, the temperature is one which prevail.

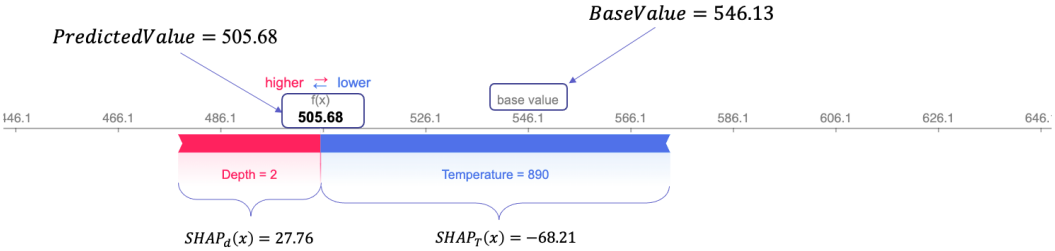

Figure 3.36: SHAP force plot

Table 3.18: Values of instance x

Instance	Depth d (mm)	Temperature T (°C)
x	2	890

For a specific instance, the plot shows the SHAP value of the input variables for model prediction. The horizontal axis determines the hardness. The base value is this the average model prediction such as:

$$BaseValue = \frac{1}{n}\sum_{k=0}^{n} f(x_k) \tag{3.38}$$

where n is the number of samples, x_k are the instances to predict, and f the hardness model to explain from SHAP.

The predicted value is the prediction by the model f for the specific point under study. The red value increases the predicted value while the blue one decreases the predicted value. The length of the displayed red and blue intervals are the SHAP values of the variables.

As illustrated, the SHAP value of the depth d added to the shap values of the temperature T balances the base value to obtain the predicted value. In fact, these plots are the graphical representation

of the following equation:

$$PredictedValue = BaseValue + \sum_{i=1}^{n} SHAP_{X_i}(x) \tag{3.39}$$

where X_i are the i variables, and $SHAP_{X_i}(x)$ are their SHAP values for the local instance x. It is then possible to find the predicted value of this instance x:

$$\begin{aligned} PredictedValue &= BaseValue + \sum_{i=1}^{n} SHAP_{X_i}(x) \\ &= BaseValue + SHAP_{Depth}(x) + SHAP_{T}(x) \\ &= 546.13 + 27.76 - 68.21 \\ &= \mathbf{505.68} \end{aligned} \tag{3.40}$$

3.4.3.3 Surrogate tree

An other possibility of XAI is to use a white-box model to ensure interpretability after a black-box modeling. This could be carried out by using an interpretable surrogate model [212]. It is possible to train a white-box model on the predicted results by black-box model with the same inputs and then extract the interpretability with the help of visuals including plots, charts or rules. This procedure is illustrated in Figure 3.37 where X are the inputs, Y is the output, and $\hat{Y}$ is the prediction :

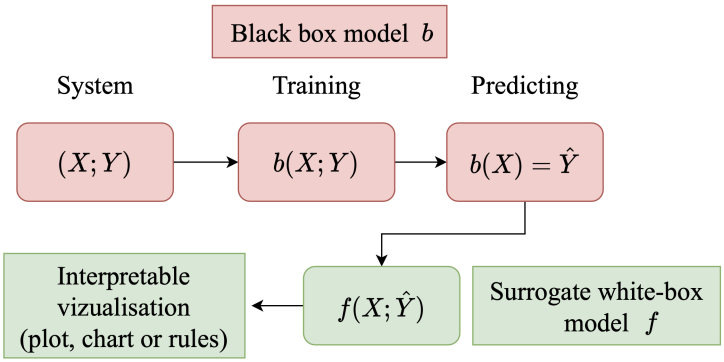

Figure 3.37: Surrogate model pipeline

For the case where the surrogate model is a decision tree, the interpretability can be based on tree visualization and rule extraction. The same matrix A, used for the previous subsection, is set for training a surrogate tree with the predicted data of an XGboost model. It is possible to visualize

the tree and highlight the conditions of thresholds that define the tree. The surrogate tree is built according to the algorithm of decision tree [213] and the obtained results are illustrated in Figure 3.38.

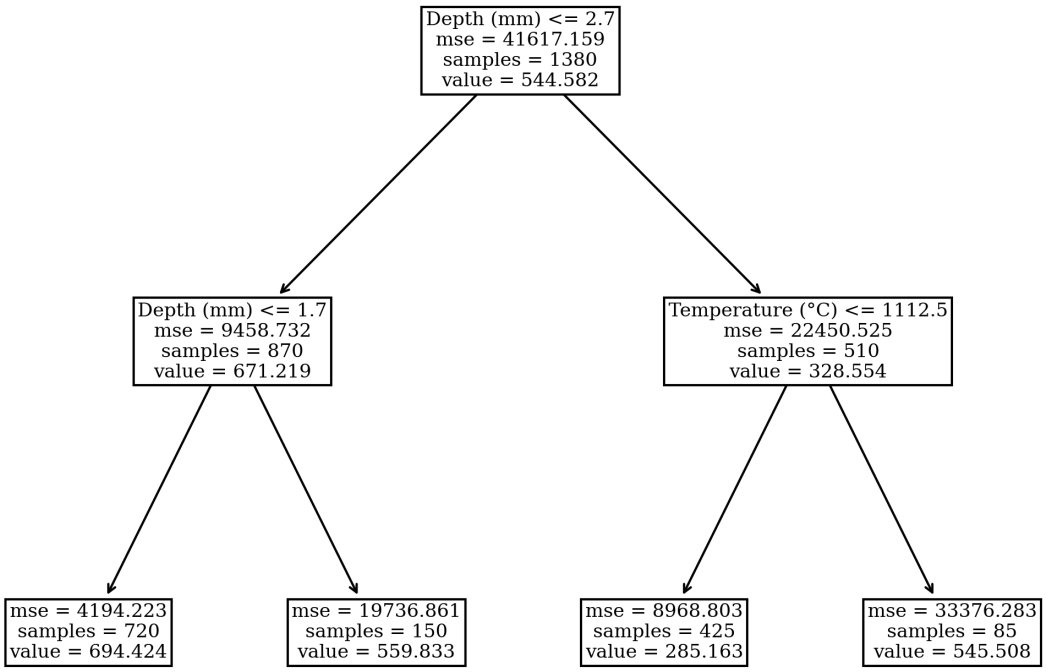

Figure 3.38: Surrogate tree

It is worth mentioning that the data validating the conditions go through the left branch. Otherwise they go through the right branch. The *samples* are the data in the node. The *value* is the value that the tree would predict for a new instance that goes through the concerned thresholds. The criterion is the Mean Squared Error (MSE). Hence, the value is the average measure of the samples that goes through the node.

It is now possible to convert the conditions of thresholds of this tree into logic and conditional instructions. The rules extracted from the illustrated tree are as follows:

```
if(Depth <= 2.70) and (Depth <= 1.70) => value = 694.42

if(Depth <= 2.70) and (Depth >  1.70) => value = 559.83

if(Depth > 2.70) and (Temperature <= 1112.50) => value = 285.16

if(Depth > 2.70) and (Temperature > 1112.50) => value = 545.51
```

Thus, for example an instance with $d = 3$ and $T = 1200$ would see its associated hardness being

predict as $\hat{y} = 545.51$. However, the precision is not the main goal here, it is more to find what is the decision making of the model, its logic. Then, it is possible to check if it meets the prior expectations.

3.4.4 Results and discussion

3.4.4.1 XGBoost feature importance

The temperature is known to be the most important variable for hardness [170] and it has been shown that its gradients in time and space are helpful to give more accurate predictions of the hardness [159]. The further observations are based on feature importance plots illustrated on Figure 3.39, 3.40, 3.41.

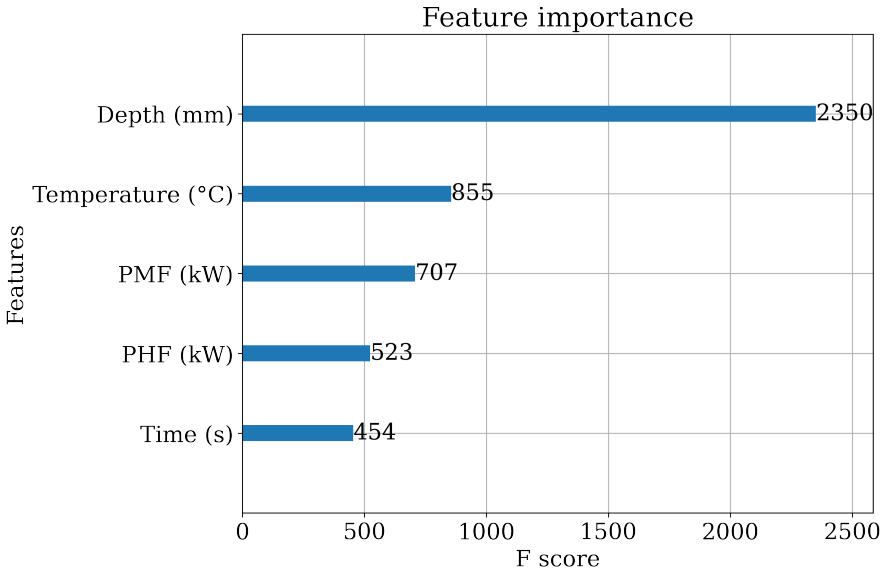

Figure 3.39: Feature importance using the weights

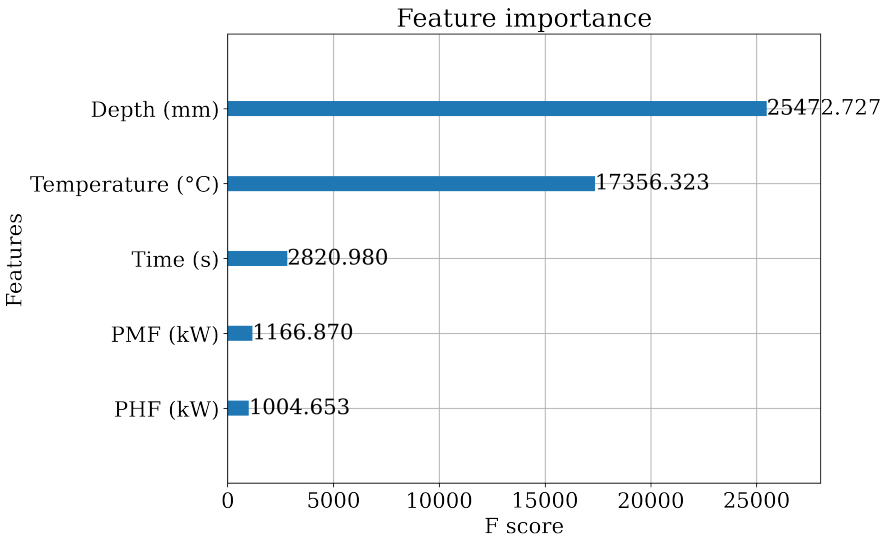

Figure 3.40: Feature importance using the gain

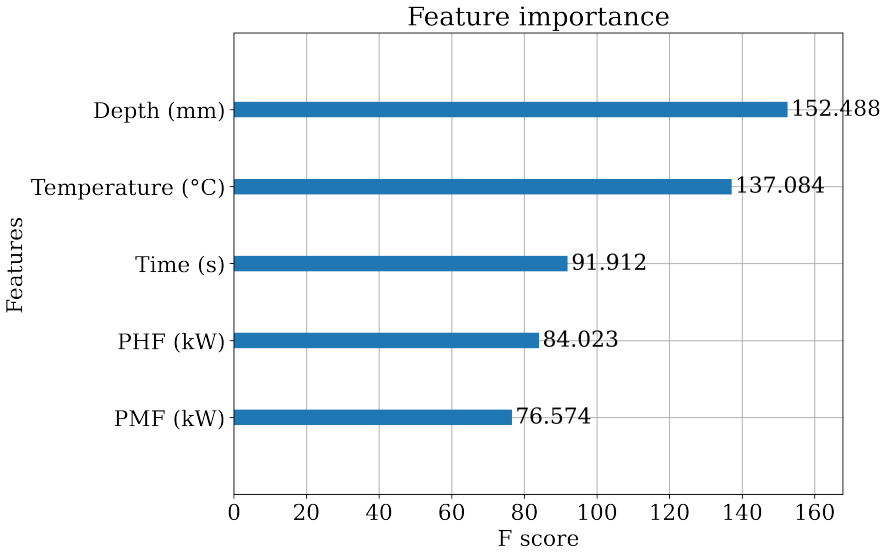

Figure 3.41: Feature importance using the coverage

The results are showing with evidence that the most important variable, whatever the metric considered, is the depth, followed by the temperature. It is clear that this result has no physical meaning. This behavior could be explained by the fact that the temperature is only available on surface and hence the model understands that the hardness is related to the depth for each run. From the machine learning point of view, it is therefore consistent to have the depth being the most

important variable.

3.4.4.2 SHAP analysis

3.4.4.2.1 Global analysis In order to emphasize the impact of all the variables on the model outputs, the shap values of all predictions are illustrated in Figures 3.42 and 3.43. Figure 3.42 presents the mean absolute SHAP value so it is easily noticeable that the depth is the most important variable for this system as previously shown. However, this does not mean that the other variables are irrelevant, but they help to discriminate the hardness between each run for a given depth.

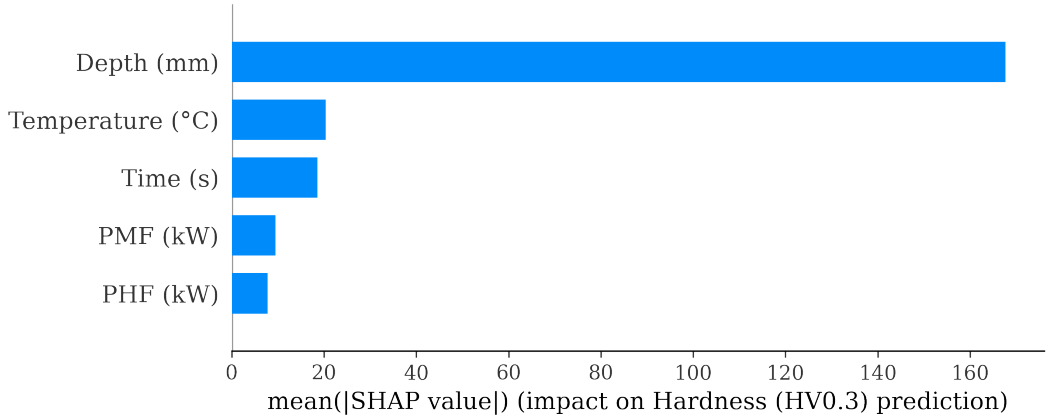

Figure 3.42: SHAP plot of basic space of variables for hardness modeling

Figure 3.43 shows all the SHAP values. It is clear that when the SHAP value of the depth is highly negative, its value is high (red) and vice versa (blue). It means that the hardness has higher values close to the treated surface and decreases with the depth. As mentioned before, the depth is the only variable being different for every hardness points while the temperature and other machine parameters remain constant for each run. Hence, the depth has the role to discriminate the in-depth hardness while in theory the in-depth temperature has this role.

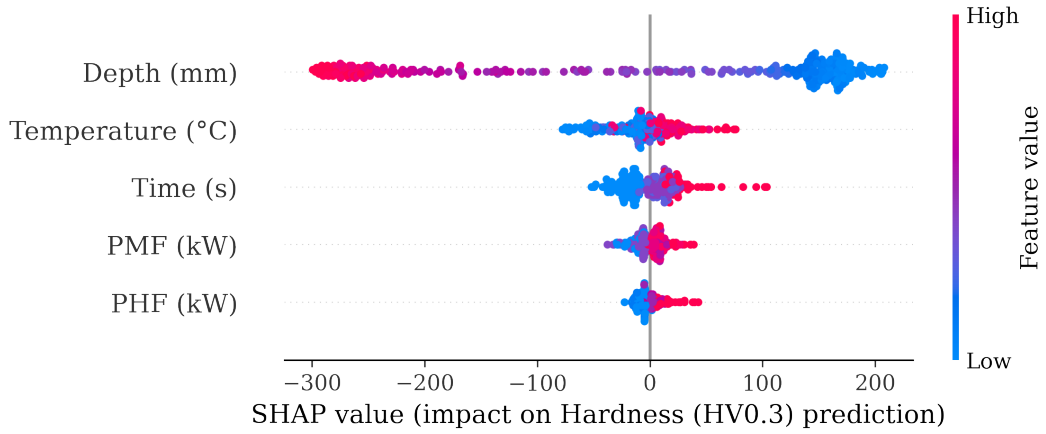

Figure 3.43: SHAP summary plot of basic space of variables for hardness modeling

When the depth can no longer discriminate the hardness between each run, it is the other variables that have an impact. Now to prove the hypothesis of a transitive rule between machine parameters, temperature, depth, and hardness. It is necessary to pursue the analysis for the other variables. In fact, it is now obvious that depth is the main parameter for the XGBoost model here but with no real meaning as process parameter.

Hence, the hardness is modeled at a fixed depth, precisely at $30\mu m$, almost where the temperature has been measured. The SHAP values are illustrated in Figure 3.44.

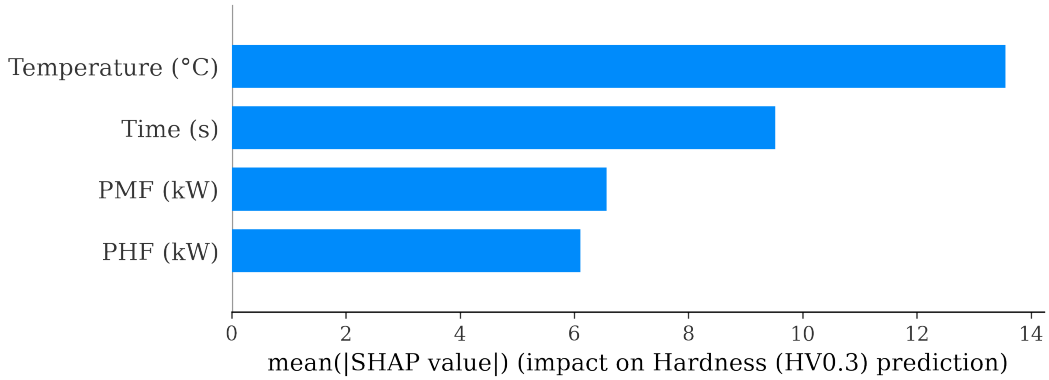

Figure 3.44: SHAP plot calculated at a depth of $30\mu m$

Here, it is shown that the temperature is the main parameter when there is no depth involved. Hence, it is considered that the temperature has the most impact on hardness prediction as expected.

To complete the analysis and to prove that the temperature history describes the hardness, a

SHAP analysis for temperature modeling was conducted. As shown in Figure 3.45, the time t has a significant impact on surface temperature prediction, followed by P_{HF} and P_{MF}, respectively.

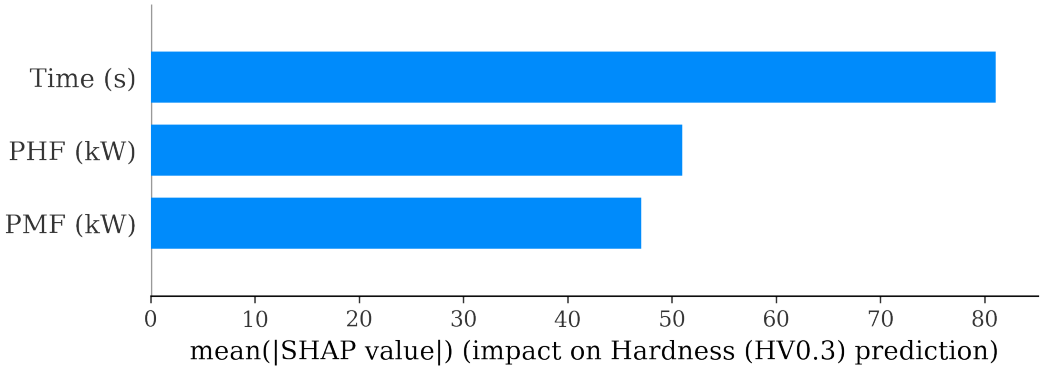

Figure 3.45: SHAP plot considering the machine parameters for temperature modeling

In Figure 3.46, it is possible to see that the time has higher impact of temperature when the time is high. This was expected because the longer the heating time, the higher the temperature. The same trend is observed for P_{HF}. On the contrary, almost all P_{MF} SHAP values are negative which means P_{MF} tends to decrease the surface temperature.

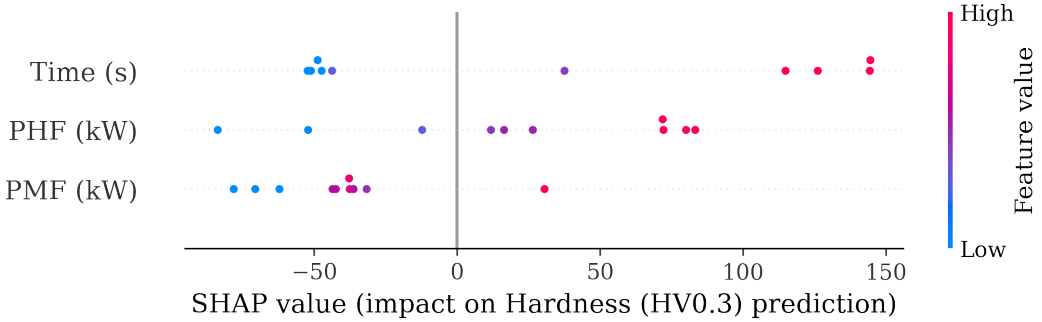

Figure 3.46: SHAP plot considering the machine parameters for temperature modeling

It has been shown that it is necessary to have an intermediate variable such as the temperature to make the link between the two different physical phenomena of the problem i.e. the induction and the hardness.

3.4.4.2.2 Local analysis Here, the aim is first to analyze a specific point where the prediction seems unclear or inconsistent according to the experimental measurement, then, to show how to analyze

the error with SHAP and finally to explain the causes of these mispredictions. SHAP force plots, as presented in the previous section, will be used. Thus, it is possible to see the impact of variables on a particular prediction. As shown in Figure 3.47 (a), one part, highlighted in Figure 3.47 (b), is poorly predicted and it is therefore interesting to analyze it using XAI tools.

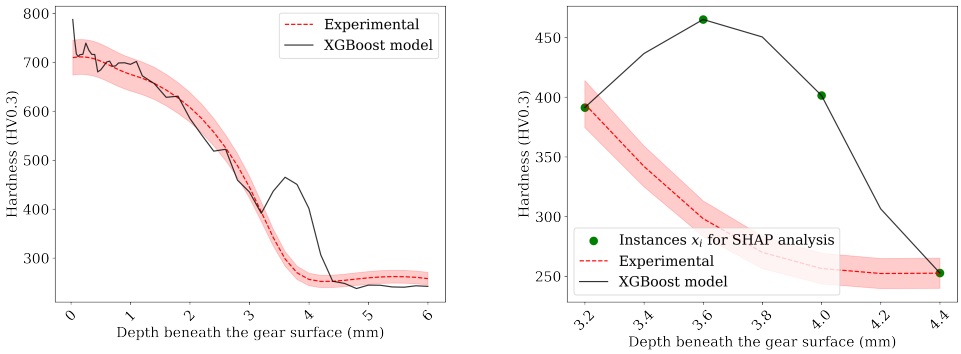

(a) (b)

Figure 3.47: Comparison of the XGBoost model with the experimental hardness - Run #14

It is worth analyzing the force plots of some instances of the Run #14 considered as mispredicted and called anomaly and compare them with those of Run #18 which is similar in terms of input and output parameters. It is clear that although similar, the parameters of the two runs are not exaclty the same as each experimental run has a unique combination of input parameters. The parameters of the two runs are listed in Table 3.19.

Table 3.19: Runs data for comparative analysis

Run #	Power of HF P_{HF} (kW)	Power of MF P_{MF} (kW)	Time t (s)	Temperature T (°C)
14	143	88	0.24	925
18	143	113	0.24	1039

The hardness profile of the Run #18 is illustrated in Figure 3.48.

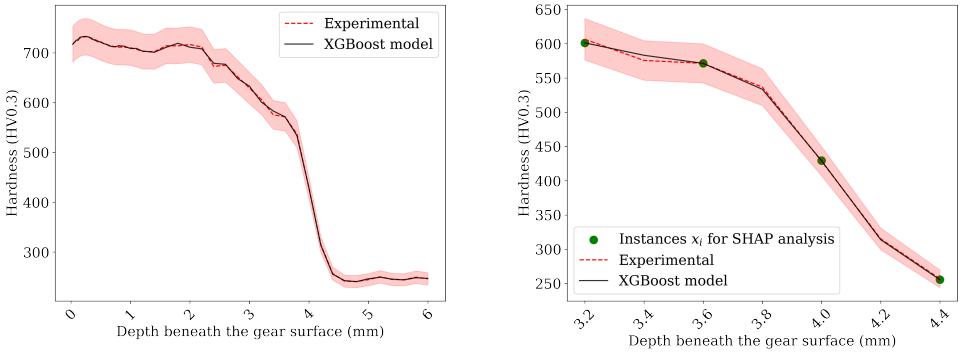

(a) (b)

Figure 3.48: Comparison of the XGBoost model with the experimental hardness - Run #18

Now, the goal is to compare the SHAP force plots of the different mentioned instances of the anomaly and the well-predicted case. What is sought is a noticeable difference in the trend of the SHAP values of the variables and to hypothesize the cause of this difference. The whole anomaly interval force plots are shown in Figure 3.49 and the different studied instances x_i of the run are listed in Table 3.20. The first and the last instances are both well predicted as it can be seen in Figure 3.47 (b). As shown in Figure 3.49 (a), the SHAP values of temperature and depth decrease the prediction while the one of the time increases the predicted value. The force plots in Figure 3.49 (b) and Figure 3.49 (c) represent the core of the anomaly. In Figure 3.49 (b), the predicted hardness should decrease (as it is known the hardness decreases in-depth) the SHAP value of time widely increases it i.e. the impact of time on this instance is higher than expected. Moreover, the SHAP values of temperature and depth don't decrease enough the predicted hardness value to have consistent value. In Figure 3.49 (c), the predicted hardness decreases as expected but with respect to the previous results it is still mispredicted as the previous hardness was higher than expected. In Figure 3.49 (d), it is an accurate prediction.

Table 3.20: Analyzed instances for the anomaly of Run #14

Instance x_i	Depth d (mm)	Predicted Hardness $\hat{H}$ (HV0.3)
(a)	3.2	391.35
(b)	3.6	465.12
(c)	4	401.50
(d)	4.4	252.72

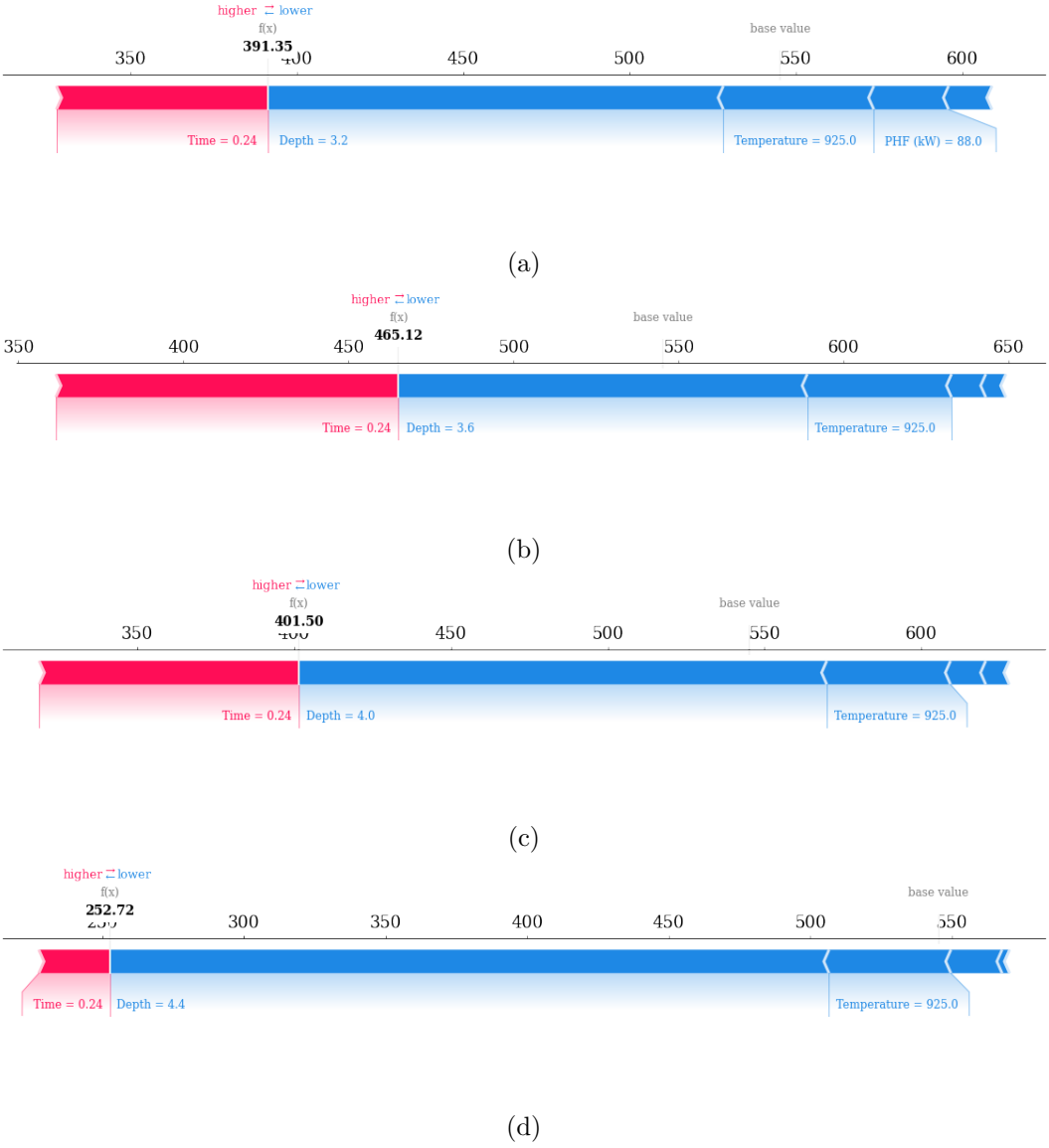

Figure 3.49: Shap force plots for the interval badly predicted

The experimental curves illustrated above in Figures 3.47 and 3.48 present slight differences too. The studied instances for comparison of Run #18 are listed in Table 3.21 and illustrated in Figure 3.48. Here, some observations can be made: the surface temperature has a value of $T = 1039$ °C, therefore, it still has a positive impact on in-depth hardness as shown in Figure 3.50 (a) and (b) until it has low effect and then decreases the hardness value as shown in Figure 3.50 (c) and (d). The increase of depth effect is proportional to the decrease of heating time incidence from Figure 3.50 (b) to (d). The effects of all variables balance themselves such that the global hardness decreases, as it was

expected from the experimental measurement. The time has always a positive effect for the hardness value: the more the gear is heated, the higher hardness will be, according to the input values. Hence, the model logic is consistent with the known physical principles.

Table 3.21: Analyzed instances for the anomaly of Run #18

Instance x_i	Depth d (mm)	Predicted Hardness $\hat{H}$ (HV0.3)
(a)	3.2	601.30
(b)	3.6	571.40
(c)	4	429.42
(d)	4.4	255.62

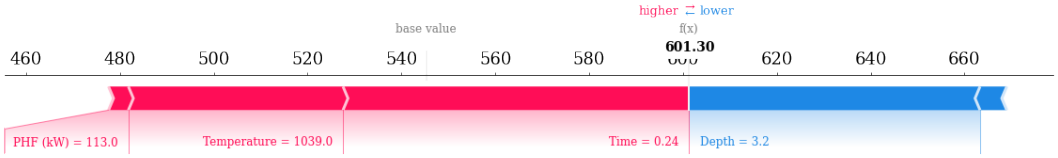

(a)

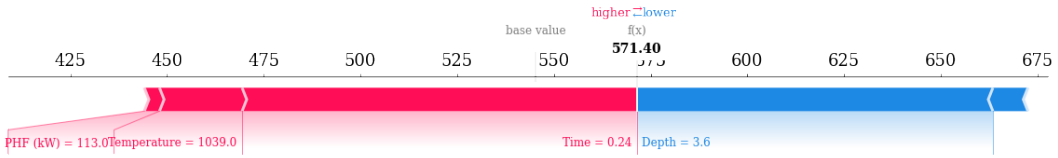

(b)

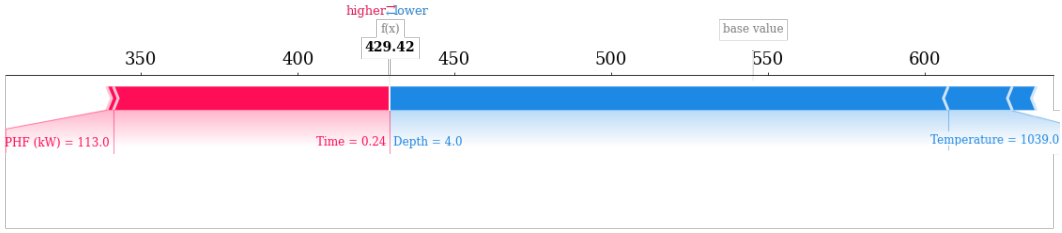

(c)

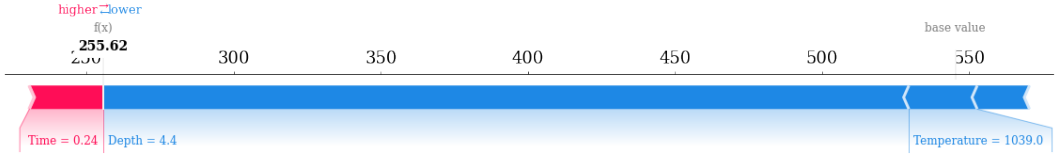

(d)

Figure 3.50: Shap force plots for comparison

The force plots of both runs show that SHAP values evolution are almost all different. In fact, only time SHAP values increase from first instance (a) to second instance (b) then decrease at the end for both runs. The evolution of the temperature SHAP values is interesting, the values strongly decrease in the Run #18 while they remain almost constant in the Run #14 which has led to increase the predicted hardness value. It is an indication that the temperature being effective in surface can lead to a good distinction from both runs, but in-depth, the temperature has no more high effect on hardness, the physical behavior changes and therefore, the model can't interpolate but copy the

training result. To support this conclusion, the misprediction seen in Run #14 is following the curve of Run #18 as illustrated in Figure 3.51.

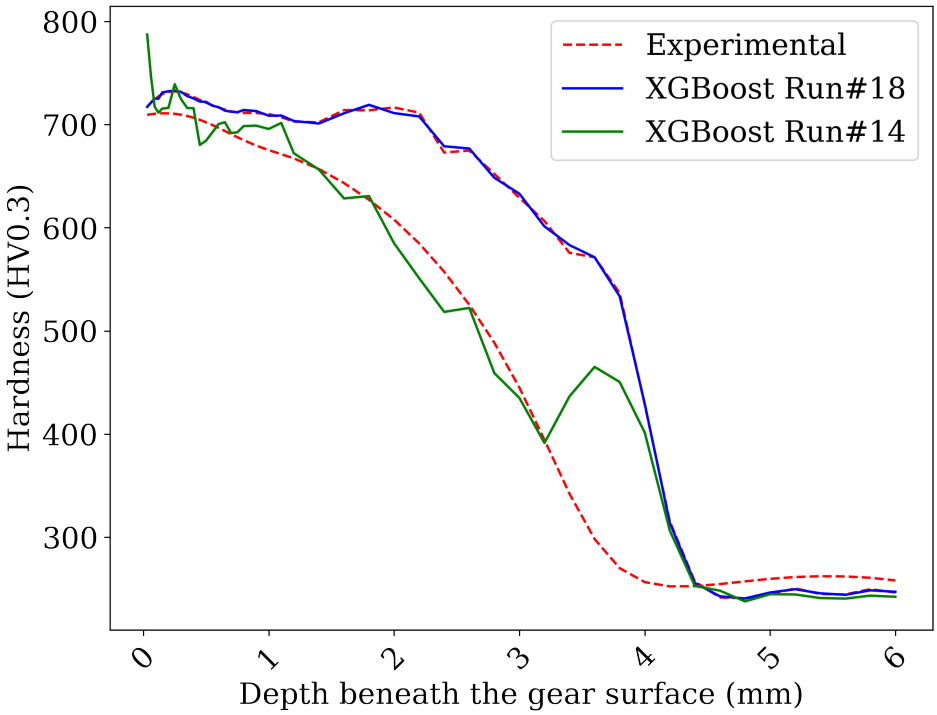

Figure 3.51: Comparison between Run#14 and Run#18 prediction

Hence, it should be possible to improve the predictions with new data, especially with several new values of heating time t and temperature T. Adding in-depth temperature should also solve the problem by allowing the model to easily discriminate hardness value with respect to its temperature.

3.4.4.3 Surrogate decision tree for model visualization

Here the proposed surrogate model is a decision tree as it is one of the most interpretable machine learning algorithm. The tree is built with conditional thresholds. These thresholds make the splitting path of the tree. It is now understandable that these conditions from the root to the leaf can be transformed as a set of decision rules which is the explicability of the model itself.

Of course, for the sake of visualization the surrogate tree is only 3-leveled deep. Therefore, it is

clear that the model is simple contrary to the XGBoost model used for accuracy purpose and so, the precision is not satisfying. Nevertheless, it is more about identifying trends than having precise results and the boundaries proposed by the decision tree illustrated in Figure 3.52 are relevant.

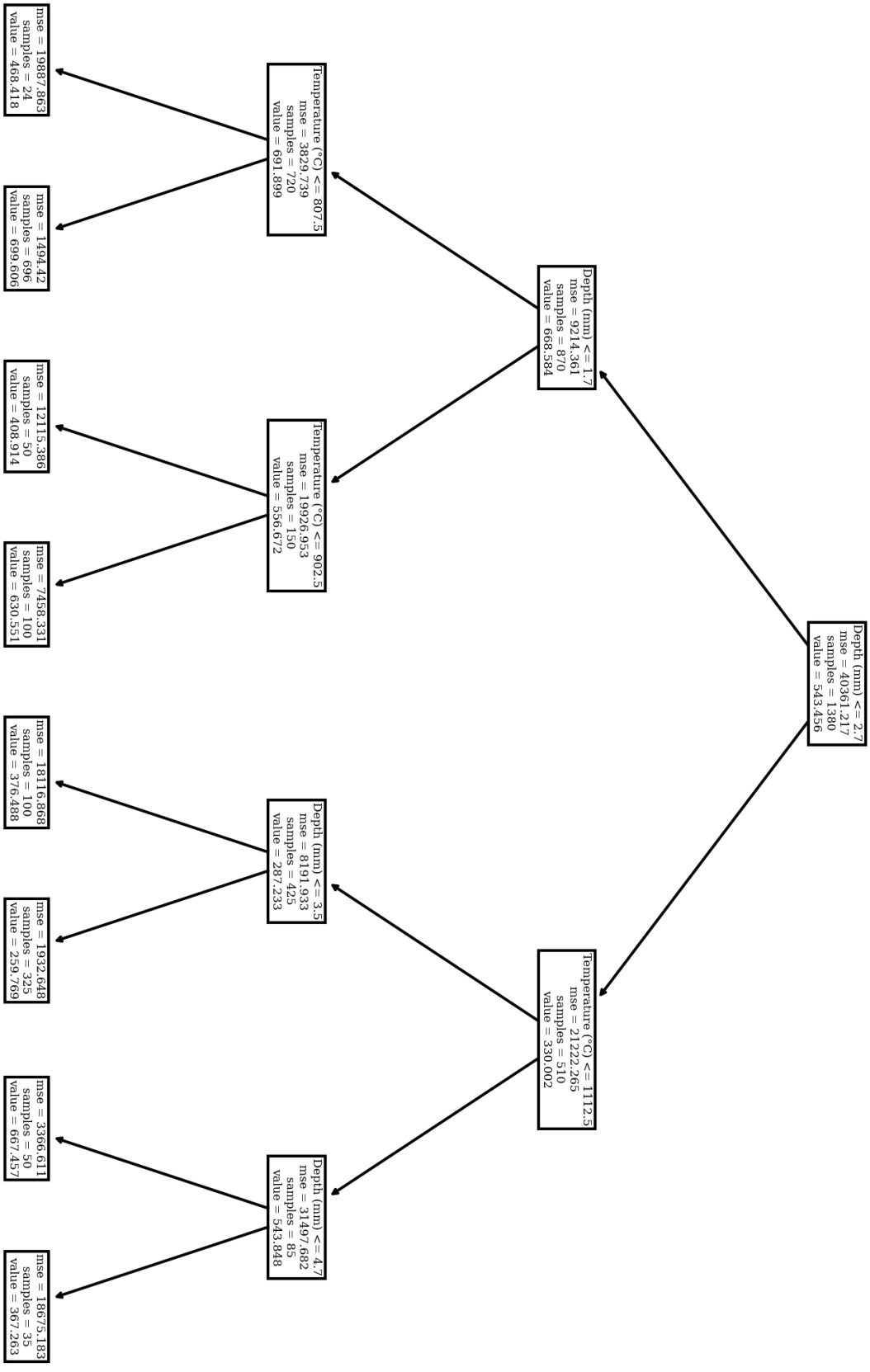

Figure 3.52: Surrogate decision tree

It is then possible to extract a series of rules from the tree by linearizing it to better understand the decisions of the model. The values of the thresholds and the predicted hardness are computed during the training of the decision tree. The set of rules are listed as follows:

```
if(Depth <= 2.70) and [(Depth <= 1.70) and (Temperature <= 807.50)] => H = 468.42
if(Depth <= 2.70) and [(Depth <= 1.70) and (Temperature >  807.50)] => H = 699.61

if(Depth <= 2.70) and [(Depth >  1.70) and (Temperature <= 902.50)] => H = 408.91
if(Depth <= 2.70) and [(Depth >  1.70) and (Temperature >  902.50)] => H = 630.55

if(Depth >  2.70) and [(Temperature <= 1112.50) and (Depth <= 3.50)] => H = 376.49
if(Depth >  2.70) and [(Temperature <= 1112.50) and (Depth > 3.50)] => H = 259.77

if(Depth > 2.70) and [(Temperature > 1112.50) and  (Depth <= 4.70)] => H = 667.46
if(Depth > 2.70) and [(Temperature > 1112.50) and  (Depth > 4.70)] => H = 367.26
```

Based on this set of rules high temperature at surface is, full austenite transformation is, leading to higher hardness. However the in-depth hardness decreases just like the in-depth temperature decreases. Therefore, if the depth is high, there will be no transformation involved by the treatment, and hence lower hardness is obtained. It is good mentioning that these rules could be considered as the proper decision making of the hardness XGBoost model as the training data of the decision tree are the actual predictions of the model.

3.4.5 Conclusion

This work has been conducted with experimental data coming from an induction hardening process carried out on C45 spur-gear and an XGBoost hardness model. In this work, an approach based on built-in tool was presented in order to investigate the model through the input variable. Then, with the help of SHAP library, a global-local explanation of an anomaly output was developed. Finally, a surrogate model was used in order to explain the principles of the model. The capability of these approaches to get a relevant explanation on all aspects of XAI of the previously made induction hardening treatment model was discussed. With this study, it is possible to conclude on several main aspects:

- when the temperature is only measured on surface, the depth d is the only variable that lead the discrimination of the hardness for each runs by law of transitivity between d and T
- the temperature T is the most important physical parameter, it has been proved when predicting hardness at a fixed depth.

- the absence of the in-depth temperature leads to some possible errors.
- the cause of anomalies are hypothetically recognizable through XAI.
- the surrogate model confirms that the depth and temperature have the most impact on hardness prediction for each runs.

The observations and hypotheses made along this study are consistent with the known physical principles of induction treatment. It is worth mentioning that the main purpose of the XAI is to validate that the results proposed by the black boxes follow a known principle (here a physical) or that at least they describe an estimate close to the known physical model. In this study, the XGBoost model predicting the hardness after induction hardening seems to follow an explainable logic when predicting accurately. To conclude, the hardness model presented in the related work is satisfactorily accurate but can be considered, thanks to this study, as a consistent model.

3.5 Article 5 : Data-driven Inverse Problem for optimizing the Induction Hardening process of C45 Spur-Gear

Sevan Garois, Monzer Daoud and Francisco Chinesta. Submitted in Metals in April 2023.

Inverse problems can be challenging and interesting to study in the context of metallurgical processes. This work aims to carry out a method for inverse modeling for simultaneous double-frequency induction hardening process. In this investigation, the experimental measured hardness profiles were considered as input data while the output data were the process parameters. For this purpose experiments were carried out on C45 steel spur-gear. The method is based on machine learning algorithms and data treatment for dealing with inverse approach issues. In addition to the inverse modeling, a forward problem-based verification completes the study. It was found according to promising results that this method is suitable and applicable for inverse problem of hardness modeling.

Keywords: Inverse problem ; machine learning ; induction hardening ; C45 steel ; spur-gear

3.5.1 Introduction

Induction hardening (IH) is a heat surface treatment process that is widely employed in various industries, such as aerospace and automotive, to improve the mechanical properties of workpieces [129, 16]. The process begins with a powerful induction heating, followed by a rapid quenching step. It has the advantage of providing rapid and localized surface heating of the desired areas without affecting the metallurgy of the bulk material, as well as good reproducibility [130]. As a result, a fine-grained martensite phase [12, 13] and a compressive residual stress field [2] are induced in the surface layer, which enhances the fatigue life behavior of engineering components [9, 10]. However, high temperatures coupled with longer heat time could lead to grain growth (causing a degradation in fatigue strength), data scatter, and excessive gear distortion [214, 215]. Accordingly, the control of the process parameters is highly important to validate the effectiveness of this heat treatment process [24]. This type of investigation is known as the forward approach.

In the inverse approach, the goal is to determine the cause of a given effect, or to reconstruct an unknown quantity from observations or measurements [216]. This approach is often regarded as a critical and challenging issue for physics, science, and engineering. In fact, it requires making assumptions and using mathematical models to estimate the unknown parameters that are responsible for the observed data. Moreover, it often involves non-unique solutions and high computational power demands. Inverse problems can be found in many fields such as computer vision and imaging [217, 218, 219, 220, 221], vibration mechanics [222], electromagnetic [223] medicine [224], groundwater modeling [225], and machine learning [226]. When the solution to such problems is not unique or sensitive to

small perturbations in the data, they represent ill-posed problems. These problems are usually more difficult to solve than well-posed problems and require additional assumptions or regularization to obtain a unique and stable solution.

Concerning the forward problem, a significant amount of research works has been conducted to study the IH process [227, 228, 229, 57, 230, 231]. While experimental approaches can provide valuable insights, they can be time-consuming and have limitations in terms of the range of validation. A more efficient method for guiding and optimizing processes is the use of numerical techniques, such as finite element modeling (FEM), which has proven to be relevant in dealing with multiphysics-based parametrized problems [175]. As a result, many studies have focused on using FEM to analyze hardness with relevant accuracy [176, 159, 177, 178, 44, 179]. However, this approach is restricted by the computational cost. Hence, machine learning algorithms have been recently employed. They tend to reduce computational time while maintaining accuracy in the modeling of parameters of interest like hardness, and residual stress [206, 159].

In the context of an inverse problem, fewer studies have been conducted for IH. They are related to the estimation of the power levels using the temperature as input in steel cylinders [117] and the heat transfer coefficient using the surface temperature in a steel billet [118]. In industry, solving the inverse problem for IH can have a number of benefits. Some of the main goals include improving efficiency by determining the optimal input parameters to meet the technical specifications for a given workpiece, reducing the amount of time and resources required to produce a desired output, and improving efficiency and precision. Moreover, it allows more flexibility in the hardening process, making it possible to treat different workpieces or geometries.

This work proposes to study the induction hardening process with inverse problem approach. The inverse problem can be defined as follows: Let A and B be two spaces and $f : A \to B$ an operator. Considering the equation

$$f(p) = h \tag{3.41}$$

where $h \in B$ is the exact datum. Finding the function f satisfying the above equation, given f and h, is the inverse problem associated to Eq. 3.41. In the present case, A and B should be the space of the induction process parameters and the space of hardness, respectively. Inverse problems can be solved using a variety of mathematical techniques such as optimization [107, 108], regularization [109, 110, 111], Bayesian inference [112, 113, 114] and machine learning algorithms [115, 116]. In this

work, a simple method based on machine learning is presented to solve the problem expressed by Eq. 3.41. Section 2 presents the experiments from which the data are collected. Section 3 is dedicated to the definition of the inverse problem in the context of induction hardening. Section 4 shows the results and the validation through the forward problem.

3.5.2 Experimental details

The series of induction hardening experiments under simultaneous double-frequency is performed on C45 steel spur gears. The gear data was summarized in Table 3.22, while the process parameters were listed in Table 3.23. During these experiments, gears were mounted on a rotating chuck. The heating phase was performed by using a rectangular shape inductor of 12.25x20mm having an air-gap of 2mm while the subsequent cooling shower of a polymer-water mixture was applied by another coaxial ring as shown in Figure 3.53. The temperature on the surface at the tooth root was measured using an Optris pyrometer. Micro-hardness Vickers (HV0.3) profiles were conducted in the normal direction to the surface of the gear at the tooth tip and root and on a transversal section, according to ISO 6507 norm [121], to determine the penetration hardening at these two locations.

Table 3.22: Main characteristics of the treated gear

Module	No. of teeth	Width	Addendum circle	Pitch circle	Root circle
2.5	22	10 mm	60 mm	55 mm	48.75 mm

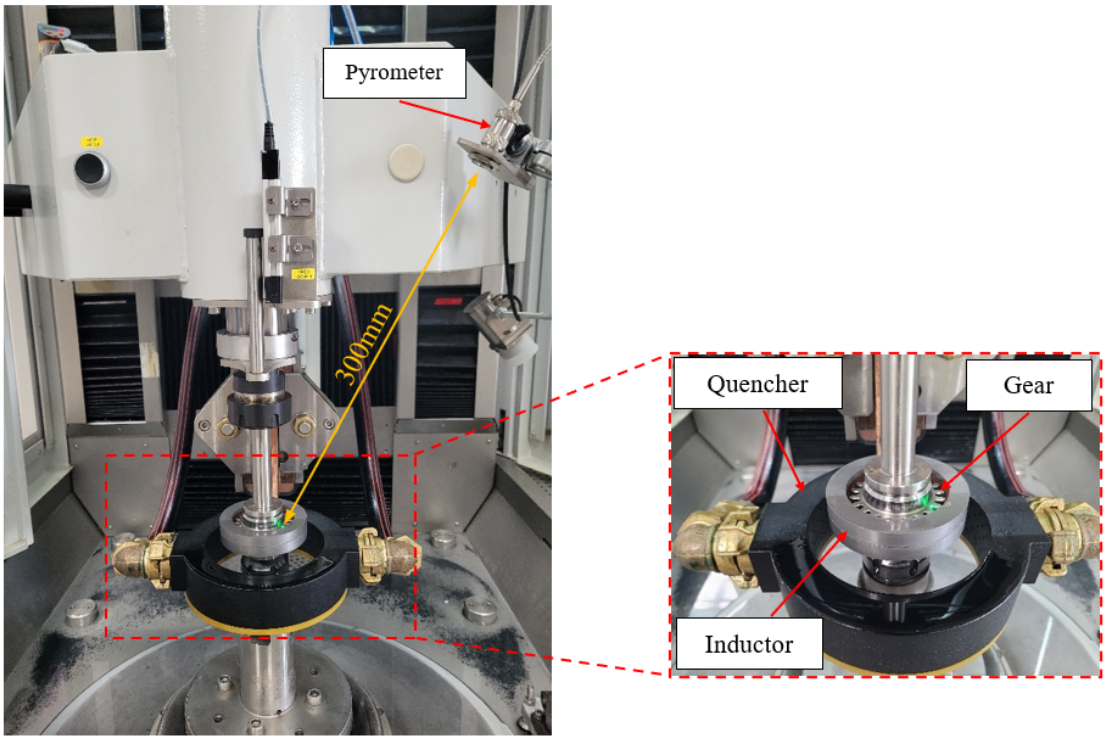

Figure 3.53: Experimental double-frequency induction hardening setup

Table 3.23: Induction heat treatment conditions

Run #	Medium Frequency MF (kHz)	High Frequency HF (kHz)	Power of HF P_{HF} (kW)	Power of MF P_{MF} (kW)	Time t (s)	Temperature T (°C)
1	13	256	143	88	0,17	780
2	12	258	225	138	0,17	1080
3	12	258	225	138	0,2	1200
4	12	257	143	113	0,17	835
5	12	258	184	113	0,17	935
6	12	258	225	113	0,17	1005
7	13	257	143	113	0,2	×
8	13	257	184	88	0,2	917
9	13	257	184	138	0,24	1189
10	13	257	143	138	0,2	1059
11	12	257	184	113	0,2	1025
12	13	257	184	88	0,24	1028
13	12	258	225	88	0,2	999
14	13	257	143	88	0,24	925
15	12	258	225	113	0,24	1167
16	12	258	225	88	0,17	900
17	12	257	184	138	0,17	1005
18	13	257	143	113	0,24	1039
19	13	257	143	138	0,24	1145
20	12	258	225	138	0,24	1217
21	12	258	225	88	0,18	884
22	12	258	198	134	0,17	920
23	×	×	238,5	94	0,17	890
24	×	×	247,5	98	0,19	958
25	12	257	202	110	0,17	884
26	×	×	175,5	102	0,19	889
27	12	257	202,5	118	0,17	887
28	×	×	193,5	102	0,19	876
29	×	×	238,5	88	0,19	906
30	×	×	247,5	88	0,19	905
31	×	×	247,5	94	0,17	858

×: missing values

3.5.3 Inverse problem

An inverse problem is the process of calculating from a set of observations the input parameters that produced them. Hence, in the present case, the measured hardness profiles should be set as input in a machine learning algorithm to predict the process parameters.

3.5.3.1 Hardness profile treatment

Based on the collected experimental data, the space X of available variables can be defined as :

$$X = \{MF, HF, P_{MF}, P_{HF}, T, d, t, H\} \tag{3.42}$$

where MF and HF are the medium and high frequency, respectively, P_{MF} and P_{HF} are their respective generator powers, T is the temperature measured at the surface close to the tooth root, d is the depth at which the hardness was measured, t is the heating duration, and H is the measured hardness. Frequencies being almost constant, they can be excluded. Hence, the studied space of variables reduces to:

$$X = \{P_{MF}, P_{HF}, T, d, t, H\} \tag{3.43}$$

The process parameters are the time and generator powers P_{MF} and P_{HF}. Hence, the problem can be described as finding a model f such as :

$$f(H) = (t, P_{MF}, P_{MF}) \tag{3.44}$$

There are 31 runs as listed in Table 3.23 composed of 60 hardness measurement point each. Hence, the hardness set as input, there are as many input variables such as:

$$f(H_1, H_2, ..., H_{60}) = (t, P_{MF}, P_{HF}) \tag{3.45}$$

However, it is preferable to have fewer variables than data points [232, 233] to allow the use of linear algorithms for modeling. It was previously shown that it is efficient to encode a profile as a few variables [159]. This procedure has the advantage of standardizing the profile to a fixed number so that any new profile would be treated equally and avoid data shape problems. Hence, in this work, each hardness profile is encoded as 5 characteristic points. The first point H_0 is at a depth of $3\mu m$. The second and third ones H_1 and H_2 correspond to the hardness measurements localized at 1/3 and 2/3 of the total depth, respectively. Then H_{08} is the hardness at the conventional depth such that $H_{08} = 0.8 \times H_0$. The last one H_3 is the last measured point of the profile which corresponds to the bulk hardness. Some profiles with their selected hardness points are illustrated in Figure 3.54.

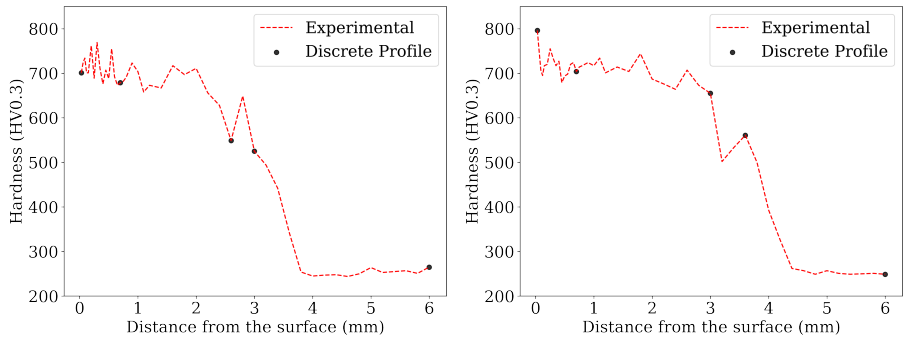

(a) Run #2

(b) Run #12

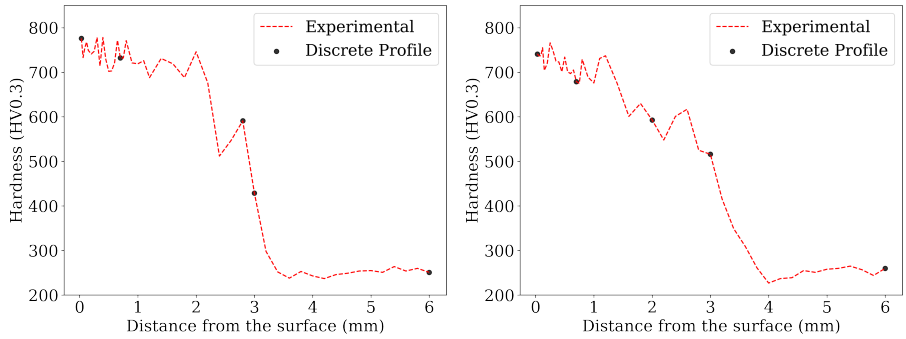

(c) Run #22

(d) Run #30

Figure 3.54: Selected hardness points from the measured hardness profiles

Then, H can be decomposed as:

$$H = \{H_0, H_1, H_{08}, H_2, H_3\} \tag{3.46}$$

The inverse problem can be now written as:

$$f(H_0, H_1, H_{08}, H_2, H_3) = (t, P_{MF}, P_{HF}) \tag{3.47}$$

3.5.3.2 Experiencing the ill-posed problem

The inverse problem encounters a major issue. A combination of the output parameters into one should be a solution. Indeed, hardness depends on temperature history, it is the product of the power of generators P_{HF} and P_{MF} and the time t. To prove the non-uniqueness of a solution, considering an artificial neural network (ANN) as f in Eq. 3.47, known as a universal function approximator, which means that, theoretically, it can learn any mathematical function, regardless of its complexity [234]. Moreover, as a global estimator, if a solution exists, a sufficient number of iterations (epochs) during

the training should let the ANN converge to it. An ANN with 3 hidden layers all composed of 120 neurons was built, and a dropout layer to ensure avoiding overfitting [235] was added to the neural architecture. The ANN was trained on several different hyperparameters and number epochs to reach convergence.

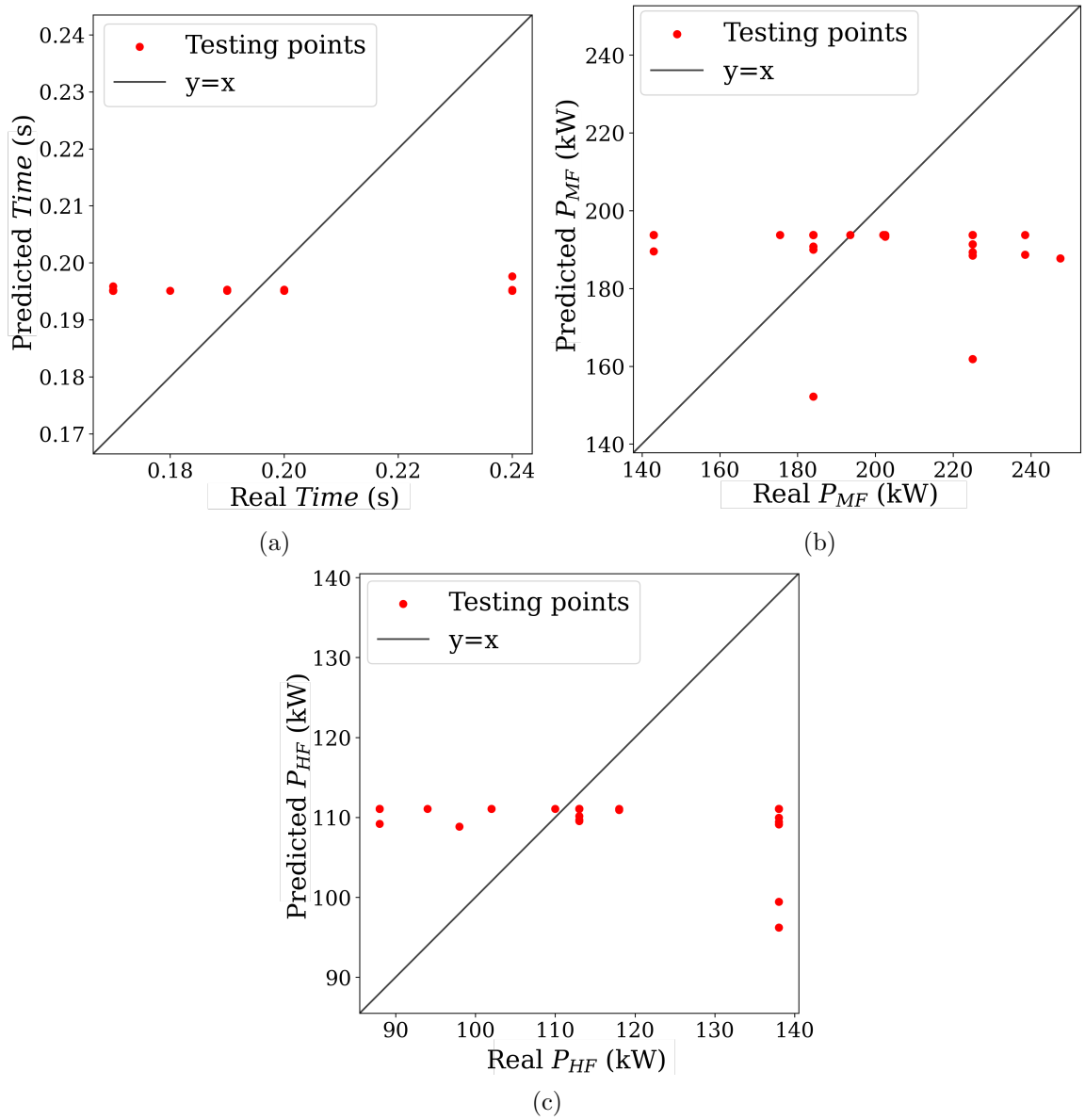

Figure 3.55: ANN process parameters predictions

The results of the ANN are almost constant for each target variables as illustrated in Figure 3.55. Moreover, the ANN doesn't converges to a unique solution, as seen in the evolution of the training

phase shown in Figure 3.56 which confirms the absence of a unique solution.

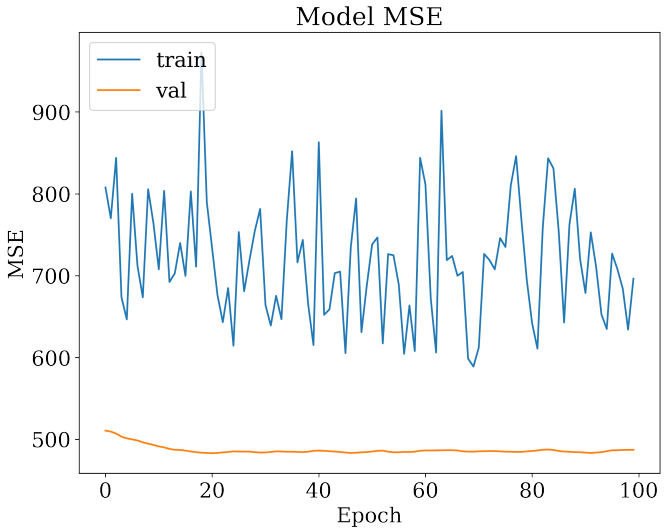

Figure 3.56: Training (train) and validation (val) error with respect to the epoch (iteration of training)

3.5.3.3 Physics-informed inverse problem

In this inverse problem, the output parameters are the powers P_{HF}, P_{MF}, and time t. As mentioned above, the major issue is the difficulty in predicting a unique vector solution of these 3 parameters. Therefore, it is essential to define a combination of the output parameters based on physical principles. The physic-based proposed combination leading to the energy reads:

$$E = t \times (P_{HF} + P_{MF}) \tag{3.48}$$

However, it is known that the tooth tip and the tooth root are influenced by the high and medium frequencies of the process, respectively [17]. The generators work simultaneously under the same heating time, hence, it is possible to consider the problem based on the specific location in the gear in order to get more information about the different process parameters such as:

$$\begin{aligned} E_{HF} &= t \times P_{HF} \\ E_{MF} &= t \times P_{MF} \end{aligned} \tag{3.49}$$

Hence, the inverse problem defined in Eq. 3.47 can be expressed as:

$$\begin{aligned} f(H_{t,0}, H_{t,08}, H_{t,1}, H_{t,2}, H_{t,3}) &= E_{HF} \\ f(H_{r,0}, H_{r,08}, H_{r,1}, H_{r,2}, H_{r,3}) &= E_{MF} \end{aligned} \tag{3.50}$$

where H_t and H_r are the hardness measured at the tooth tip and tooth root, respectively.

Finally, the initial inverse modeling is reduced to a simple regression problem. The tested algorithms and results are presented in the next section.

3.5.4 Inverse modeling and results

The modeling was divided into 2 stages. First, data were used in several machine learning techniques and tested to evaluate the best algorithm. These algorithms vary from complex such as XGBoost to multi-linear regression. It is important to use quite simple algorithms when it is possible to save computational time. Second, the results of the inverse model were used in the forward problem for validation purpose.

3.5.4.1 Inverse modeling

The dataset was composed of 60 runs (30 runs in both, the tooth root and tooth tip). It is worth mentioning that 70% of the dataset was considered for training, and 30% for test. As mentioned above, different models were selected to predict the energy such as XGBoost regressor [125], Random Forest (RF) [236, 237], Multi-linear regression [238], and Support Vector Regressor (SVR) [239, 240].

The obtained results listed in Table 3.24 show a satisfying performance for each model as the error is relatively low ($< 10\%$). It suggests that the inverse problem is now properly defined.

Table 3.24: Test results for inverse modeling

Position	Error	XGBoost	Random Forest	Multi-Linear Regression	SVR
Tooth tip	RMSE	1.07	1.42	0.74	1.34
	RMSPE	5.78%	7.23%	3.71%	7.99%
Tooth root	RMSE	0.84	2.58	0.78	2.27
	RMSPE	4.53%	6.78%	3.93%	5.65%

The characteristic hardness measurements chosen for variables are meaningful according to the promising obtained results. As the error differs depending on the data that are randomly put in training and testing during the split, the selection of the data was optimized with respect to test

results. However, cross-validation technique [153] was used to ensure the robustness of the model but is unstable because of the small number of samples [241, 242]. With this amount of data, the presented models cannot be generalized. Results from multi-linear regression model were illustrated in Figure 3.57.

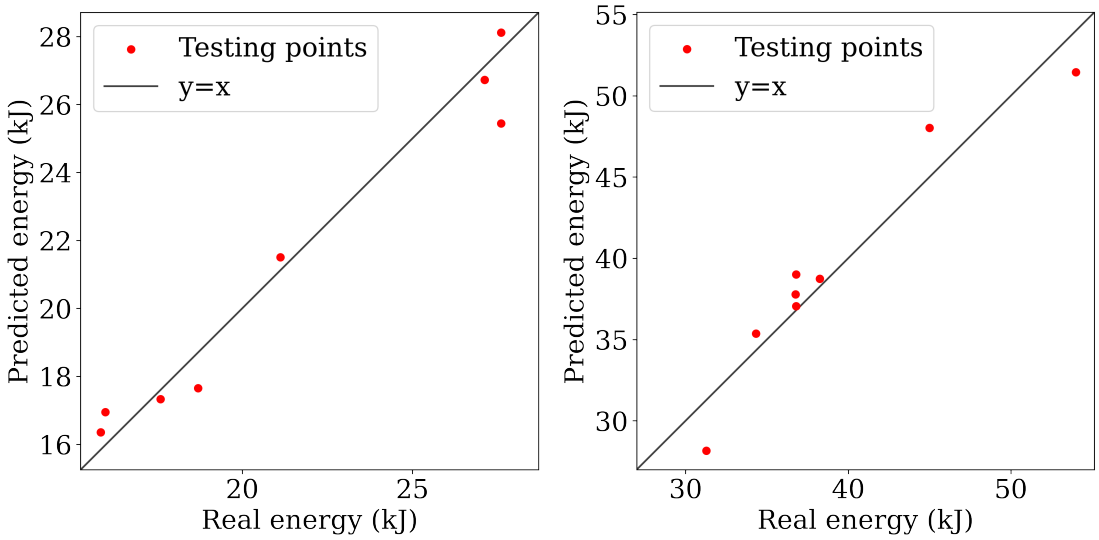

(a) Tooth tip (b) Tooth root

Figure 3.57: Predicted versus real energy at the tooth tip and the tooth root

It is worth noticing that the data are well predicted within the fixed ranges of energy. Moreover, these results show that a simple algorithm such as multi-linear regression can handle the simplified problem.

3.5.4.2 Forward problem consistency

In order to ensure that it is possible to turn back to the forward problem with the available variables presented in the previous section, the next step of this work is to predict the hardness with the previous output parameters i.e. the energy. The problem could be expressed as:

$$\begin{aligned} f(E_{MF}) &= (H_0, H_{08}, H_1, H_2, H_3) \\ f(E_{HF}) &= (H_0, H_{08}, H_1, H_2, H_3) \end{aligned} \tag{3.51}$$

Predicting multiple outputs with one variable as input is fairly complex in regression when the variables are dependent on each other. Since the hardness points $(H_0, H_{08}, H_1, H_2, H_3)$ were selected from fixed

depth to keep the data homogeneity, it is possible to divide the hardness and depth into 2 variables. The depth being known, it can be considered as an input variable.

Hence the input space of the variables could be written as :

$$X = \{E, loc, d\} \tag{3.52}$$

where E is the energy of the location of the point, loc is the location, either the root or tip of the tooth, and d is the depth of the measured hardness. Therefore, the problem is such as:

$$f(E, d, loc) = H \tag{3.53}$$

There are some differences between the inverse and forward approaches. The location in the gear is now considered as the input variable *loc*. Contrary to the inverse approach using one model per location, in the forward problem the locations are encoded and only one model is needed. Also, in the inverse problem, one instance represents a hardness profile, in the forward problem an instance is now a single hardness measurement linked to its depth. Because of this difference and to ensure consistency of the profiles while splitting for training and testing sets, the data are split according to their respective profile. Therefore, 24 profiles were considered for training, leaving 7 profiles for the testing phase. The obtained results are listed in Table 3.25:

Table 3.25: Test results of the hardness prediction

Error	XGBoost	Multi-Linear Regression	Random Forest	SVR
RMSE	**45.55**	134.25	**47.15**	137.59
RMSPE	**8.5%**	28.75%	**9.2%**	37.26%

It is clear that the XGBoost and Random Forest algorithms comparatively give a much better prediction of the hardness. The best models are illustrated in Figure 3.58. Bulk and surface hardness ($\approx$ 300HV and 700HV) are well predictedw while both models showed difficulties when predicting hardness in the transition phase (between surface and core hardness). This difficulty can be explained by several factors. Indeed, not only the problem is already complex, but also the number of samples used is fairly low. Moreover, the variables are limited to those that have already been used in the inverse problem. However, it is known that the surface and in-depth temperatures [206] or the austenite ratio [159] can highly increase the accuracy of the predictions for the hardness in transition. Beyond

this method, such variables could be used to enhance the efficiency of the model.

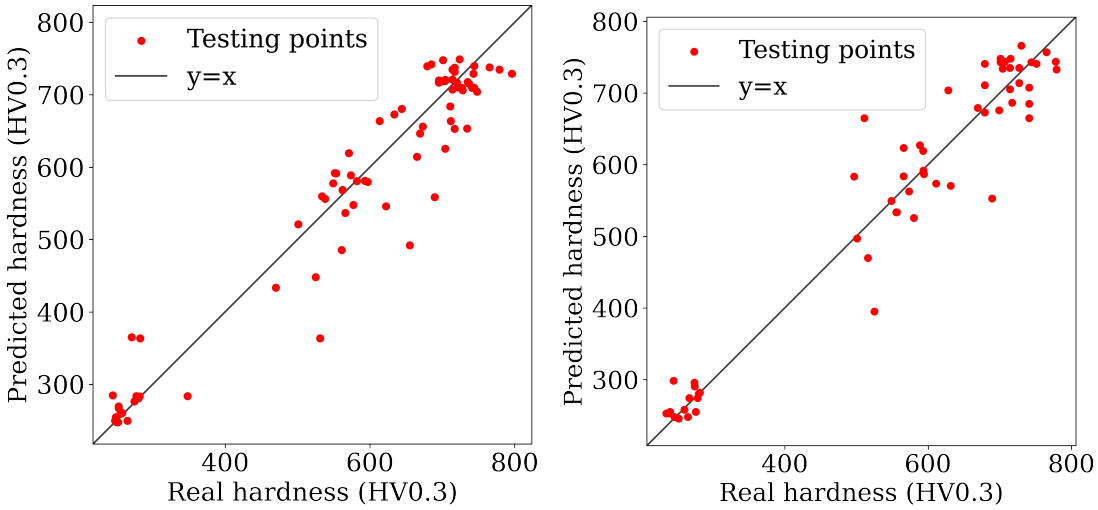

(a) Random Forest (b) XGBoost

Figure 3.58: Predicted versus real hardness for forward problem in both tooth tip and root of the gear

3.5.5 Conclusions

This work proposed an inverse approach of the hardness. Data were collected from induction hardening experiments carried out on C45 spur-gear. In this work, an inverse modeling based on machine learning was presented. This method consists of predicting process parameters of induction hardening treatment based on the hardness profiles. The method proceeded by discretizating the profiles, the combination of the process parameters, and the forward problem-based verification. The main conclusions were as follows:

- The discretization of hardness profile and the physics-based combination of the output variables of the data were essential to conduct the inverse modeling.
- It was shown that simple algorithms were efficient to predict the energy.
- The number of available samples was too small to prove the generalization of the model.
- The results of the forward problem verification proved the efficiency of the proposed approach.

It is worth outlining that the inverse approach model has the advantage to be simple and easy to conduct with no data shape issues. Also, the developed method have the advantages of a shorter time

response than complex inverse methods which is highly suitable for process optimization. In the light of the results, the proposed inverse approach can be used in induction hardening optimization.

Conclusion and perspectives

3.5.6 Outcomes

This thesis investigated the process of induction hardening (IH) under the scope of AI. Several types of process with different kind of workpieces have been studied including simultaneous double-frequency IH on C45 steel spur-gear and single-frequency IH on 300M steel cylinders. The purpose was to propose different approaches to model, explain and optimize the process of IH in a global manner with the insurance of industrial issues to be considered.

First, an exploration of synthetic data generated from simulation from the software FORGE was proposed along with the prediction of the hardness. The simulations were carried out on C45 steel-spur gear with physical properties taken from literature. Then, a XGBoost model with feature selection and combination presented promising results, while the hybrid model, augmented with austenite ratio, showed appealing predictions for post-treatment hardness. Next, a similar study was conducted to predict the residual stress with relevant results too. The exploration of synthetic data and the predictions of hardness and residual stresses are a start and have somehow proven the feasibility of using machine learning for this kind of problem. However, experimental data are more relevant and interesting to use as they involve unique and challenging issues such as bias, noise, missing data, to name a few.

Hence, experimental data have been collected from diverse experiments with different process. 300M steel cylinders treated by single-frequency IH allowed to start modeling with a simple geometry. Moreover, with the help of in-depth temperature given by FEM, the prediction of hardness showed excellent results. Next, experiments on C45 steel spur-gear have been carried out with different geometry parameters. The resulted data were collected and gathered with respect to different factors about the considered input features, leading to multiple cases to study, including a case with profile-based hardness prediction. The results showed that the model was quite efficient, accurate and in good agreement with the experimental hardness measurements.

After exploring the prediction of hardness thanks to machine learning, it appeared that it was meaningful to study the consistency and the veracity of the results under the scope of eXplanable Artificial Intelligence (XAI) tools. The data considered for such a study was the profile-based hardness modeling. Different tools were utilized to highlights the behavior of the model when predicting the hardness. First, the XGBoost in-built tool was used to show feature importance. Then, the SHAP

library was utilized explored with shap values the involvement of each features in each prediction, including the study of mispredictions. Next, a surrogate model was built to illustrate in the form of rules the decision-making of the model. In the end, every tool confirmed that the model is physically consistent.

To conclude the work, a simple method for inverse modeling was proposed. The data considered are also the ones considered in the profile-based hardness case. This method includes descritization of the profiles to insure data shape consistency and physics-based feature creation to decrease the number of ouput variables. After promising results, a forward problem-based verification was carried out.

3.5.7 Perspectives

With the presented outcomes of this work, several openings can be highlighted for further studies:

- This work presented the hardness predictions as promising while knowing that the impact of the in-depth temperature was important for the differentiation of the in-depth hardnesses and especially for those belonging to the heat affected zone (HAZ), known as the hardnesses in the transition phase between the surface and the bulk material. It should be mentioned that this requires the use of a thermocouple during the experiments which can be complex and expensive. However, once the data is obtained, it is possible to model the temperature and to have a trustful and indicative in-depth temperature which allows a better reliability of the results of the in-depth hardnesses.

- Only the hardness was experimentally studied due to lack of data on the other parameters of interest such as residual stresses and distortion. As a complementary work, it should be interesting to model these parameters just like the hardness. Indeed, predicting all the parameters of interest could lead to a quality criteria of given process and hence, to the validation or reject of a treated gear.

- It should be also possible to generalize this method to other geometries. Indeed, the thesis focused on simple geometry (cylinders) and complex geometry (spur-gear). However, other complex geometries such as helical gears which are of high interest but also bevel gears or worm gears which can be also be subjects of hardening treatments. Hence, not only the work should

focus on process parameters but also to encode geometric parameters as euclidean data such as tuples or geometric data such as graphs. The latter involves a new type of deep learning called Geometric Neural Networks (GNN)

- In this thesis the studied treatment was the induction hardening process. However, a study on different kind of hardening treatments such as shot-peening, nitruration or carburizing should be promising. Also, the integration of different materials in the data could also lead to a more generalizing method. It appeared that the chemical composition of a material had an important effect for some treatment. Mobilizing all these new parameters should lead to a more generalizing method and could be of high interest.

- The lack of data and representation in the space has been an issue during the thesis. New experiments with different process parameters could enrich the data already obtained and studied to enhance a new trained model. The latter could be more generalizing and accurate. Another solution could be the use of data augmentation technique which numerically increase the number of samples by slightly modifying the existing data.

- It was shown that the hybrid way using physical knowledge directly or indirectly in the model was a suitable solution for more accurate predictions and physical consistency. Hence, building physics-informed model including physical equation-based verification during the training is highly recommended for further works in the field of metallurgy involving complex multi-physics processes.

- Develop a user-friendly tool for engineers or technicians that are not into the data field to allow them use and visualize the results of the modeling, but also the justification brought by XAI to ensure their consistency.

Bibliography

[1] Rexnord, "Failure analysis: Gears-shafts-bearings-seals," tech. rep., August 1978.

[2] D. Hömberg, Q. Liu, J. Montalvo-Urquizo, D. Nadolski, T. Petzold, A. Schmidt, and A. Schulz, "Simulation of multi-frequency-induction-hardening including phase transitions and mechanical effects," *Finite Elements in Analysis and Design*, vol. 121, pp. 86–100, 2016.

[3] V. I. Rudnev, "Single-coil dual-frequency induction hardening of gears," *Heat treating progress*, vol. 9, pp. 9–11, 2009.

[4] A. Cubillo, S. Perinpanayagam, and M. Esperon-Miguez, "A review of physics-based models in prognostics: Application to gears and bearings of rotating machinery," *Advances in Mechanical Engineering*, vol. 8, no. 8, p. 1687814016664660, 2016.

[5] P. Ku, "Gear failure modes—importance of lubrication and mechanics," *ASLe Transactions*, vol. 19, no. 3, pp. 239–249, 1976.

[6] S. P. Radzevich and D. W. Dudley, *Handbook of practical gear design*. CRC press, 1994.

[7] A. Olver, "The mechanism of rolling contact fatigue: an update," *Proceedings of the Institution of Mechanical Engineers, Part J: Journal of Engineering Tribology*, vol. 219, no. 5, pp. 313–330, 2005.

[8] M. F. Aswad, A. J. Mohammed, and S. R. Faraj, "Induction surface hardening: a review," in *Journal of Physics: Conference Series*, vol. 1973, p. 012087, IOP Publishing, 2021.

[9] F. Maresca, V. Kouznetsova, M. Geers, and W. Curtin, "Contribution of austenite-martensite transformation to deformability of advanced high strength steels: from atomistic mechanisms to microstructural response," *Acta Materialia*, vol. 156, pp. 463–478, 2018.

[10] S. Xu, J. Li, Y. Cui, Y. Zhang, L. Sun, J. Li, J. Luan, Z. Jiao, X.-L. Wang, C. Liu, *et al.*, "Mechanical properties and deformation mechanisms of a novel austenite-martensite dual phase steel," *International Journal of Plasticity*, vol. 128, p. 102677, 2020.

[11] V. Rudnev, D. Loveless, and R. L. Cook, *Handbook of induction heating.* CRC press, 2017.

[12] G. Qiu, D. Zhan, C. Li, Y. Yang, M. Qi, Z. Jiang, and H. Zhang, "Effects of yttrium and heat treatment on the microstructure and mechanical properties of clam steel," *Journal of Materials Engineering and Performance*, vol. 29, no. 1, pp. 42–52, 2020.

[13] C. Celada-Casero, B. Huang, J.-R. Yang, and D. San-Martin, "Microstructural mechanisms controlling the mechanical behaviour of ultrafine grained martensite/austenite microstructures in a metastable stainless steel," *Materials & Design*, vol. 181, p. 107922, 2019.

[14] D. Hömberg, "A mathematical model for induction hardening including mechanical effects," *Nonlinear Analysis: Real World Applications*, vol. 5, no. 1, pp. 55–90, 2004.

[15] V. Savaria, *Contraintes résiduelles et leurs impacts sur l'amorçage de fissures en fatigue de flexion dans des engrenages aéronautiques durcis superficiellement par induction.* PhD thesis, École de technologie supérieure, 2014.

[16] A. Candeo, C. Ducassy, P. Bocher, and F. Dughiero, "Multiphysics modeling of induction hardening of ring gears for the aerospace industry," *IEEE Transactions on Magnetics*, vol. 47, no. 5, pp. 918–921, 2011.

[17] A. A. M. Al Salkhadi, *Modélisation et simulation du procédé de durcissement par induction appliqué à des pignons à chaîne-chauffage à double fréquence.* PhD thesis, Université du Québec à Rimouski, 2021.

[18] J. Barglik, K. Ducki, D. Kukla, J. Mizera, G. Mrówka-Nowotnik, J. Sieniawski, and A. Smalcerz, "Comparison of single and consecutive dual frequency induction surface hardening of gear wheels," in *IOP Conference Series: Materials Science and Engineering*, vol. 355, p. 012015, IOP Publishing, 2018.

[19] J. T. Oden and J. N. Reddy, *Variational methods in theoretical mechanics.* Springer Science & Business Media, 2012.

[20] G. Strang, G. J. Fix, *et al.*, "An analysis of the finite element method," 1969.

[21] J. C. Simo and T. J. Hughes, *Computational inelasticity*, vol. 7. Springer Science & Business Media, 2006.

[22] D. Boffi, F. Brezzi, M. Fortin, *et al.*, *Mixed finite element methods and applications*, vol. 44. Springer, 2013.

[23] M. Spezzapria, F. Dughiero, M. Forzan, and A. Candeo, "Multiphysics fem simulation of contour induction hardening process on aeronautical gears," *Journal of Iron and Steel Research International*, vol. 19, no. S1, pp. 95–98, 2012.

[24] M. Areitioaurtena, U. Segurajauregi, I. Urresti, M. Fisk, and E. Ukar, "Predicting the induction hardened case in 42crmo4 cylinders," *Procedia CIRP*, vol. 87, pp. 545–550, 2020.

[25] K. Gao, X. Qin, Z. Wang, H. Chen, S. Zhu, Y. Liu, and Y. Song, "Numerical and experimental analysis of 3d spot induction hardening of aisi 1045 steel," *Journal of Materials Processing Technology*, vol. 214, no. 11, pp. 2425–2433, 2014.

[26] K. Wang, S. Chandrasekar, and H. T. Yang, "Finite-element simulation of induction heat treatment," *Journal of Materials Engineering and Performance*, vol. 1, no. 1, pp. 97–112, 1992.

[27] N. Hoa Ngan and P. Bocher, "Finite element analysis simulation of the effect of induction hardening on rolling contact fatigue," *Journal of tribology*, vol. 140, no. 6, p. 061404, 2018.

[28] T. J. Hughes, *The finite element method: linear static and dynamic finite element analysis*. Courier Corporation, 2012.

[29] R. D. Cook *et al.*, *Concepts and applications of finite element analysis*. John wiley & sons, 2007.

[30] J. N. Reddy, *An Introduction to Nonlinear Finite Element Analysis Second Edition: with applications to heat transfer, fluid mechanics, and solid mechanics*. OUP Oxford, 2014.

[31] K. Kurek and D. Dolega, "Modeling of induction hardening," in *Int. Sci. Colloquium: Modeling of Electromagnetic Processing, Hannover, Germany*, pp. 125–130, 2003.

[32] M. W. Kennedy, S. Akhtar, J. A. Bakken, and R. E. Aune, "Analytical and experimental validation of electromagnetic simulations using comsol®, re inductance, induction heating and magnetic fields," in *COMSOL Users Conference, Stuttgart Germany*, pp. 1–9, Citeseer, 2011.

[33] N. Barka, P. Bocher, J. Brousseau, M. Galopin, and S. Sundararajan, "Modeling and sensitivity study of the induction hardening process," in *Advanced Materials Research*, vol. 15, pp. 525–530, Trans Tech Publ, 2007.

[34] M. Leitner, R. Aigner, and F. Grün, "Numerical fatigue analysis of induction-hardened and mechanically post-treated steel components," *Machines*, vol. 7, no. 1, p. 1, 2019.

[35] M. W. Kennedy, S. Akhtar, J. A. Bakken, and R. E. Aune, "Review of classical design methods as applied to aluminum billet heating with induction coils," in *EPD Congress 2011-TMS 2011 Annual Meeting and Exhibition; San Diego, CA, United States, 27 February-3 March, 2011*, pp. 707–722, 2011.

[36] X. Geng, Z. Cheng, S. Wang, C. Peng, A. Ullah, H. Wang, and G. Wu, "A data-driven machine learning approach to predict the hardenability curve of boron steels and assist alloy design," *Journal of Materials Science*, vol. 57, no. 23, pp. 10755–10768, 2022.

[37] F. Dalipi, S. Yildirim Yayilgan, and A. Gebremedhin, "Data-driven machine-learning model in district heating system for heat load prediction: A comparison study," *Applied Computational Intelligence and Soft Computing*, vol. 2016, 2016.

[38] S. Seyedzadeh, F. P. Rahimian, S. Oliver, I. Glesk, and B. Kumar, "Data driven model improved by multi-objective optimisation for prediction of building energy loads," *Automation in Construction*, vol. 116, p. 103188, 2020.

[39] S. Cohen, "The evolution of machine learning: Past, present, and future," in *Artificial intelligence and deep learning in pathology*, pp. 1–12, Elsevier, 2021.

[40] I. Lee and Y. J. Shin, "Machine learning for enterprises: Applications, algorithm selection, and challenges," *Business Horizons*, vol. 63, no. 2, pp. 157–170, 2020.

[41] V. Champaney, F. Chinesta, and E. Cueto, "Engineering empowered by physics-based and data-driven hybrid models: A methodological overview," *International Journal of Material Forming*, vol. 15, no. 3, p. 31, 2022.

[42] F. Chinesta, E. Cueto, E. Abisset-Chavanne, J. L. Duval, and F. E. Khaldi, "Virtual, digital and hybrid twins: a new paradigm in data-based engineering and engineered data," *Archives of computational methods in engineering*, vol. 27, pp. 105–134, 2020.

[43] J. Chen, F. Zhao, Y. Sun, L. Zhang, and Y. Yin, "Prediction model based on xgboost for mechanical properties of steel materials," *International Journal of Modelling, Identification and Control*, vol. 33, no. 4, pp. 322–330, 2019.

[44] M. Daoud, R. Kubler, A. Bemou, P. Osmond, and A. Polette, "Prediction of residual stress fields after shot-peening of trip780 steel with second-order and artificial neural network models based on multi-impact finite element simulations," *Journal of Manufacturing Processes*, vol. 72, pp. 529–543, 2021.

[45] P. Rokicki, E. Bąk, G. Mrówka-Nowotnik, and A. Nowotnik, "Single-frequency induction hardening of structural steel," *Journal of Achievements in Materials and Manufacturing Engineering*, vol. 86, no. 2, 2018.

[46] P. Rokicki, "Induction hardening of tool steel for heavily loaded aircraft engine components," *Archives of Metallurgy and Materials*, vol. 62, 2017.

[47] J. Grum, "Induction hardening," *Handbook of residual stress and deformation of steel*, vol. 2, pp. 220–247, 2002.

[48] V. Bukanin, A. Ivanov, A. Zenkov, and V. Vologdin, "Induction hardening of external gear," in *IOP Conference Series: Materials Science and Engineering*, vol. 327, p. 022016, IOP Publishing, 2018.

[49] W. Schwenk, "Sdf induction heating provides accurate contour hardening of pm parts.," *Industrial heating*, vol. 70, no. 5, pp. 51–53, 2003.

[50] M. Elamin, P. Lombard, A. Rodriguez, and P. Wendling, "Optimization of the heating phase for the bi-frequency heat treat process of a gear," in *HT2019*, pp. 56–62, ASM International, 2019.

[51] V. Esteve, J. Jordan, E. Dede, E. Sanchis-Kilders, and E. Maset, "Induction heating inverter with simultaneous dual-frequency output," in *Twenty-First Annual IEEE Applied Power Electronics Conference and Exposition, 2006. APEC'06.*, pp. 5–pp, IEEE, 2006.

[52] O. Lucía, P. Maussion, E. J. Dede, and J. M. Burdío, "Induction heating technology and its applications: past developments, current technology, and future challenges," *IEEE Transactions on industrial electronics*, vol. 61, no. 5, pp. 2509–2520, 2013.

[53] A. Smalcerz, "The use of multifrequency induction heating for temperature distribution control," *Archives of metallurgy and materials*, vol. 60, no. 2A, pp. 721–725, 2015.

[54] T. Zedler, A. Nikanorov, and B. Nacke, "Investigation of relative magnetic permeability as input data for numerical simulation of induction surface hardening," in *International Scientific Colloquium Modelling for Electromagnetic Processing Hannover*, pp. 27–29, 2008.

[55] J. Zgraja, "Dual-frequency induction heating generator with adjustable impedance matching," *IEEE Transactions on Industrial Electronics*, vol. 66, no. 11, pp. 8308–8317, 2018.

[56] A. Kohli and H. Singh, "Optimization of processing parameters in induction hardening using response surface methodology," *Sadhana*, vol. 36, pp. 141–152, 2011.

[57] M. MUHAMMAD, M. A. Siddiqui, and S. Muhammad, "Experimental investigation and optimization of process parameters for through induction hardening using factorial design of experiments," *Journal of Engineering Research*, vol. 5, no. 3, 2017.

[58] M. Onan, K. Baynal, and H. İ. Ünal, "Determining the influence of process parameters on the induction hardening of aisi 1040 steel by an experimental design method," 2015.

[59] H. Hammi, N. Barka, and A. El Ouafi, "Effects of induction heating process parameters on hardness profile of 4340 steel bearing shoulder using 2d axisymmetric model," *Mathematics, Computer, and Engineering Department, the University of Quebec at Rimouski, Rimouski, Quebec, Canada*, 2015.

[60] S. M. Walley, "Historical origins of indentation hardness testing," *Materials Science and Technology*, vol. 28, no. 9-10, pp. 1028–1044, 2012.

[61] P. Panagiotidis, A. Antonatos, and G. Tsananas, "Case depth determination by using vickers micro-hardness test method at trsc/ppc sa," *4th ICNDT of HSNT*, 2007.

[62] K. Clarke, C. Van Tyne, C. Vigil, and R. Hackenberg, "Induction hardening 5150 steel: effects of initial microstructure and heating rate," *Journal of materials engineering and performance*, vol. 20, pp. 161–168, 2011.

[63] A. Asgharzadeh, S. A. Nazari Tiji, R. Esmaeilpour, T. Park, and F. Pourboghrat, "Determination of hardness-strength and-flow behavior relationships in bulged aluminum alloys and verification by fe analysis on rockwell hardness test," *The International Journal of Advanced Manufacturing Technology*, vol. 106, pp. 315–331, 2020.

[64] R. Hill, B. Storåkers, and A. Zdunek, "A theoretical study of the brinell hardness test," *Proceedings of the Royal Society of London. A. Mathematical and Physical Sciences*, vol. 423, no. 1865, pp. 301–330, 1989.

[65] C. Azevedo and J. B. Neto, "Failure analysis of forged and induction hardened steel cold work rolls," *Engineering failure analysis*, vol. 11, no. 6, pp. 951–966, 2004.

[66] N. Shamsaei and A. Fatemi, "Deformation and fatigue behaviors of case-hardened steels in torsion: Experiments and predictions," *International Journal of Fatigue*, vol. 31, no. 8-9, pp. 1386–1396, 2009.

[67] W.-B. Kim and S.-J. Na, "A study on residual stresses in surface hardening by high frequency induction heating," *Surface and Coatings Technology*, vol. 52, no. 3, pp. 281–288, 1992.

[68] H. Kristoffersen and P. Vomacka, "Influence of process parameters for induction hardening on residual stresses," *Materials & Design*, vol. 22, no. 8, pp. 637–644, 2001.

[69] P. S. Prevey *et al.*, "X-ray diffraction residual stress techniques," *ASM International, ASM Handbook.*, vol. 10, pp. 380–392, 1986.

[70] O. Anderoglu, *Residual stress measurement using X-ray diffraction.* PhD thesis, Texas A&M University, 2005.

[71] M. E. Fitzpatrick, A. T. Fry, P. Holdway, F. Kandil, J. Shackleton, and L. Suominen, "Determination of residual stresses by x-ray diffraction.," 2005.

[72] D. Coupard, T. Palin-luc, P. Bristiel, V. Ji, and C. Dumas, "Residual stresses in surface induction hardening of steels: Comparison between experiment and simulation," *Materials Science and Engineering: A*, vol. 487, no. 1-2, pp. 328–339, 2008.

[73] T. Palin-Luc, D. Coupard, C. Dumas, and P. Bristiel, "Simulation of multiaxial fatigue strength of steel component treated by surface induction hardening and comparison with experimental results," *International journal of fatigue*, vol. 33, no. 8, pp. 1040–1047, 2011.

[74] W. Jomaa, V. Songmene, and P. Bocher, "An investigation of machining-induced residual stresses and microstructure of induction-hardened aisi 4340 steel," *Materials and Manufacturing Processes*, vol. 31, no. 7, pp. 838–844, 2016.

[75] N. S. Bailey, W. Tan, and Y. C. Shin, "Predictive modeling and experimental results for residual stresses in laser hardening of aisi 4140 steel by a high power diode laser," *Surface and Coatings Technology*, vol. 203, no. 14, pp. 2003–2012, 2009.

[76] V. Savaria, F. Bridier, and P. Bocher, "Predicting the effects of material properties gradient and residual stresses on the bending fatigue strength of induction hardened aeronautical gears," *International Journal of Fatigue*, vol. 85, pp. 70–84, 2016.

[77] Y. Cao, J. Sun, F. Ma, Y. Chen, X. Cheng, X. Gao, and K. Xie, "Effect of the microstructure and residual stress on tribological behavior of induction hardened gcr15 steel," *Tribology International*, vol. 115, pp. 108–115, 2017.

[78] Y. Lee, J. Lim, and Y. Moon, "Mechanical characteristics of low-carbon-steel pipe bent by local induction heating with small bending radii," *Materials Transactions*, vol. 53, no. 5, pp. 847–852, 2012.

[79] G. Schajer, "Measurement of non-uniform residual stresses using the hole-drilling method. part i—stress calculation procedures," 1988.

[80] A. Niku-Lari, J. Lu, and J. Flavenot, "Measurement of residual stress distribution by the incremental hole-drilling method," *Pergamon Press, Advances in Surface Treatments. Technology–Applications–Effects.*, vol. 4, pp. 199–219, 1987.

[81] K. C. A. Khanzode and R. D. Sarode, "Advantages and disadvantages of artificial intelligence and machine learning: A literature review," *International Journal of Library & Information Science (IJLIS)*, vol. 9, no. 1, p. 3, 2020.

[82] S. Das, A. Dey, A. Pal, and N. Roy, "Applications of artificial intelligence in machine learning: review and prospect," *International Journal of Computer Applications*, vol. 115, no. 9, 2015.

[83] A. Singh, N. Thakur, and A. Sharma, "A review of supervised machine learning algorithms," in *2016 3rd International Conference on Computing for Sustainable Global Development (INDIACom)*, pp. 1310–1315, Ieee, 2016.

[84] F. Hahne, W. Huber, R. Gentleman, S. Falcon, R. Gentleman, and V. Carey, "Unsupervised machine learning," *Bioconductor case studies*, pp. 137–157, 2008.

[85] L. P. Kaelbling, M. L. Littman, and A. W. Moore, "Reinforcement learning: A survey," *Journal of artificial intelligence research*, vol. 4, pp. 237–285, 1996.

[86] B. Nenchev, Q. Tao, Z. Dong, C. Panwisawas, H. Li, B. Tao, and H. Dong, "Evaluating data-driven algorithms for predicting mechanical properties with small datasets: A case study on gear steel hardenability," *International Journal of Minerals, Metallurgy and Materials*, vol. 29, no. 4, pp. 836–847, 2022.

[87] N. J. Sai, P. Rathore, and A. Chauhan, "Machine learning-based predictions of fatigue life for multi-principal element alloys," *Scripta Materialia*, vol. 226, p. 115214, 2023.

[88] C. Krause, B. Uysal, M. Engler, C. Radek, and M. Schaudig, "Application of machine learning techniques to determine surface hardness based on the barkhausen effect," *HTM Journal of Heat Treatment and Materials*, vol. 77, no. 6, pp. 409–424, 2022.

[89] J. Sha, M. Fan, B. Cao, and B. Liu, "Noncontact and nondestructive evaluation of heat-treated bearing rings using pulsed eddy current testing," *Journal of Magnetism and Magnetic Materials*, vol. 521, p. 167516, 2021.

[90] A. Agrawal, S. Goel, W. B. Rashid, and M. Price, "Prediction of surface roughness during hard turning of aisi 4340 steel (69 hrc)," *Applied Soft Computing*, vol. 30, pp. 279–286, 2015.

[91] H. Yang, Z. Zhang, J. Zhang, and X. C. Zeng, "Machine learning and artificial neural network prediction of interfacial thermal resistance between graphene and hexagonal boron nitride," *Nanoscale*, vol. 10, no. 40, pp. 19092–19099, 2018.

[92] F. Lambiase, A. Di Ilio, and A. Paoletti, "Prediction of laser hardening by means of neural network," *Procedia CIRP*, vol. 12, pp. 181–186, 2013.

[93] P. D. Deshpande, B. Gautham, U. Gupta, and D. Khan, "Modeling the steel case carburizing quenching process using statistical and machine learning techniques," in *2014 9th International Conference on Industrial and Information Systems (ICIIS)*, pp. 1–6, IEEE, 2014.

[94] J. Wróbel and A. Kulawik, "Using the artificial neural networks in the modelling of the induction heating," in *AIP Conference Proceedings*, vol. 1648, p. 850090, AIP Publishing LLC, 2015.

[95] M. Z. Asadzadeh, P. Raninger, P. Prevedel, W. Ecker, and M. Mücke, "Hybrid modeling of induction hardening processes," *Applications in Engineering Science*, vol. 5, p. 100030, 2021.

[96] K. Kato, M. Sakawa, K. Ishimaru, S. Ushiro, and T. Shibano, "Heat load prediction through recurrent neural network in district heating and cooling systems," in *2008 IEEE international conference on systems, man and cybernetics*, pp. 1401–1406, IEEE, 2008.

[97] Y. Feng, Y. Liu, J. Wang, and R. Li, "Research on an svm prediction of welding deformation rectification for high-strength steel fillet-welded joints after traveling induction heating," *Journal of Ship Production and Design*, vol. 39, no. 01, pp. 43–53, 2023.

[98] J. Shen, X. Hu, D. Mi, Z. Qian, X. Teng, X. Song, Y. Jiang, and X. Nie, "Thermomechanical fatigue behavior and lifetime modeling of powder metallurgy superalloy considering phase angle effect," *International Journal of Fatigue*, vol. 164, p. 107164, 2022.

[99] A. B. Arrieta, N. Díaz-Rodríguez, J. Del Ser, A. Bennetot, S. Tabik, A. Barbado, S. García, S. Gil-López, D. Molina, R. Benjamins, *et al.*, "Explainable artificial intelligence (xai): Concepts, taxonomies, opportunities and challenges toward responsible ai," *Information fusion*, vol. 58, pp. 82–115, 2020.

[100] A. Adadi and M. Berrada, "Peeking inside the black-box: a survey on explainable artificial intelligence (xai)," *IEEE access*, vol. 6, pp. 52138–52160, 2018.

[101] R. Guidotti, A. Monreale, S. Ruggieri, F. Turini, F. Giannotti, and D. Pedreschi, "A survey of methods for explaining black box models," *ACM computing surveys (CSUR)*, vol. 51, no. 5, pp. 1–42, 2018.

[102] R. Dwivedi, D. Dave, H. Naik, S. Singhal, R. Omer, P. Patel, B. Qian, Z. Wen, T. Shah, G. Morgan, *et al.*, "Explainable ai (xai): Core ideas, techniques, and solutions," *ACM Computing Surveys*, vol. 55, no. 9, pp. 1–33, 2023.

[103] E. Tjoa and C. Guan, "A survey on explainable artificial intelligence (xai): Toward medical xai," *IEEE transactions on neural networks and learning systems*, vol. 32, no. 11, pp. 4793–4813, 2020.

[104] S. M. Lundberg, G. G. Erion, and S.-I. Lee, "Consistent Individualized Feature Attribution for Tree Ensembles," *arXiv:1802.03888 [cs, stat]*, Mar. 2019. arXiv: 1802.03888.

[105] M. T. Ribeiro, S. Singh, and C. Guestrin, "Model-agnostic interpretability of machine learning," *arXiv preprint arXiv:1606.05386*, 2016.

[106] R. Guidotti, A. Monreale, S. Ruggieri, D. Pedreschi, F. Turini, and F. Giannotti, "Local rule-based explanations of black box decision systems," *arXiv preprint arXiv:1805.10820*, 2018.

[107] C. L. Byrne, *Iterative optimization in inverse problems*. CRC Press, 2014.

[108] N. Ye, F. Roosta-Khorasani, and T. Cui, "Optimization methods for inverse problems," *2017 MATRIX Annals*, pp. 121–140, 2019.

[109] G. Peyré, S. Bougleux, and L. Cohen, "Non-local regularization of inverse problems," in *Computer Vision–ECCV 2008: 10th European Conference on Computer Vision, Marseille, France, October 12-18, 2008, Proceedings, Part III 10*, pp. 57–68, Springer, 2008.

[110] H. Egger and H. W. Engl, "Tikhonov regularization applied to the inverse problem of option pricing: convergence analysis and rates," *Inverse problems*, vol. 21, no. 3, p. 1027, 2005.

[111] M. Benning and M. Burger, "Modern regularization methods for inverse problems," *Acta Numerica*, vol. 27, pp. 1–111, 2018.

[112] D. Calvetti and E. Somersalo, "Inverse problems: From regularization to bayesian inference," *Wiley Interdisciplinary Reviews: Computational Statistics*, vol. 10, no. 3, p. e1427, 2018.

[113] D. M. Schmidt, J. S. George, and C. C. Wood, "Bayesian inference applied to the electromagnetic inverse problem," *Human brain mapping*, vol. 7, no. 3, pp. 195–212, 1999.

[114] X. Ma and N. Zabaras, "An efficient bayesian inference approach to inverse problems based on an adaptive sparse grid collocation method," *Inverse Problems*, vol. 25, no. 3, p. 035013, 2009.

[115] B. Sridharan, M. Goel, and U. D. Priyakumar, "Modern machine learning for tackling inverse problems in chemistry: molecular design to realization," *Chemical Communications*, vol. 58, no. 35, pp. 5316–5331, 2022.

[116] L. Pilozzi, F. A. Farrelly, G. Marcucci, and C. Conti, "Machine learning inverse problem for topological photonics," *Communications Physics*, vol. 1, no. 1, p. 57, 2018.

[117] M. Z. Asadzadeh, P. Raninger, P. Prevedel, W. Ecker, and M. Mücke, "Inverse model for the control of induction heat treatments," *Materials*, vol. 12, no. 17, p. 2826, 2019.

[118] K. T. Nguyen and A. Bendada, "An inverse approach for the prediction of the temperature evolution during induction heating of a semi-solid casting billet," *Modelling and Simulation in Materials Science and Engineering*, vol. 8, no. 6, p. 857, 2000.

[119] J. V. Beck, B. Blackwell, and C. R. S. Clair Jr, *Inverse heat conduction: Ill-posed problems*. James Beck, 1985.

[120] M. Dreher, R. Quintanilla, and R. Racke, "Ill-posed problems in thermomechanics," *Applied Mathematics Letters*, vol. 22, no. 9, pp. 1374–1379, 2009.

[121] E. ISO, "6507-1: 2018—metallic materials—vickers hardness test—part 1: Test method," *ISO: Geneva, Switzerland*, 2018.

[122] J. Bergstra and Y. Bengio, "Random search for hyper-parameter optimization.," *Journal of machine learning research*, vol. 13, no. 2, 2012.

[123] S. B. Kotsiantis, "Decision trees: a recent overview," *Artificial Intelligence Review*, vol. 39, pp. 261–283, 2013.

[124] T. Chen, T. He, M. Benesty, V. Khotilovich, Y. Tang, H. Cho, K. Chen, R. Mitchell, I. Cano, T. Zhou, *et al.*, "Xgboost: extreme gradient boosting," *R package version 0.4-2*, vol. 1, no. 4, pp. 1–4, 2015.

[125] T. Chen and C. Guestrin, "Xgboost: A scalable tree boosting system," in *Proceedings of the 22nd acm sigkdd international conference on knowledge discovery and data mining*, pp. 785–794, 2016.

[126] C. Wuppermann and E. Míček, "Importance of heat treatment for the variety of applications of modern materials," *Prozesswarme*, vol. 2018, pp. 95–101, 01 2018.

[127] M. E. Grayley, "Guide to the selection of surface treatments for the improvement of fatigue strength of steels," *Engineering Sciences Data Unit (ESDU)*, 09 1989.

[128] H. Oppermann, "Surface treatments improve the structural fatigue strength of metallic components," vol. 37, pp. 82–85, 03 1995.

[129] P. Rokicki, "Induction hardening of tool steel for heavily loaded aircraft engine components," *Archives of Metallurgy and Materials*, vol. 62, pp. 315–320, 03 2017.

[130] V. Rudnev, D. Loveless, and R. Cook, *Handbook of Induction Heating.* CRC Press, 2nd ed., 08 2017.

[131] D. Hömberg, "A mathematical model for induction hardening including mechanical effects," *NONLINEAR ANAL-REAL WORLD APP*, vol. 5, pp. 55–90, 02 2004.

[132] M. Spezzapria, F. Dughiero, M. Forzan, and A. Candeo, "Multiphysics fem simulation of contour induction hardening process on aeronautical gears," *J. Iron Steel Res.*, vol. 19, pp. 95–98, 01 2012.

[133] K. Wang, S. Chandrasekar, and H. Yang, "Finite-element simulation of induction heat treatment," *Journal of Materials Engineering and Performance*, vol. 1, pp. 97–112, 02 1992.

[134] M. Samiuddin and M. Muzamil, "Experimental investigation and optimization of process parameters for through induction hardening using factorial design of experiments," *Journal of Engineering Research*, vol. 5, pp. 174–185, 12 2016.

[135] D. Hutton, *Fundamentals of Finite Element Analysis*. McGraw-Hill Higher Education, Boston, 1st ed., 01 2004.

[136] P. Astrid, *Reduction of process simulation models : a proper orthogonal decomposition approach*. Thesis, Technische Universiteit Eindhoven, 2004.

[137] O. Lucia, P. Maussion, E. Dede, and J. Burdio, "Induction heating technology and its applications: Past developments, current technology, and future challenges," *Industrial Electronics, IEEE Transactions on*, vol. 61, pp. 2509–2520, 05 2014.

[138] I. Magnabosco, P. Ferro, A. Tiziani, and F. Bonollo, "Induction heat treatment of a iso c45 steel bar: Experimental and numerical analysis," *Computational Materials Science*, vol. 35, pp. 98–106, 02 2006.

[139] H. Ding and Y. Shin, "A metallo-thermomechanically coupled analysis of orthogonal cutting of aisi 1045 steel," *Journal of Manufacturing Science and Engineering*, vol. 134, p. 051014, 10 2012.

[140] A. Gorni, "Steel forming and heat treating handbook," tech. rep., 01 2015.

[141] S.-J. Lee, E. Pavlina, and C. Vantyne, "Kinetics modeling of austenite decomposition for an end-quenched 1045 steel," *MATER SCI ENG A-STRUCT MATER*, vol. 527, pp. 3186–3194, 05 2010.

[142] P. BARBA, "Field models of induction heating for industrial applications," *PRZEGLĄD ELEKTROTECHNICZNY*, vol. 1, pp. 3–7, 03 2018.

[143] D. Cardinaux, *Étude et modélisation numérique 3D par éléments finis d'un procédé de traitement thermique de tôles embouties après chauffage par induction : Application à un renfort de pied central automobile*. Thesis, École Nationale Supérieure des Mines de Paris, Nov. 2008.

[144] M. Stein, "Large sample properties of simulations using latin hypercube sampling," *Technometrics*, vol. 29, pp. 143–151, 05 1987.

[145] R. Ibáñez Pinillo, E. Abisset-Chavanne, A. Ammar, D. González, E. Cueto, A. Huerta, J. Duval, and F. Chinesta, "A multidimensional data-driven sparse identification technique: The sparse proper generalized decomposition," *Complexity*, vol. 2018, pp. 1–11, 11 2018.

[146] V. Limousin, X. Delgerie, E. Leroy, R. Ibáñez, C. Argerich, F. Daim, J. Duval, and F. Chinesta, "Advanced model order reduction and artificial intelligence techniques empowering advanced structural mechanics simulations: application to crash test analyses," *Mechanics & Industry*, vol. 20, p. 804, 01 2019.

[147] W. Johnson and R. Mehl, "Reaction kinetics in process of nucleation and growth," *Transaction of American Institute of Mining, Metallurgical, and Petroleum Engineers*, vol. 135, p. 416, 01 1939.

[148] M. Avrami, "Kinetics of phase change. i general theory," *J. Chem. Phys.*, vol. 7, pp. 1103–1112, 12 1939.

[149] M. Avrami, "Kinetics of phase change ii. transformation-time relations for random distribution nuclei," *J. Chem. Phys.*, vol. 8, pp. 212–224, 12 1940.

[150] M. Avrami, "Kinetics of phase change iii. granulation, phase change and microstructure," *J. Chem. Phys.*, vol. 9, pp. 177–184, 12 1941.

[151] S. Kim and H. Kim, "A new metric of absolute percentage error for intermittent demand forecasts," *International Journal of Forecasting*, vol. 32, pp. 669–679, 07 2016.

[152] T. Hastie, R. Tibshirani, and J. Friedman, *The elements of statistical learning: data mining, inference, and prediction*. Springer Science & Business Media, 2009.

[153] M. S. Santos, J. P. Soares, P. H. Abreu, H. Araujo, and J. Santos, "Cross-validation for imbalanced datasets: Avoiding overoptimistic and overfitting approaches [research frontier]," *IEEE Computational Intelligence Magazine*, vol. 13, no. 4, pp. 59–76, 2018.

[154] J. Macqueen, "Some methods for classification and analysis of multivariate observations," in *In 5-th Berkeley Symposium on Mathematical Statistics and Probability*, pp. 281–297, 1967.

[155] L. I. Kuncheva and J. J. Rodríguez, "On feature selection protocols for very low-sample-size data," *Pattern Recognition*, vol. 81, pp. 660–673, 2018.

[156] S. Pafka, "benchm-ml." `https://github.com/szilard/benchm-ml`, 2019.

[157] P. Orzechowski, W. La Cava, and J. H. Moore, "Where are we now?," *Proceedings of the Genetic and Evolutionary Computation Conference*, Jul 2018.

[158] L. Prechelt, "Early stopping-but when?," in *Neural Networks: Tricks of the trade*, pp. 55–69, Springer, 1998.

[159] K. Derouiche, S. Garois, V. Champaney, M. Daoud, K. Traidi, and F. Chinesta, "Data-driven modeling for multiphysics parametrized problems-application to induction hardening process," *Metals*, vol. 11, no. 5, p. 738, 2021.

[160] I. Magnabosco, P. Ferro, A. Tiziani, and F. Bonollo, "Induction heat treatment of a iso c45 steel bar: Experimental and numerical analysis," *Computational materials science*, vol. 35, no. 2, pp. 98–106, 2006.

[161] H. Ding and Y. C. Shin, "A metallo-thermomechanically coupled analysis of orthogonal cutting of aisi 1045 steel," *Journal of manufacturing science and engineering*, vol. 134, no. 5, 2012.

[162] H. J. Geijselaers, "Numerical simulation of stresses due to solid state transformations: the simulation of laser hardening," 2003.

[163] S.-J. Lee, E. J. Pavlina, and C. J. Van Tyne, "Kinetics modeling of austenite decomposition for an end-quenched 1045 steel," *Materials Science and Engineering: A*, vol. 527, no. 13-14, pp. 3186–3194, 2010.

[164] P. Di Barba, M. E. Mognaschi, M. Bullo, F. Dughiero, M. Forzan, S. Lupi, and E. Sieni, "Field models of induction heating for industrial applications," *Organ*, vol. 3, p. 18, 2018.

[165] M. Stein, "Large sample properties of simulations using latin hypercube sampling," *Technometrics*, vol. 29, no. 2, pp. 143–151, 1987.

[166] R. Shwartz-Ziv and A. Armon, "Tabular data: Deep learning is not all you need," *Information Fusion*, vol. 81, pp. 84–90, 2022.

[167] P. J. Withers and H. Bhadeshia, "Residual stress. part 1–measurement techniques," *Materials science and Technology*, vol. 17, no. 4, pp. 355–365, 2001.

[168] R. E. Haimbaugh, *Practical induction heat treating*. ASM international, 2015.

[169] H. Kristoffersen and P. Vomacka, "Influence of process parameters for induction hardening on residual stresses," *Materials & Design*, vol. 22, pp. 637–644, Dec. 2001.

[170] J. Li, Z. Cao, L. Liu, X. Liu, and J. Peng, "Effect of Microstructure on Hardness and Wear Properties of 45 Steel after Induction Hardening," *steel research international*, vol. 92, p. 2000540, Apr. 2021.

[171] J. Hájek, D. Rot, and J. Jiřinec, "Distortion in Induction-Hardened Cylindrical Part," *Defect and Diffusion Forum*, vol. 395, pp. 30–44, Aug. 2019.

[172] J. Grum, "A review of the influence of grinding conditions on resulting residual stresses after induction surface hardening and grinding," *Journal of Materials Processing Technology*, p. 15, 2001.

[173] D. Rodman, C. Krause, F. Nürnberger, F.-W. Bach, K. Haskamp, M. Kästner, and E. Reithmeier, "Induction Hardening of Spur Gearwheels Made from 42CrMo4 Hardening and Tempering Steel by Employing Spray Cooling," *steel research international*, vol. 82, pp. 329–336, Apr. 2011.

[174] J. Yi, M. Gharghouri, P. Bocher, and M. Medraj, "Distortion and residual stress measurements of induction hardened AISI 4340 discs," *Materials Chemistry and Physics*, vol. 142, pp. 248–258, Oct. 2013.

[175] D. V. Hutton, *Fundamentals of finite element analysis*. McGraw-Hill Science Engineering, 2003.

[176] Y. Guo, M. Liu, and Y. Yan, "Hardness prediction of grind-hardening layer based on integrated approach of finite element and cellular automata," *Materials*, vol. 14, no. 19, p. 5651, 2021.

[177] Y. Zhang, J. Ruan, T. Huang, X. Yang, H. Zhu, and G. Yang, "Calculation of temperature rise in air-cooled induction motors through 3-d coupled electromagnetic fluid-dynamical and thermal finite-element analysis," *IEEE Transactions on Magnetics*, vol. 48, no. 2, pp. 1047–1050, 2012.

[178] V. Javaheri, A. Pohjonen, J. I. Asperheim, D. Ivanov, and D. Porter, "Physically based modeling, characterization and design of an induction hardening process for a new slurry pipeline steel," *Materials & Design*, vol. 182, p. 108047, 2019.

[179] M. Fisk, L.-E. Lindgren, W. Datchary, and V. Deshmukh, "Modelling of induction hardening in low alloy steels," *Finite elements in analysis and design*, vol. 144, pp. 61–75, 2018.

[180] P. Sumithra and D. Thiripurasundari, "Review on computational electromagnetics," *Advanced Electromagnetics*, vol. 6, no. 1, pp. 42–55, 2017.

[181] W. Li, Z. Yuan, and Z. Chen, "Adaptive mesh morphing method for numerical analysis of electromagneto-mechanical coupling using lagrangian approach," in *Proc. 19th Int. Conf. Comput. Electromagn. Fields COMPUMAG*, pp. 1–2, 2013.

[182] M. Areitioaurtena, U. Segurajauregi, V. Akujärvi, M. Fisk, I. Urresti, and E. Ukar, "A semi-analytical coupled simulation approach for induction heating," *Advanced Modeling and Simulation in Engineering Sciences*, vol. 8, no. 1, pp. 1–19, 2021.

[183] D. Hömberg, T. Petzold, and E. Rocca, "Analysis and simulations of multifrequency induction hardening," *Nonlinear Analysis: Real World Applications*, vol. 22, pp. 84–97, 2015.

[184] S. Smokvina Hanza, T. Marohnić, D. Iljkić, and R. Basan, "Artificial neural networks-based prediction of hardness of low-alloy steels using specific jominy distance," *Metals*, vol. 11, no. 5, p. 714, 2021.

[185] A. Sorsa, K. Leiviskä, S. Santa-aho, and T. Lepistö, "Quantitative prediction of residual stress and hardness in case-hardened steel based on the Barkhausen noise measurement," *NDT & E International*, vol. 46, pp. 100–106, Mar. 2012.

[186] J. Ghaisari, H. Jannesari, and M. Vatani, "Artificial neural network predictors for mechanical properties of cold rolling products," *Advances in Engineering Software*, vol. 45, no. 1, pp. 91–99, 2012.

[187] L. Ruisen, D. Songyi, W. Chen, C. Peng, T. Zuodong, Y. YanMei, and W. Shixiong, "Bagging of xgboost classifiers with random under-sampling and tomek link for noisy label-imbalanced data," in *IOP Conference series: Materials science and engineering*, vol. 428, p. 012004, IOP Publishing, 2018.

[188] M. Schwenk, M. Fisk, T. Cedell, J. Hoffmeister, V. Schulze, and L.-E. Lindgren, "Process simulation of single and dual frequency induction surface hardening considering magnetic nonlinearity," *Materials Performance and Characterization*, vol. 1, no. 1, pp. 1–20, 2012.

[189] M. Schwenk, J. Hoffmeister, and V. Schulze, "Experimentally validated residual stresses and distortion prediction for dual frequency induction hardening," *International Journal of Applied Electromagnetics and Mechanics*, vol. 44, no. 2, pp. 127–135, 2014.

[190] D. Yun, H. Park, J.-H. Koo, S. Ham, and S. Lee, "Investigation of heat treatment of gears using a simultaneous dual frequency induction heating method," *IEEE Transactions on Magnetics*, vol. 51, no. 11, pp. 1–4, 2015.

[191] D. Tamayo, A. Silburt, D. Valencia, K. Menou, M. Ali-Dib, C. Petrovich, C. X. Huang, H. Rein, C. Van Laerhoven, A. Paradise, *et al.*, "A machine learns to predict the stability of tightly packed planetary systems," *The Astrophysical Journal Letters*, vol. 832, no. 2, p. L22, 2016.

[192] A. Möller, V. Ruhlmann-Kleider, C. Leloup, J. Neveu, N. Palanque-Delabrouille, J. Rich, R. Carlberg, C. Lidman, and C. Pritchet, "Photometric classification of type ia supernovae in the supernova legacy survey with supervised learning," *Journal of Cosmology and Astroparticle Physics*, vol. 2016, no. 12, p. 008, 2016.

[193] F. Giannakas, C. Troussas, A. Krouska, C. Sgouropoulou, and I. Voyiatzis, "Xgboost and deep neural network comparison: The case of teams' performance," in *International Conference on Intelligent Tutoring Systems*, pp. 343–349, Springer, 2021.

[194] M. Zamani Joharestani, C. Cao, X. Ni, B. Bashir, and S. Talebiesfandarani, "Pm2. 5 prediction based on random forest, xgboost, and deep learning using multisource remote sensing data," *Atmosphere*, vol. 10, no. 7, p. 373, 2019.

[195] T. S. Jaakkola and D. Haussler, "Probabilistic kernel regression models," in *Seventh International Workshop on Artificial Intelligence and Statistics*, PMLR, 1999.

[196] M. Langer, D. Oster, T. Speith, H. Hermanns, L. Kästner, E. Schmidt, A. Sesing, and K. Baum, "What do we want from explainable artificial intelligence (xai)?–a stakeholder perspective on xai and a conceptual model guiding interdisciplinary xai research," *Artificial Intelligence*, vol. 296, p. 103473, 2021.

[197] E. Tjoa and C. Guan, "A Survey on Explainable Artificial Intelligence (XAI): towards Medical XAI," p. 21, 2019.

[198] O. Loyola-Gonzalez, "Black-box vs. white-box: Understanding their advantages and weaknesses from a practical point of view," *IEEE Access*, vol. 7, pp. 154096–154113, 2019.

[199] R. Guidotti, A. Monreale, S. Ruggieri, F. Turini, F. Giannotti, and D. Pedreschi, "A Survey of Methods for Explaining Black Box Models," *ACM Computing Surveys*, vol. 51, pp. 1–42, Jan. 2019.

[200] A. Das and P. Rad, "Opportunities and challenges in explainable artificial intelligence (xai): A survey," *arXiv preprint arXiv:2006.11371*, 2020.

[201] M. V. García and J. L. Aznarte, "Shapley additive explanations for no2 forecasting," *Ecological Informatics*, vol. 56, p. 101039, 2020.

[202] A. Abdollahi and B. Pradhan, "Urban vegetation mapping from aerial imagery using explainable ai (xai)," *Sensors*, vol. 21, no. 14, p. 4738, 2021.

[203] A. Dikshit and B. Pradhan, "Interpretable and explainable ai (xai) model for spatial drought prediction," *Science of the Total Environment*, vol. 801, p. 149797, 2021.

[204] S. Yoo and N. Kang, "Explainable artificial intelligence for manufacturing cost estimation and machining feature visualization," *Expert Systems with Applications*, vol. 183, p. 115430, 2021.

[205] J. Jeon, N. Seo, J.-G. Jung, S. B. Son, and S.-J. Lee, "Prediction and mechanism explain of austenite-grain growth during reheating of alloy steel using xai," *Journal of Materials Research and Technology*, 2022.

[206] S. Garois, M. Daoud, K. Traidi, and F. Chinesta, "Artificial intelligence modeling of induction contour hardening of 300m steel bar and c45 steel spur-gear," *International Journal of Material Forming*, Submitted.

[207] H. Zheng, J. Yuan, and L. Chen, "Short-term load forecasting using emd-lstm neural networks with a xgboost algorithm for feature importance evaluation," *Energies*, vol. 10, no. 8, p. 1168, 2017.

[208] C. Goutte and E. Gaussier, "A probabilistic interpretation of precision, recall and f-score, with implication for evaluation," in *European conference on information retrieval*, pp. 345–359, Springer, 2005.

[209] M. T. Ribeiro, S. Singh, and C. Guestrin, ""Why Should I Trust You?": Explaining the Predictions of Any Classifier," in *Proceedings of the 22nd ACM SIGKDD International Conference on Knowledge Discovery and Data Mining*, (San Francisco California USA), pp. 1135–1144, ACM, Aug. 2016.

[210] R. Guidotti, A. Monreale, S. Ruggieri, D. Pedreschi, F. Turini, and F. Giannotti, "Local Rule-Based Explanations of Black Box Decision Systems," *arXiv:1805.10820 [cs]*, May 2018. arXiv: 1805.10820.

[211] S. M. Lundberg and S.-I. Lee, "A Unified Approach to Interpreting Model Predictions," in *Advances in Neural Information Processing Systems*, vol. 30, Curran Associates, Inc., 2017.

[212] C. B. Azodi, J. Tang, and S.-H. Shiu, "Opening the black box: interpretable machine learning for geneticists," *Trends in genetics*, vol. 36, no. 6, pp. 442–455, 2020.

[213] J. R. Quinlan, "Learning decision tree classifiers," *ACM Computing Surveys (CSUR)*, vol. 28, no. 1, pp. 71–72, 1996.

[214] Z. Li and B. L. Ferguson, "Controlling gear distortion and residual stresses during induction hardening," *Gear Technology*, 2012.

[215] V. Nemkov, R. Goldstein, J. Jackowski, L. Ferguson, and Z. Li, "Stress and distortion evolution during induction case hardening of tube," *Journal of materials engineering and performance*, vol. 22, pp. 1826–1832, 2013.

[216] S. I. Kabanikhin, "Definitions and examples of inverse and ill-posed problems," 2008.

[217] Z. Pizlo, "Perception viewed as an inverse problem," *Vision research*, vol. 41, no. 24, pp. 3145–3161, 2001.

[218] A. Mohamad-Djafari, *Inverse problems in vision and 3D tomography*. John Wiley & Sons, 2013.

[219] M. Bertero, P. Boccacci, and C. De Mol, *Introduction to inverse problems in imaging*. CRC press, 2021.

[220] M. T. McCann, K. H. Jin, and M. Unser, "Convolutional neural networks for inverse problems in imaging: A review," *IEEE Signal Processing Magazine*, vol. 34, no. 6, pp. 85–95, 2017.

[221] G. Ongie, A. Jalal, C. A. Metzler, R. G. Baraniuk, A. G. Dimakis, and R. Willett, "Deep learning techniques for inverse problems in imaging," *IEEE Journal on Selected Areas in Information Theory*, vol. 1, no. 1, pp. 39–56, 2020.

[222] G. M. Gladwell, "Inverse problems in vibration," 1986.

[223] G. D. Egbert and A. Kelbert, "Computational recipes for electromagnetic inverse problems," *Geophysical Journal International*, vol. 189, no. 1, pp. 251–267, 2012.

[224] R. S. MacLeod and D. H. Brooks, "Recent progress in inverse problems in electrocardiology," *IEEE Engineering in Medicine and Biology Magazine*, vol. 17, no. 1, pp. 73–83, 1998.

[225] N.-Z. Sun, *Inverse problems in groundwater modeling*, vol. 6. Springer Science & Business Media, 2013.

[226] E. De Vito, L. Rosasco, A. Caponnetto, U. De Giovannini, F. Odone, and P. Bartlett, "Learning from examples as an inverse problem.," *Journal of Machine Learning Research*, vol. 6, no. 5, 2005.

[227] A. Vieweg, G. Ressel, P. Prevedel, P. Raninger, M. Panzenböck, S. Marsoner, and R. Ebner, "Induction hardening: Differences to a conventional heat treatment process and optimization of its parameters," in *IOP Conference Series: Materials Science and Engineering*, vol. 119, p. 012019, IOP Publishing, 2016.

[228] D.-h. Xu and Z.-B. Kuang, "A study on the distribution of residual stress due to surface induction hardening," 1996.

[229] J.-K. Choi, K.-S. Park, and S.-S. Lee, "Prediction of high-frequency induction hardening depth of an aisi 1045 specimen by finite element analysis and experiments," *International journal of precision engineering and manufacturing*, vol. 19, pp. 1821–1827, 2018.

[230] M. K. Misra, B. Bhattacharya, O. Singh, and A. Chatterjee, "Multi response optimization of induction hardening process-a new approach," *IFAC Proceedings Volumes*, vol. 47, no. 1, pp. 862–869, 2014.

[231] D. Kaiser, J. Damon, F. Mühl, B. de Graaff, D. Kiefer, S. Dietrich, and V. Schulze, "Experimental investigation and finite-element modeling of the short-time induction quench-and-temper process of aisi 4140," *Journal of Materials Processing Technology*, vol. 279, p. 116485, 2020.

[232] R. O. Duda, P. E. Hart, *et al.*, *Pattern classification and scene analysis*, vol. 3. Wiley New York, 1973.

[233] J. Gareth, W. Daniela, H. Trevor, and T. Robert, *An introduction to statistical learning: with applications in R.* Spinger, 2013.

[234] M. Kubat, "Neural networks: a comprehensive foundation by simon haykin, macmillan, 1994, isbn 0-02-352781-7.," *The Knowledge Engineering Review*, vol. 13, no. 4, pp. 409–412, 1999.

[235] A. Labach, H. Salehinejad, and S. Valaee, "Survey of dropout methods for deep neural networks," *arXiv preprint arXiv:1904.13310*, 2019.

[236] L. Breiman, "Random forests," *Machine learning*, vol. 45, pp. 5–32, 2001.

[237] A. Cutler, D. R. Cutler, and J. R. Stevens, "Random forests," *Ensemble machine learning: Methods and applications*, pp. 157–175, 2012.

[238] R. A. Bottenberg and J. H. Ward, *Applied multiple linear regression*, vol. 63. 6570th Personnel Research Laboratory, Aerospace Medical Division, Air Force ..., 1963.

[239] A. J. Smola and B. Schölkopf, "A tutorial on support vector regression," *Statistics and computing*, vol. 14, pp. 199–222, 2004.

[240] M. Awad, R. Khanna, M. Awad, and R. Khanna, "Support vector regression," *Efficient learning machines: Theories, concepts, and applications for engineers and system designers*, pp. 67–80, 2015.

[241] R. B. Rao, G. Fung, and R. Rosales, "On the dangers of cross-validation. an experimental evaluation," in *Proceedings of the 2008 SIAM international conference on data mining*, pp. 588–596, SIAM, 2008.

[242] A. Isaksson, M. Wallman, H. Göransson, and M. G. Gustafsson, "Cross-validation and bootstrapping are unreliable in small sample classification," *Pattern Recognition Letters*, vol. 29, no. 14, pp. 1960–1965, 2008.